TURUN
YLIOPISTO
UNIVERSITY
OF TURKU

Enhancing Lyme Neuroborreliosis Diagnostics with UHPLC–MS/MS-based Metabolomics and Machine Learning

Ilari Kuukkanen

TURUN YLIOPISTON JULKAISUJA – ANNALES UNIVERSITATIS TURKUENSIS
SARJA – SER. AI OSA – TOM. 761 | ASTRONOMICA – CHEMICA – PHYSICA – MATHEMATICA | TURKU 2026

TURUN
YLIOPISTO
UNIVERSITY
OF TURKU

ENHANCING LYME NEUROBORRELIOSIS DIAGNOSTICS WITH UHPLC–MS/MS-BASED METABOLOMICS AND MACHINE LEARNING

Ilari Kuukkanen

TURUN YLIOPISTON JULKAISUJA – ANNALES UNIVERSITATIS TURKUENSIS
SARJA – SER. AI OSA – TOM. 761 | ASTRONOMICA - CHEMICA - PHYSICA – MATHEMATICA | TURKU 2026

University of Turku

Faculty of Science
Department of Chemistry
Chemistry
Doctoral programme in Exact Sciences

Supervised by

Docent, Maarit Karonen, PhD
Department of Chemistry
University of Turku
Turku, Finland

Professor, Jukka Hytönen, MD, PhD
Institute of Biomedicine
University of Turku
Turku, Finland

Reviewed by

Dr, Linda Ahonen, PhD
Novo Nordisk Foundation Center for Biosustainability
Technical University of Denmark
Lyngby, Denmark

Docent, Satu Kurkela, MD, PhD
HUS Diagnostic Center
Clinical Microbiology
University of Helsinki and
Helsinki University Hospital
Helsinki, Finland

Opponent

Associate Professor, Marko Lehtonen, PhD
School of Pharmacy
Faculty of Health Sciences
University of Eastern Finland
Kuopio, Finland

ISBN 978-952-02-0686-4 (PRINT)
ISBN 978-952-02-0687-1 (PDF)
ISSN 0082-7002 (Print)
ISSN 2343-3175 (Online)
Painosalama, Turku, Finland 2026

To my beloved wife, whose unwavering support, love, and patience carried me through the most challenging moments of this journey.
And to my children, whose joy, curiosity, and resilience inspired me every day. You remind me of what truly matters and why perseverance is worth it.

UNIVERSITY OF TURKU
Faculty of Science
Department of Chemistry
Chemistry
ILARI KUUKKANEN: Enhancing Lyme neuroborreliosis diagnostics with UHPLC–MS/MS-based metabolomics and machine learning
Doctoral Dissertation, 153 pp.
Doctoral Programme in Exact Sciences
March 2026

ABSTRACT

This multidisciplinary doctoral dissertation focused on development of untargeted ultrahigh-performance liquid chromatography–tandem mass spectrometry (UHPLC–MS/MS) -based metabolomics of serum and cerebrospinal fluid (CSF), integrated with supervised machine learning (ML), to identify metabolic alterations and candidate molecular features (MFs) for enhanced diagnostics of Lyme neuroborreliosis (LNB). Due to limitations of current biomarkers in Lyme borreliosis (LB) diagnostics, a paired, within-patient design was implemented to enhance sensitivity to disease-related changes. Serum profiling paired pretreatment LNB with 12 months after treatment samples. CSF profiling paired pretreatment LNB with samples three weeks after treatment initiation. LNB cohorts were companied with *Borrelia* antibody-negative, non-LNB controls in serum and CSF, and with other laboratory confirmed central nervous system infections in CSF, enabling assessment of disease specificity.

Across matrices, pathway alterations were characterized by the tryptophan-kynurenine axis, broad lipid-signaling alterations (lysophospholipids, sphingomyelins, sphingoid bases, fatty acid amides, cyclic phosphatidic acids), and amino acid metabolism. Acetylcarnitine exhibited matrix-specific dynamics, elevated in pretreatment CSF, declining after treatment and higher in other CNS infections, but increased in post-treatment serum, indicating distinct compartmental responses. Several CSF MFs associated with chemokine CXCL13 concentration, thus supporting linkage to neuroinflammation.

Supervised ML classifiers trained on serum profiles yielded strong discrimination with high sensitivity and specificity, and robust performance across comparisons. LNB induced detectable metabolic alterations, however, treated LNB retained a distinct serum signature versus non-LNB controls. Overlapping discriminatory features across models indicate an infection-linked signal rather than purely treatment-driven observations.

UHPLC–MS/MS-based MF panels and ML classifiers emerge as potential complementary tools to enhance diagnostics and monitoring of disseminated LB.

KEYWORDS: *Borrelia burgdorferi*; cerebrospinal fluid; Lyme neuroborreliosis; machine learning; metabolomics; UHPLC–MS/MS; serum

TURUN YLIOPISTO
Matemaattis-luonnontieteellinen tiedekunta
Kemian laitos
Luonnonyhdistekemian tutkimusryhmä
ILARI KUUKKANEN: Lymen neuroborrelioosin diagnostiikan tehostaminen UHPLC–MS/MS-perusteisella metabolomiikalla ja koneoppimisella
Väitöskirja, 153 s.
Eksaktien tieteiden tohtoriohjelma
Maaliskuu 2026

TIIVISTELMÄ

Tässä poikkitieteellisessä väitöskirjassa kehitettiin ultrakorkean erotuskyvyn nestekromatografiaan ja tandemmassaspektrometriaan (UHPLC–MS/MS) perustuvaa metabolomiikkamenetelmää seerumi- ja aivo-selkäydinnestenäytteille (likvori). Menetelmä yhdistettiin koneoppimiseen Lymen neuroborrelioosiin (LNB) liittyvien aineenvaihduntaprofiilien sekä potentiaalisten merkkiaineiden tunnistamiseksi. Tutkimusasetelma perustui pääosin samoilta potilailta ennen hoitoa ja hoidon jälkeen kerättyihin näytteisiin, mikä paransi analyysien luotettavuutta taudin aiheuttamien aineenvaihdunnallisten muutosten tunnistamiseksi.

Seerumien profiloinnissa ennen antibioottihoitoa otettuja näytteitä verrattiin näytteisiin, jotka kerättiin 12 kuukautta hoidon päättymisen jälkeen. Likvorien profiloinnissa vastaava vertailu tehtiin ennen hoitoa ja kolme viikkoa hoidon aloituksen jälkeen otettujen näytteiden välillä. Lisäksi LNB-potilaiden seerumi- ja likvoriprofiileja verrattiin *Borrelia*-vasta-ainenegatiivisten kontrollipotilaiden näytteisiin. Likvoridatan osalta tehtiin myös vertailuja muihin tunnettuihin keskushermostoinfektioihin, mikä mahdollisti havaittujen muutosten tautispesifisyyden arvioinnin.

Tulokset osoittivat, että eri näytematriiseissa havaitut aineenvaihduntatuotteiden muutokset kohdistuivat erityisesti tryptofaani-aineenvaihduntaan, lipidivälitteisen signaloinnin muutoksiin, sekä muuhun aminohappoaineenvaihduntaan. Useat likvorissa tunnistetut merkkiaineet korreloivat kemokiini CXCL13 -pitoisuuden kanssa, mikä tukee niiden välistä yhteyttä neuroinflammaatioon.

Koneoppimiseen perustuvat binääriluokittelijat saavuttivat eri vertailuasemissa hyvän erottelukyvyn korkealla spesifisyydellä. Lisäksi eri luokittimien välillä toistuvasti havaitut aineenvaihduntatuotteet viittaavat ensisijaisesti infektion aiheuttamiin aineenvaihdunnallisiin muutoksiin.

Yhteenvetona voidaan todeta, että UHPLC–MS/MS-menetelmään perustuvat biomarkkeripaneelit yhdistettynä koneoppimiseen näyttäytyvät lupaavina ja käytännöllisinä työkaluina, jotka voivat täydentää nykyisiä diagnostisia menetelmiä sekä tukea LNB:n hoidon seurantaa.

ASIASANAT: aivo-selkäydinneste; *Borrelia burgdorferi*; koneoppiminen; Lymen neuroborrelioosi; metabolomiikka; UHPLC–MS/MS; seerumi

Table of Contents

Abbreviations

ACA	Acrodermatitis chronica atrophicans
AGC	Automated gain control
APAP	Acetaminophen (paracetamol)
APCI	Atmospheric pressure chemical ionization
APPI	Atmospheric pressure photoionization
AUC	Area under curve
CerP	Phosphoceramide
CNS	Central nervous system
cPA	Cyclic phosphatidic acid
CSF	Cerebrospinal fluid
CXCL13	C-X-C motif chemokine ligand 13
DDA	Data-dependent acquisition
dd-MS^2	Data-dependent-MS/MS
DIA	Data-independent acquisition
EFNS	European Federation of Neurological Societies
EIA	Enzyme immunoassay
EM	Erythema migrans
ESI	Electrospray ionization
GC–MS	Gas chromatography–mass spectrometry
HESI	Heated electrospray ionization
HILIC	Hydrophilic interaction liquid chromatography
HMDB	Human Metabolome Database
HSV	Herpes simplex virus
IS	Internal standard
IT	Injection time
KEGG	Kyoto Encyclopedia of Genes and Genomes
LASSO	Least absolute shrinkage and selection operator
LB	Lyme borreliosis
LC–MS	Liquid chromatography–mass spectrometry
LNB	Lyme neuroborreliosis
LysoPC	Lysophosphatidylcholine
LysoPE	Lysophosphatidylethanolamine

LysoPL	Lysophospholipid
MALDI	Matrix-assisted laser desorption/ionization
m/*z*	Mass-to-charge ratio
MF	Molecular feature
ML	Machine learning
MS	Mass spectrometry
MS/MS	Tandem mass spectrometry
MSE	Metabolite set enrichment
MSI	Metabolomics Standards Initiative
MSX	Multiplexed PRM
NAAG	*N*-acetylaspartylglutamate
NMDA	*N*-methyl-D-aspartate
NMR	Nuclear magnetic resonance
non-LNB	*Borrelia* antibody-negative
PCA	Principal component analysis
PDA	Photodiode array
PRM	Parallel reaction monitoring
PTFE	Polytetrafluoroethylene
PTLDS	Post-treatment Lyme disease syndrome
RaMP-DB	Relational Database of Metabolomic Pathways
RCF	Relative centrifugal force
ROC	Receiver operating characteristic
RT	Retention time
SD	Standard deviation
SM	Sphingomyelin
TBE	Tick-borne encephalitis
UHPLC	Ultrahigh-performance liquid chromatography
VZV	Varicella zoster virus

An artificial intelligence-based large language model (Microsoft 365 Copilot, version bizchat.20260129.44.2, Microsoft Corporation, Redmond, WA, USA) with enterprise data protection was used to improve grammar, spelling, readability, and consistency. The tool was not used for generating original content or drawing conclusions. All substantive intellectual work is the author's own, and all changes were verified by the author.

List of Original Publications

This dissertation is based on the following original publications, which are referred to in the text by their Roman numerals I-III:

I Kuukkanen, I., Pietikäinen, A., Rissanen, T., Hurme, S., Kortela, E., Kanerva, M., Oksi, J., Hytönen, J., Karonen, M. UHPLC–MS/MS-based untargeted metabolite profiling of Lyme neuroborreliosis. *Scientific Reports*, **2025**, *15*, 8442. https://doi.org/10.1038/s41598-025-92189-0

II Kuukkanen, I., Geraldson, M., Klisura, Đ., Kortela, E., Pietikäinen, A., Lahti, L., Hytönen, J., Karonen, M. A mass spectrometry-based machine learning approach for biomarkers prediction of Lyme neuroborreliosis. *ACS Omega*, **2026**, *11*, 17521-17529. https://doi.org/10.1021/acsomega.5c10792

III Kuukkanen, I., Pietikäinen, A., Rissanen, T., Hurme, S., Kortela, E., Hytönen, J., Karonen, M. Metabolomic insights into Lyme neuroborreliosis: exploring cerebrospinal fluid for diagnostic clues. *Ticks and Tick-borne Diseases,* **2026**, *17*, 102645. https://doi.org/10.1016/j.ttbdis.2026.102645

1 Introduction

Lyme borreliosis (LB) is the most common tick-borne infectious disease in the Northern Hemisphere[1] and is caused by spirochetes of the *Borrelia burgdorferi* sensu lato complex (hereafter referred to as *Borrelia*). In natural ecosystems, vertebrates such as small mammals (e.g., mice and voles) and certain bird species serve as primary reservoir hosts for *Borrelia*[2–5], thereby enabling transmission of the bacteria to ticks of the genus *Ixodes*, the principal vectors responsible for human infections.[1,6]

Ticks rely on different hosts during their life cycle (Figure 1).[5] Progression between developmental stages of ticks (larva, nymph, and adult) depends on the successful completion of a blood meal. During a blood meal, infected ticks can transmit *Borrelia* from their midgut to the host through their saliva. Adult females also require a blood meal to produce eggs. It is generally accepted that *Borrelia* spirochetes are not transmitted transovarially and, as a result, eggs and newly hatched larvae remain uninfected.[7] However, recent studies suggest that *Borrelia* infection may also occur in larvae[8], although this is not yet well established.

The generalist feeding habits of *Ixodes* spp. ticks increase the risk of human infection.[9] Humans are considered dead-end hosts for *Borrelia*[5], but feeding by an infected tick can still lead to LB. In contrast, large mammals such as deer are incompetent reservoir hosts for *Borrelia*.[10] However, they play an important ecological role in sustaining tick populations, as adult ticks feed and mate on them.[11]

Because *Borrelia* transmission generally requires several hours to days of tick attachment[12], the risk of transmission increases with longer attachment duration and with multiple simultaneous tick attachments.[13] Previous episodes of LB do not provide protective immunity, making a new infection possible after subsequent exposure to an infected tick. If LB remains untreated during the early localized stage, *Borrelia* spirochetes may disseminate from the initial tick feeding site to surrounding tissues and organs[14], potentially leading to early disseminated LB manifestations.[15]

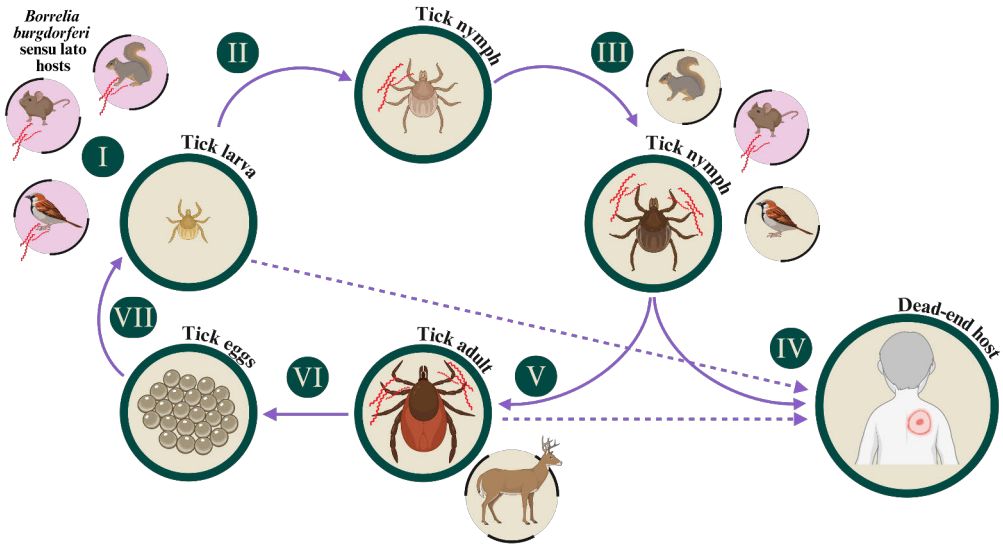

Figure 1. Life cycle of *Ixodes* spp. ticks and their role as vectors of *Borrelia burgdorferi* sensu lato: (**I**) Larval tick feeds on its first host; (**II**) after engorgement, the larva moults into the nymphal stage; (**III**) the nymph feeds on a second host; (**IV**) humans and other incidental hosts may serve as dead-end hosts; (**V**) following repletion, the nymph moults into the adult stage, which feeds on a third host; (**VI**) the engorged female lays eggs; (VII) eggs hatch into spirochete-free larvae. Adapted from Radolf et al., 2012.[5]

Diagnosis of early localized LB is clinical and based on the characteristic manifestation of erythema migrans (EM), the expanding skin lesion around the tick feeding site.[16] The production of *Borrelia*-specific antibodies takes several weeks, which complicates diagnosis in cases that lack detectable hallmark features such as EM and that present with nonspecific or heterogeneous symptoms.[17,18] This delay limits the utility of serology-based antibody assays, the current cornerstone of LB diagnostics, during early infection. Nevertheless, these assays are highly effective for detecting disseminated manifestations of LB.[19,20] However, *Borrelia*-specific antibodies can remain elevated for months after successful antibiotic treatment, reflecting persistent seropositivity among the patients.[21–23] This persistence may lead to false-positive diagnostic results and unnecessary antibiotic treatments in patients with prior LB episodes but no active disease.

LB progression includes early and late disseminated disease stages, as well as a condition known as post-treatment Lyme disease syndrome (PTLDS), which remains poorly understood. These stages, presented in Figure 2, are characterized by systemic spread of the pathogen to multiple organs.

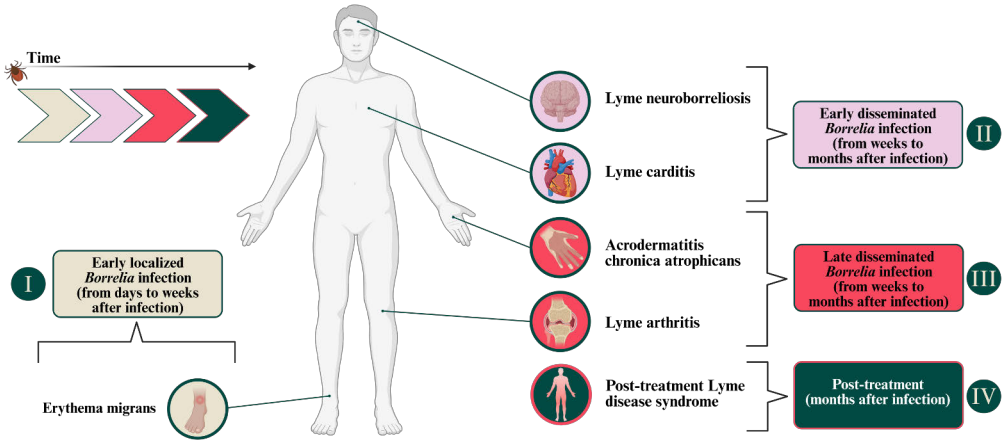

Figure 2. Examples of clinical manifestations of Lyme borreliosis (LB), categorized into following disease stages: (**I**) early localized disease, typically characterized by erythema migrans; (**II**) early disseminated disease, which may manifest as Lyme carditis or Lyme neuroborreliosis; (**III**) late disseminated disease, including conditions such as acrodermatitis chronica atrophicans and Lyme arthritis; and (**IV**) post-treatment persistent symptoms, often referred to as post-treatment Lyme disease syndrome.

In early disseminated LB, *Borrelia* may invade critical organs such as the heart (Lyme carditis) and the nervous system (Lyme neuroborreliosis, LNB), while late disseminated infection is typically associated with involvement of joints (Lyme arthritis) and chronic dermatological manifestations (acrodermatitis chronica atrophicans, ACA) that occur months after the initial tick bite. Disseminated LB reflects not only a more advanced pathological state but also increased diagnostic complexity. LNB is one of the most clinically significant complications of early disseminated LB, in which *Borrelia* starts to affect and harm the peripheral nervous system and, in some cases, the central nervous system (CNS). This typically occurs within weeks of initial exposure.[15,24] Neurological involvement in LB is observed in approximately 10-15% of adult patients in North America and Europe[24–26], while among European pediatric populations the incidence is reported to be even higher[27–29]. In Europe, LNB is most frequently associated with *Borrelia garinii*, although *Borrelia afzelii* and *Borrelia burgdorferi* sensu stricto are also reported.[30–32]

Diagnosis of definite LNB in Europe requires a combination of clinical symptoms and laboratory findings, including the detection of intrathecally produced *Borrelia*-specific antibodies, cerebrospinal fluid (CSF) pleocytosis, and neurological symptoms.[19,20,33] Obtaining a CSF sample always necessitates an invasive and painful lumbar puncture. These challenges with LNB diagnostics underscore the urgent need for more robust, sensitive, and reliable methodologies for the detection and confirmation of both early and disseminated manifestations.

Advances in LB biomarker research have introduced a chemokine CXCL13 (C-X-C motif chemokine ligand 13) as a diagnostic biomarker for acute LNB.[34–36] CXCL13 is an immune system signaling molecule that guides B cell migration.[37,38] Studies have shown that CSF CXCL13 concentrations rise more rapidly than *Borrelia*-specific antibody levels during the early phase of LNB.[39] CXCL13 levels also decline rapidly following successful antibiotic treatment.[40] This makes CXCL13 a valuable early CSF biomarker for LNB, especially in cases where traditional serological tests may be inconclusive. However, CXCL13 is not an LNB-specific marker, and it should not be used as a stand-alone test for acute LNB. Elevated CSF CXCL13 levels can also occur in other neuroinflammatory conditions, such as viral tick-borne encephalitis (TBE), herpetic CNS infections and neurosyphilis.[41] Therefore, CXCL13's diagnostic value is optimized when interpreted together with clinical symptoms, CSF pleocytosis, and evidence of *Borrelia*-specific intrathecal antibody production.[34]

Interest in metabolomics, i.e., the comprehensive study of small molecules in biological systems, is a broadly used field within omics research in clinical settings. Metabolomics is used to interpret how genetics, environment, and disease influence metabolism and is a major discipline within the omics sciences alongside genomics, transcriptomics, and proteomics.

Metabolites are small molecules, generally with a molecular mass <1,500 Da. They function as intermediates or end products of numerous metabolic pathways and play crucial roles in sustaining cellular processes, supporting growth, and maintaining physiological functions.[42] Thus, the metabolome can provide a dynamic and sensitive picture of both physiological and pathological states.[43–45] This sensitivity, however, increases its vulnerability to external variables such as environmental factors, diet, and preanalytical sample handling.[46] An overview of the major omic levels and their example associations with physiological and environmental factors is shown in Figure 3.

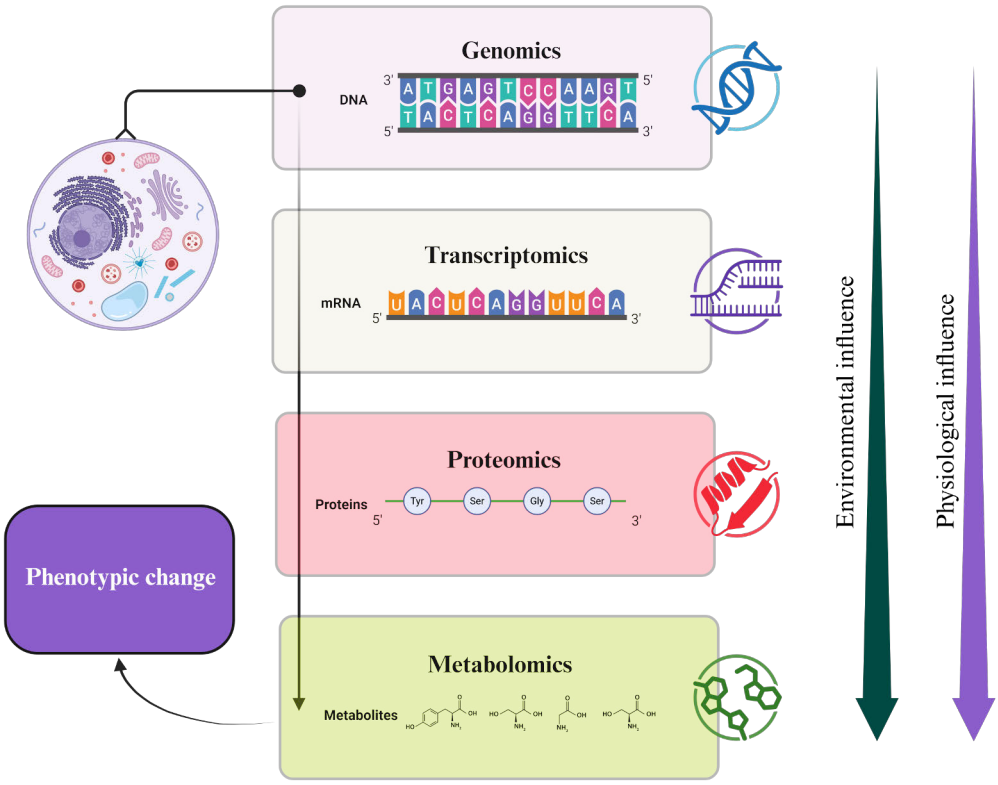

Figure 3. Overview of the main omics levels (genomics, transcriptomics, proteomics, and metabolomics) within biological systems. Each of the omics level reflects a different layer of biological regulation. Metabolomics provides the most immediate and dynamic snapshot of an organism's physiological state. While this responsiveness enhances its potential for detecting subtle biological changes, this also complicates its use in clinical diagnostics, where controlling for confounding variables is required to ensure reproducibility and interpretability.

The human metabolome contains immense chemical diversity. Metabolites can be broadly classified into primary metabolites and specialized metabolites (formerly referred to as secondary metabolites). Primary metabolites are directly involved in normal growth, development, and reproduction. These include compounds such as carbohydrates, proteins, nucleic acids, and lipids that form the basis for everyday life and serve as energy sources. In contrast, specialized metabolites are not essential for everyday functions but play critical roles, for example, in ecological interactions, defense mechanisms, and signaling. Examples of these include alkaloids, polyphenols, and steroids. Despite their different roles, both primary and specialized metabolites contribute to the overall chemical processes in biological systems.

Even with immense complexity, metabolomics enables the systematic investigation of chemical signatures produced in cellular processes, including host-

pathogen interactions.[47] Unlike single-molecule diagnostics, metabolomics captures a near-real-time "snapshot" of the chemical space of an organism.[48] The metabolome, however, is chemically highly diverse, spanning polar and nonpolar compounds, volatile and nonvolatile metabolites, and molecules with widely differing concentrations and physicochemical properties. As a result, no single analytical platform can comprehensively cover the entire metabolome, and many metabolomics laboratories therefore analyze the same sample using multiple complementary techniques. Metabolomic techniques, such as mass spectrometry (MS) and nuclear magnetic resonance (NMR) spectroscopy, are commonly used to measure these metabolites with high sensitivity, selectivity, and reproducibility.[49,50]

Among MS-based approaches, liquid chromatography–mass spectrometry (LC–MS) is particularly suitable for a broad range of chemically diverse, nonvolatile metabolites[51], whereas gas chromatography–mass spectrometry (GC–MS) is especially valuable for volatile compounds and for small primary metabolites after derivatization[52,53]. In LC–MS, metabolome coverage is also strongly influenced by the chromatographic separation.[51,54] Reversed-phase LC is typically more suitable for less polar and more hydrophobic metabolites, whereas hydrophilic interaction liquid chromatography (HILIC) provides improved retention of highly polar compounds.[55,56] Accordingly, the selected column chemistry further constrains which metabolite classes are efficiently retained, separated, and ultimately detected in a given workflow.[54,55] In addition to chromatographic separation, metabolome coverage in LC–MS is also influenced by the ionization technique.[57,58] Electrospray ionization (ESI) is the most commonly applied ionization method in LC–MS metabolomics, whereas atmospheric pressure chemical ionization (APCI) and atmospheric pressure photoionization (APPI) may be more suitable for selected less polar analytes or in situations where ESI is less effective.[57–59] Matrix-assisted laser desorption/ionization (MALDI) is also widely used in metabolomics, although more commonly in direct-analysis and MS imaging applications than in conventional LC-coupled metabolomic profiling.[60,61]

The limited coverage of any single metabolomics platform is particularly relevant in complex infectious diseases such as LB, where clinically meaningful metabolic alterations may occur across several metabolite classes and therefore may not be detected by conventional serological or molecular tests.[62–67] Preliminary studies have demonstrated the utility of metabolomics in distinguishing different stages of LB [68–73], though comprehensive metabolomic profiling of disseminated LNB remains limited.[69,74] At the same time, the analytical window achieved in any individual study is shaped not only by the instrumental platform but also by sample preparation.[51,75] In metabolomics, commonly used pretreatment strategies include macromolecule precipitation, liquid–liquid extraction, solid-phase extraction, filtration-based cleanup, and, in the case of GC–MS, chemical derivatization to improve volatility and thermal stability.[52,76–78] Because each preparation method enriches certain compound

classes while underrepresenting others, the selected pretreatment workflow should always be interpreted as a compromise between metabolome coverage, reproducibility, throughput, and compatibility with the analytical platform.[75–77] In the present work, the chosen sample preparation and liquid chromatography–electrospray ionization–tandem mass spectrometry (LC–ESI–MS/MS) workflow were designed to provide robust and reproducible coverage of a broad subset of serum and CSF metabolites under clinically realistic conditions.

Selecting relevant sample matrices is critical in metabolomic research, as it directly determines the interpretability and significance of the findings. Biofluids, such as blood and CSF, provide snapshots of systemic and nervous system-related metabolic profiles, respectively. Blood is composed of a cellular component (i.e., red and white blood cells, platelets) and a liquid plasma fraction. Plasma is obtained by centrifuging anticoagulated blood and removing the cellular fraction. However, when blood is allowed to clot before centrifugation, the supernatant is known as serum. Serum lacks clotting factors (e.g. fibrinogen and prothrombin) that are present in plasma.[79] However, clotting activates platelets and enzyme cascades, making the serum metabolome more affected by platelet-derived metabolites to some extent.[80] Nevertheless, serum provides a view of systemic metabolism and is relatively easy to collect, making it suitable for large-scale clinical studies and biomarker discovery.[81] Serum is mainly an aqueous solution (~95% water) that contains various macromolecules such as proteins and peptides (e.g. albumin, globulins, lipoproteins, enzymes, hormones), nutrients (e.g. carbohydrates, lipids, amino acids), electrolytes, by-products, and small organic molecules.[81,82] For metabolomic studies, precipitation of large macromolecules from the sample matrix is required prior to analysis.

In contrast, CSF is a clear fluid that surrounds and protects the brain and spinal cord. It maintains CNS homeostasis, helps to clear metabolic waste, and serves as interface with peripheral circulation.[83] CSF consists of ~99% water and carries various metabolites, including glucose, lactate, amino acids, neurotransmitter precursors, and lipids.[83,84] Because CSF reflects the metabolomic state of the CNS, it is a highly informative sample matrix for neurological disorders such as LNB, multiple sclerosis, and Alzheimer's disease.[24,85–88] However, CSF collection is invasive and requires strict sampling protocols, most importantly with regard to patient safety, but also to avoid contamination of the samples.

Both serum and CSF are highly complex sample matrices with wide dynamic concentration ranges. This complicates comprehensive metabolite coverage and requires robust extraction protocols and analytical strategies.[75,83] As with serum samples, precipitation of large macromolecules in CSF is required prior to analysis. Standardization of pre-analytical steps is critical to minimize variability arising from environmental factors.[75] Ultimately, the selection and handling of biological matrices are the cornerstones of metabolomics, influencing data quality, biomarker validity, and clinical translation.[89,90]

Metabolomics is typically divided into untargeted and targeted strategies. Untargeted metabolomics aims to detect as many metabolites as possible without prior selection of target analytes, providing a global view of chemical space (global metabolomics).[91,92] This discovery-driven approach is used to identify novel biomarkers and pathways linked to the phenomena of interest.[93] For example, untargeted profiling of CSF can reveal metabolic signatures linked to neuroinflammation and immune activation. After the candidate biomarkers are identified, the untargeted workflow typically moves to targeted metabolomics for verification and validation. Targeted methods focus on a defined set of metabolites, with precise quantification, optimized sensitivity, and reproducibility.[92,94] In practice, targeted metabolomic approaches often employ optimized MS methods to ensure robustness and scalability for routine clinical use.[95]

Metabolomic "fingerprint" profiling typically begins with the detection of metabolites using high-resolution MS. Analytes are ionized, and the resulting ions are separated based on their mass-to-charge ratio (m/z). This allows differentiation among compounds with similar chemical structures and is critical for identification and quantification.[96] The detected peak intensity or peak area in the generated chromatogram reflects the relative or absolute abundance of a specific compound. Prior to data analysis, peak areas are typically integrated, aligned, and normalized. The next step in the metabolomic workflow is structural characterization, in which MS/MS fragmentation patterns, exact masses, and predicted molecular formulae are evaluated to assign compound identities and confidence levels. Examples of serum and CSF total ion chromatograms are presented in Figure 4.

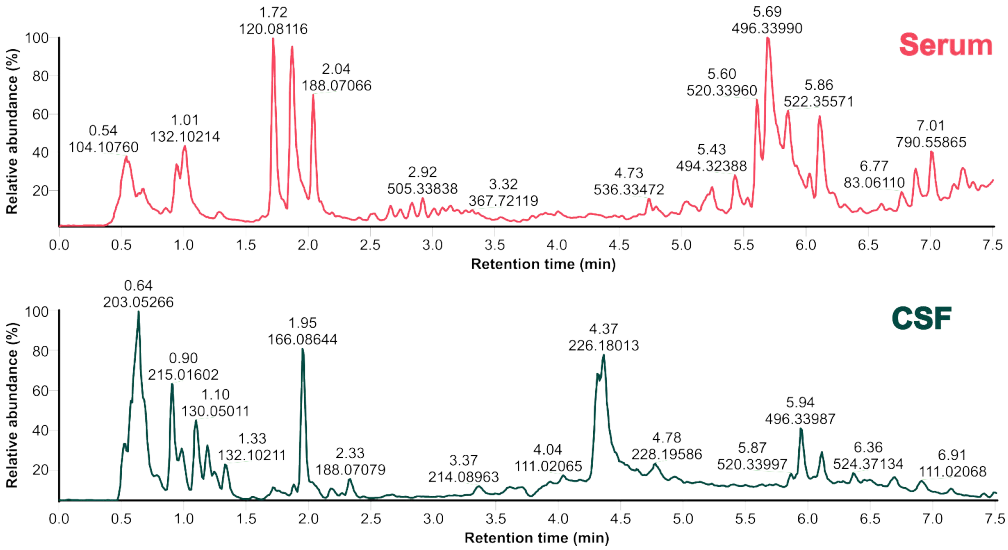

Figure 4. Examples of total ion chromatograms of paired serum and cerebrospinal fluid (CSF) samples from a same individual with acute Lyme neuroborreliosis.

Two main acquisition strategies are used to acquire MS/MS data: data-dependent acquisition (DDA) and data-independent acquisition (DIA). In DDA, the most intense precursor ions are selected and fragmented to generate high-quality MS/MS spectra. DDA approach is highly effective for structural elucidation and building spectral libraries because it produces characteristic fragmentation patterns and simplifies interpretation.[97] DDA is particularly useful for generating comprehensive reference MS/MS spectra and supporting compound annotation workflows. However, its selectivity towards the most abundant ions can create biased results, potentially missing relevant low-abundance metabolites. In contrast, DIA fragments all ions within predefined isolation windows, producing multiplexed MS/MS spectra and capturing a broader range of molecular features (MFs). Although DIA requires advanced computational deconvolution, it offers improved reproducibility and coverage, making it increasingly attractive for untargeted metabolomics studies.[98] Recent advances, for example in ultrahigh-resolution MS, ion mobility, and DIA, have significantly enhanced metabolite coverage and quantitative accuracy, supporting both targeted and untargeted workflows.[99–103] These improvements are notable for clinical metabolomics, where subtle biochemical changes can help disease characterization and treatment monitoring.[104]

Untargeted metabolomic analyses create large datasets of high-dimensional LC–MS data that must be preprocessed *in silico* prior to statistical analysis. Standard metabolomic workflows typically include raw data conversion, chromatographic peak detection and deconvolution, LC–MS feature reconstruction, RT alignment, feature grouping across samples, gap filling, background/blank filtering, normalization, and

stabilization of variance via transformation (e.g., log transformation), batch effect correction, and preliminary feature identification (MS library matching for exact masses and fragmentation patterns), and pathway analysis.[105–107]

Metabolomic data is inherently complex, and untargeted LC–MS analyses can include tens of thousands of features. At the same time, sample sizes are often limited (e.g. by sample availability and eligibility), creating a setting where the number of features exceeds the number of observations ($p \gg n$), increasing the risk of statistical overfitting.[108] In biomarker-focused metabolomic studies, both univariate and multivariate statistical approaches are commonly used.[89] In clinical contexts, disease-related MFs are also subtle, especially in between-individual variability comparisons.[109,110] Consequently, unsupervised methods such as principal component analysis (PCA) may fail to separate patient and control groups because dominant variance reflects demographic factors, medication, or lifestyle rather than the studied disease state itself.[89,110,111] While LC–MS data processing typically involves variable fragmentation behavior and platform-specific strategies, data processing in GC–MS with electron ionization (EI) is partly different because EI produces more standardized fragmentation patterns and retention index information, which are often used for spectral matching, deconvolution, and metabolite identification. Thus, although the general statistical challenges associated with high-dimensional metabolomics are shared across platforms, the detailed preprocessing and annotation workflows remain method-dependent.

Statistical analysis of high-dimensional metabolomic data requires strategies that take into account relevant covariates, along with MF normalization and batch effect correction.[112–114] Approaches such as stratified analyses can reveal data patterns that are specific to particular subgroups, with the use of additional matched controls improving comparability within heterogeneous samples.[115] The use of linear mixed models is typically suited for handling within individual correlations (e.g. time point measurements), and multivariable regression adjustment for known confounders in the data (e.g. age, sex, and use of medication).[116] In addition, properly implemented cross-validation is crucial for limiting overfitting and obtaining reliable effect estimations.[108] Combined, these statistical analyses enhance analytical performance, limit bias, and strengthen the robustness of conclusions.[117] Nonetheless, external validation of selected biomarker candidates remains essential to establish their statistical reliability and clinical relevance.[118]

Among the most promising tools for interpreting highly complex metabolomic data are machine learning (ML) models.[119–126] ML is a branch of artificial intelligence that focuses on algorithms capable of learning patterns from training datasets. The performance of ML models typically improves as the amount of available training data increases. ML models can identify relationships between features and outcomes to make accurate predictions and classifications.[119,126]

ML strategies can be divided into supervised and unsupervised learning approaches. Supervised ML uses "labeled" data to train models for prediction or classification tasks, such as distinguishing disease stages based on LC–MS metabolite profiles.[127–129] Commonly used algorithms include Random Forest[130], support vector machines[131], and neural networks[132]. Unsupervised ML models identify hidden structures in unknown data, such as clustering patients by metabolic similarity or detecting novel biomarker fingerprints.[119,133]

Feature selection is a crucial step in metabolomic-based ML workflows, as it helps to reduce dimensionality and improve model interpretability.[134] Algorithms such as the regression method LASSO (least absolute shrinkage and selection operator) or recursive feature elimination, can help identify the most informative features.[135] In conclusion, ML models can classify samples, predict treatment response, or integrate metabolomics with other omics for a better understanding of systems-level insights.[136–140]

This doctoral dissertation represents a step toward the development of a fast and sensitive MS-based metabolomics approach designed to serve as a complementary tool for the diagnosis of LNB. The aims of the doctoral dissertation were:

1. To establish an analytical workflow for comprehensive metabolomic profiling of potential serum biomarkers related to LNB (**Article I**).
2. To utilize serum MS data to create a ML model with three classifiers to separate, acute pretreatment LNB, post-treatment LNB, and age- and sex-matched *Borrelia* antibody-negative (non-LNB) controls (**Article II**).
3. To investigate and identify nervous system-specific metabolic alterations associated with LNB by performing comprehensive metabolomic profiling of CSF samples related to LNB and other CNS infections compared with non-LNB controls (**Article III**).

Article I utilized clinically well-characterized serum samples from a previous LNB study[141] to develop a robust metabolomics workflow based on ultrahigh-performance liquid chromatography (UHPLC) coupled with MS/MS. Metabolomic profiles were compared between the acute pretreatment phase of LNB and 12 months after antibiotic treatment, both within-patients and across LNB individuals. The MS dataset was processed *in silico* prior to statistical analysis, and the most prominent MFs altered in LNB were characterized to create serum biomarker panels. MS data generated served as the foundation for developing ML-based predictive models for disease classification (**Article II**). Finally, the methodology was extended to CSF samples (**Article III**).

Article II focused on the development of ML models based on three patient cohorts: serum samples from the pretreatment LNB state, post-treatment LNB samples (from the same individual as the pretreatment sample), and non-LNB control samples. Paired samples from the same individuals enabled within-patient analyses, improving sensitivity to treatment-related metabolic changes. The non-LNB control group was age- and sex-matched to the LNB patients, while the treated LNB cohort served as a reference for recovery. Serum samples underwent *in silico* metabolomic analysis and dimensionality reduction prior to ML model development. Three supervised ML classifiers were trained with two-thirds of the serum profiles, while one-third was used to evaluate model performance.

Article III analyzed clinically well-characterized CSF samples from the same LNB individuals[141], applying the metabolomic workflow from **Article I** and modifying it to accommodate the smaller CSF volumes available. The CSF patient cohort included individuals with acute definite LNB as well as a subgroup sampled three weeks after the initiation of antibiotic treatment. Non-LNB samples were age- and sex-matched to the LNB patients. Cases of other laboratory-confirmed CNS infections, including TBE, Herpes simplex virus (HSV), and Varicella zoster virus (VZV), were included to investigate biomarkers associated with CNS infections more broadly. Furthermore, metabolomic differences between acute LNB patients with and without radiculitis were investigated. MS data was processed *in silico* prior to statistical analysis, and the most prominent MFs were characterized to create CSF biomarker panels for LNB.

2 Materials and Methods

2.1 Patient samples

2.1.1 Serum

LNB serum samples used in **Articles I** and **II** were collected during routine serological diagnostics and originate from a previous study comparing treatment outcomes of oral doxycycline and intravenous ceftriaxone in patients with LNB.[141] For the ML model in **Article II**, age- and sex-matched non-LNB serum samples were collected during routine serological diagnostics from individuals suspected of LNB, but showed no detectable intrathecal *Borrelia*-specific antibody production. These individuals were also seronegative for *Borrelia* by an in-house enzyme immunoassay (EIA).[142] All serum samples were stored at –20 °C, the standard temperature for routine diagnostic samples, and no freezers with automated defrost cycles were used.

For **Article I**, serum samples (n = 149) from 81 patients were selected for UHPLC–MS/MS analysis. All patients had definite acute LNB, with the diagnosis confirmed according to the European Federation of Neurological Societies (EFNS) guidelines and criteria.[33] Of the 81 patients, 68 had both pretreatment and post-treatment samples available, with the post-treatment samples serving as controls for their corresponding pretreatment samples. The median age of the patients was 60 years (range: 17–88 years), including 28 females (35%) and 53 males (65%). Antibiotic treatment consisted of doxycycline in 40 patients and ceftriaxone in 41 patients.

For **Article II**, a subgroup of 34 patients with paired pre- and post-treatment serum samples (n = 64) from the **Article I** cohort was selected. In addition, 34 non-LNB samples were matched for comparison, and 28 unpaired non-LNB samples were included in the analysis.

2.1.2 Cerebrospinal fluid

CSF samples from patients with definite LNB in **Article III** were collected at the same time as the corresponding serum counterparts in the previously described

study.[141] A total of 63 pretreatment CSF samples were available. Of these, 19 (30%) were from female patients and 44 (70%) from male patients, with a median age of 58 years (range: 18–79 years). For two pretreatment LNB patients, matching non-LNB controls were not available. Radiculitis was observed in 40 patients, while 23 did not exhibit symptoms.

In a subgroup of 36 LNB patients, an additional CSF sample was collected three weeks after treatment initiation, as specified in the original study protocol, from those patients with ≥50 leukocytes/μL in the pretreatment CSF sample.[141] In this subgroup, 13 (36%) were female and 23 (64%) were male, with a median age of 59 years (range: 28–78 years). Oral doxycycline was administered to 22 patients, and intravenous ceftriaxone was administered to 14 patients.

Non-LNB control CSF samples (n = 61) were obtained during routine diagnostics and were age- and sex-matched to the LNB patient cohort. These samples were collected from individuals suspected of LB/LNB but lacking intrathecal *Borrelia*-specific antibody production and testing negative for *Borrelia* antibodies using an in-house whole-cell antigen preparation-based EIA. In addition, 21 CSF samples from patients with other confirmed CNS infections were also included: TBE (n = 9), HSV (n = 6), and VZV (n = 6). All CSF samples were stored at –20 °C and no freezers with automated defrost cycles were used.

2.1.3 Ethics approval and informed consent

Written informed consent had been obtained from all participants in the original study, during which the LNB patients' serum and CSF samples were collected.[141] Ethical approval had been granted by the National Committee on Medical Research Ethics in Finland, and institutional permission had been provided by the Wellbeing Services County of South-West Finland (T13_2019-1/381700, T012/004/19). Definite LNB diagnoses were confirmed according to the guidelines and criteria of the EFNS.[33] Serum *Borrelia* antibody-negative non-LNB control samples, together with CSF samples from other CNS infections, were identified retrospectively via the laboratory information management system of the Clinical Microbiology Laboratory of Turku University Hospital. The non-LNB samples had been collected with written informed consent from patients suspected of having LB/LNB as part of routine clinical practice. All serum and CSF samples were coded to ensure strict anonymity. The study followed the ethical principles of the Declaration of Helsinki for research involving human participants and biological data.

2.1.4 Sample preparation

Deuterated L-tryptophan-(indole-d_5) and DL-phenyl-d_5-alanine were used as internal standards (IS) during sample preparation and analysis in **Articles I-III**. L-tryptophan-(indole-d_5) was used to monitor possible analyte loss during sample preparation, while DL-phenyl-d_5-alanine was used to assess UHPLC–MS/MS performance and matrix effects in both serum and CSF analyses. Prior to method development, the identities of both ISs were confirmed by matching retention time (RT) and MS/MS fragmentation patterns, and accurate masses to those of the correct authentic standards. The ISs were detectable in both positive and negative ion modes and exhibited moderate UV absorbance. UV detection was primarily used to evaluate aqueous mixtures of pure compounds during method development. For the actual analysis of serum and CSF samples, standard correction factors were based on integrated MS peak areas, as UV detection was affected by interference from their naturally occurring counterparts in these matrices.

All samples were processed in random order, with matched samples from individual patients analyzed within the same batch. All steps were performed at consistent vortex speeds and centrifugal forces to preserve analytical comparability across matrices. Following slow thawing in ice, serum samples were vortexed at 750 rpm, and 150 µL of serum was transferred to a new microcentrifuge tube, to which 50 µL of a deuterated L-tryptophan-(indole-d_5) IS solution (7.125 µM, aq.) was added. The mixture was then vortexed for 15 min at 750 rpm. To precipitate macromolecules (e.g., proteins), 750 µL of cold methanol was added, and the suspension was vortexed for 30 min at 750 rpm. After precipitation, the samples were centrifuged for 20 min at a relative centrifugal force (RCF) of 21,913 *g*. The supernatant (700 µL) was transferred to a new microcentrifuge tube and dried under vacuum. Dried residues were dissolved in 150 µL of a deuterated DL-phenyl-d_5-alanine IS solution (10 µM, aq.), vortexed for 15 min at 750 rpm, and spin-filtered through 0.2 µm polytetrafluoroethylene (PTFE) microcentrifugal filters for 20 min at an RCF of 9,056 *g*. Following filtration, the samples were pipetted into 700 µL 96-well plates for UHPLC–QOrbitrap–MS/MS analysis. Aqueous control blanks, prepared identically to the serum samples, were included to monitor sample preparation performance and assess matrix effects throughout the analysis.

CSF samples were processed using the same workflow as serum, with proportional scaling to accommodate the lower available sample volumes (50 µL). Reagent and reconstitution volumes were proportionally adjusted to maintain established solvent-to-matrix and IS-to-analyte ratios, e.g., IS added at 1:3 (*v*:*v*) relative to the sample volume and methanol at 5:1 (*v*:*v*). All subsequent processing steps, including mixing, macromolecule precipitation, centrifugation, drying, filtration, and analysis conditions, were maintained identical to ensure methodological consistency.

2.2 UHPLC–MS/MS analysis

All samples for **Articles I-III** were analyzed using an Acquity UPLC® unit (for **Article I-II**) or an Acquity Premier UPLC® unit (for **Article III**) equipped with a photodiode array (PDA) detector (Waters Corporation, Milford, MA, USA), coupled to a Q Exactive™ hybrid quadrupole-Orbitrap™ MS (Thermo Fisher Scientific GmbH, Bremen, Germany) via a heated electrospray ionization (HESI) source.

Chromatographic separation was achieved on an Acquity UPLC® BEH Phenyl column (1.7 µm, 2.1 × 100 mm; Waters Corporation, Wexford, Ireland). Elution was carried out using acetonitrile (A) and 0.1% aqueous formic acid (B) at a flow rate of 0.5 mL × min^{-1}. The gradient program was as follows: 0.0–0.5 min, 0.1% A; 0.5–7.5 min, 90% A; 7.5–8.5 min, 90% A; 8.5–8.6 min, 0.1% A; and 8.6–10.1 min, 0.1% A. The injection volume was 5 µL with a full-loop overfill factor of three. UV data (190–500 nm) was collected throughout the run, while MS data was acquired between 0.0–7.5 min. During column wash and stabilization, the UHPLC flow was diverted to waste. The autosampler kept the sample temperature stable at 4 °C. The column temperature was maintained at 40 °C.

MS analysis was performed in positive ion mode over a mass range of *m*/*z* 70–1,050. Full scans were acquired at a resolution of 70,000, with an Automatic Gain Control™ (AGC) target of 3×10^6 and a maximum injection time (IT) of 200 ms. Data-dependent MS/MS (dd-MS^2) scans were recorded at a resolution of 17,500, with an AGC target of 1×10^5 and a maximum IT of 50 ms. The dd-MS^2 method employed a Top N technique, selecting the five most intense ions per cycle for fragmentation (MSX count = 1; loop count = 5). A lock mass of *m*/*z* 214.08963 was applied to improve mass accuracy.

HESI source parameters were as follows: capillary temperature 380 °C, spray voltage 3,800 V, sheath gas (N_2) flow rate 60 (arbitrary units), auxiliary gas flow rate 20 (arbitrary units), S-lens RF level 60, and probe heater temperature 300 °C. IS solutions of DL-phenyl-d_5-alanine and L-tryptophan-(indole-d_5) were injected in duplicate every 10 samples. Prior to analysis, sample order was randomized, and the instrument was calibrated using Thermo Scientific™ Pierce™ LTQ Velos ESI positive ion calibration solution.

2.3 *In silico* metabolomic analysis

For **Articles I-III,** UHPLC–MS/MS data in RAW format was processed with Compound Discoverer 3 (Thermo Fisher Scientific Inc., Waltham, MA, USA; version 3.1.0.305). The *in silico* workflow *"Untargeted Metabolomics with Statistics Detect Unknowns with ID using Online Databases and mzLogic"* was employed for all data analysis. The workflow integrated peak detection, RT alignment across samples, automated preliminary compound annotation, and the mzLogic scoring

algorithm. The resulting feature tables contained metabolite-specific information for each detected MF, including accurate mass (*m*/*z*), RTs, MS/MS fragmentation spectra (where available), and integrated MF peak areas. The MS peak quantification results were exported to CSV format for statistical analysis in **Articles I** and **III** and for ML model development in **Article II**.

2.4 Statistical analysis

In **Article I**, differences between the pretreatment LNB and post-treatment LNB samples were summarized with descriptive statistics, and due to the non-normality of the distributions, studied with the Wilcoxon signed-rank test. Statistically significant MFs ($p < 0.001$) in raw and standardized datasets were examined. The most prominent MFs were selected based on the MF filtering criteria. Changes in serum MF peak areas were required to be at least two-fold, with the alteration in median MF peak area $\geq 5 \times 10^5$ (counts × seconds) between the pretreatment and post-treatment group medians.

Linear mixed models were used to evaluate the effects of patients' characteristics. The applied statistical models included a within-factor (time point: pretreatment and post-treatment) and between-factors: sex, age, antibiotic treatment, hospital, estimated use of acetaminophen (APAP), and reported LNB symptom duration. To account for correlations among repeated measurements within-individuals, the compound symmetry covariance structure was used for the time-factor. Logarithmic transformation was used. Normality of variables was evaluated and tested with the Shapiro-Wilk test. Tests were performed as two-sided ($p < 0.05$). The analyses were carried out using RStudio (version 2023.03.0.386) based on R (version 4.3.0; RStudio, PBC, Boston, MA, USA).

For **Article III,** statistical analyses were carried out separately across relevant CSF comparisons: between pretreatment LNB samples and three weeks after treatment initiation samples (comparison **A**), between pretreatment LNB samples and matched non-LNB control samples (comparison **B**), between pretreatment LNB samples and other known CNS infection samples (comparison **C**), and subgroup analysis between pretreatment LNB patients with and without radiculitis (comparison **D**).

Comparisons **A** and **B** were carried out using the Wilcoxon signed rank test due to the paired observations. Statistical analysis of comparison **C** was based on independent samples and was evaluated using the Wilcoxon rank sum test. The MF differences in comparison **D** were studied with the same analysis methods as in comparison **C**. Due to the non-normality of the distributions, non-parametric methods were applied.

Statistically significant MFs ($p < 0.001$) in both raw and standardized datasets were examined. Multivariable models were used to evaluate the effects of patients' characteristics. Linear mixed models for repeated measurements, with compound symmetry covariance structure, were performed in comparisons **A** and **B**. Logarithmic transformations were used. In comparison **A**, models included a within-factor (time point: pretreatment and three weeks after treatment initiation) and between-factors (age, sex, CSF leukocyte count, use of APAP, and CSF CXCL13 concentration). In comparison **B**, models included a within-factor (matched pair: pretreatment sample and non-LNB controls) and between-factors (age, sex, and use of APAP). Linear regression models were used in comparisons **C** and **D**. These models included three independent variables (age, sex, and use of APAP). The normality of variables was evaluated visually and tested with the Shapiro-Wilk test. Tests were performed as two-sided ($p < 0.05$). The analyses were carried out using RStudio (version 2024.09.1 Build 394) based on R (version 4.4.3; RStudio, PBC, Boston, MA, USA).

2.5 Molecular feature identification

Preliminary identification of the detected MFs was conducted *in silico* by screening detected MFs against several online databases, including mzCloud™, ChemSpider[143], KEGG[144] (Kyoto Encyclopedia of Genes and Genomes), and HMDB[145] (Human Metabolome Database). These databases were used to generate automatic candidate identifications by comparing experimental fragmentation patterns against reference spectra, and by evaluating biological plausibility based on suitable metabolic pathways and metabolite classes.

Manual evaluations and characterizations were performed with Xcalibur™ software (version 4.1.31.9; Thermo Fisher Scientific GmbH, Bremen, Germany), integrating multiple criteria such as exact mass (accurate *m*/*z*), RT, isotopic patterns, adduct formation, charge state, neutral losses, and MS/MS fragmentation behavior to assign identification confidence levels. This classification followed the five-level system[146] proposed by Schymanski *et al.* (2014), which is aligned with the Metabolomics Standards Initiative (MSI) framework[118] by Sumner *et al.* (2007):

- **Level 1**: Confirmed structure (validated identification with an authentic reference standard)
- **Level 2**: Putative identification (MS/MS match to the literature)
- **Level 3**: Tentative structure (database or literature matches to a molecular formula)
- **Level 4**: Molecular formula only (including isotope distribution, charge state, and possible adduct formation)
- **Level 5**: Unique feature (no structural assignment)

2.6 Machine learning model

In **Article II**, the *in silico* processed MS feature table was imported into the TreeSummarizedExperiment structure in R/Bioconductor[147,148] for data management. The ML dataset comprised 130 serum samples: pretreatment LNB (n = 34), post-treatment LNB (n = 34), and non-LNB controls (n = 62). These samples were organized into 62 analytical data cases, including 34 complete matched triplets (pretreatment, post-treatment, and matched non-LNB control) and 28 individual non-LNB control cases. Two-thirds of the data cases (n = 41) were used for model training, and one-third (n = 21) were reserved for final testing of the model. MF peak areas underwent logarithmic transformation, and MFs directly associated with medication use were excluded from the dataset.

Supervised classification was performed using Random Forest algorithms implemented in the mikropml R package.[128] Pairwise classifiers were trained for group comparisons: **i**) pretreatment vs. post-treatment, **ii**) pretreatment vs. non-LNB control, **iii**) post-treatment vs. non-LNB control. Model development within the training partition used five-fold cross-validation (80% training fraction per fold).

Evaluation of the model performance was based on the independent test set to compare predicted and known group labels.[130] Receiver operating characteristic area under the curve (ROC/AUC) was calculated to assess the model's ability to discriminate between classes. Performance was also compared against a random baseline to see how much better the model performed than it would by chance.

Importantly, data was partitioned at the case-level rather than the sample-level to prevent information leakage across matched triplets and to provide a cautious estimate of how well the model would perform on new datasets, thus reducing the risk of overfitting. Random Forest were selected for their robustness to nonlinear relationships and minimal parametric assumptions, and feature importance was assessed using mean decrease in Gini to identify the most discriminative MFs.

2.7 Metabolite set enrichment analysis

In **Article III**, Metabolite set enrichment (MSE) analysis was conducted with MetaboAnalyst (version 6.0)[149]. Pathway connections and metabolite-lipid annotations were screened from the Relational Database of Metabolomic Pathways[150] (RaMP-DB) that integrated cross-references to KEGG[144] via HMDB[145], Reactome[151], and WikiPathways.[152] RaMP-DB metabolite sets containing ≥ three entries were required to ensure pathway coverage and reduce instability in MSE analysis. Features selected for the MSE analysis comprised a subset of the most

prominent and well-characterized MFs with positive HMDB library matches. This targeted selection of the subset was made to minimize identification uncertainties and strengthen biological interpretability.

3 Results and Discussion

3.1 UHPLC–MS/MS method performance

To establish a stable and high-throughput UHPLC–MS/MS workflow for untargeted metabolomic profiling of serum and CSF from patients with LNB, particular attention was first given to sample pretreatment and analytical robustness. Efficient removal of macromolecules proved critical for maintaining instrument stability and sensitivity over time. Six precipitation ratios were evaluated, and a methanol ratio of 5:1 (*v*:*v*) was selected to ensure effective precipitation, thereby supporting consistent chromatographic separation and stable ionization. Method robustness was further ensured by randomized injection order and the systematic use of deuterated ISs, which were applied during both method development and routine analyses to monitor sensitivity, repeatability, and matrix effects. In addition, a lock mass function was used to improve mass accuracy. On this basis, a rapid, reproducible, and readily adoptable UHPLC–MS/MS workflow for untargeted metabolomic profiling of serum and CSF samples from patients with LNB was established. The MS platform was operated in positive ion mode across an *m*/*z* range of 70–1,050 and configured for high-throughput analysis, with 10.1 min chromatographic runs and automated sample injections. This configuration enabled large batches of serum and CSF samples to be analyzed efficiently within a single analytical time frame.

Instrument performance was monitored in both serum and CSF samples. Examples of IS peak area integration in analyzed serum (**Article I**) and CSF (**Article III**) samples are presented in Figure 5. Samples exhibiting an IS peak area standard deviation (SD) greater than ±30% relative to the dataset average were reanalyzed together with their corresponding matched pair(s). To harmonize MF peak areas, IS-based normalization was applied. For each sample, all detected MF peak areas were scaled using a correction factor calculated as the ratio of the average IS peak area across the run to the IS peak area of each sample.

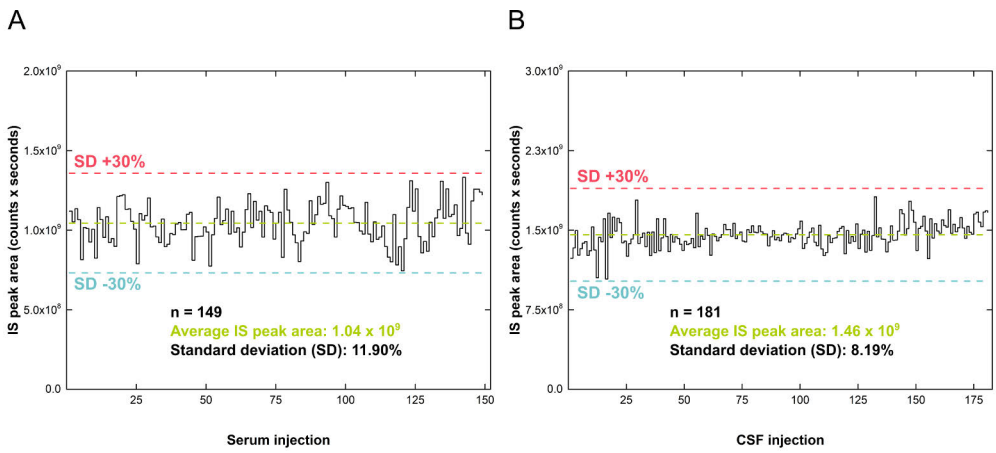

Figure 5. Example plots of internal standard (IS) DL-phenyl-d_5-alanine's mass spectrometric (MS) peak areas in **Article I** in serum (panel **A**) and in **Article III** in cerebrospinal fluid (CSF; panel **B**) samples.

3.2 Serum metabolomics workflow

3.2.1 Serum sample cohort

Serum samples in **Article I** were obtained from 81 individual patients diagnosed with definite LNB. Samples were collected at two clinically relevant time points: prior to diagnosis (acute, pretreatment) and 12 months after antibiotic treatment (healthy, post-treatment). Paired serum samples were available for 68 patients. In addition, six pretreatment samples and seven post-treatment samples were available. The serum metabolomics workflow is presented in Figure 6.

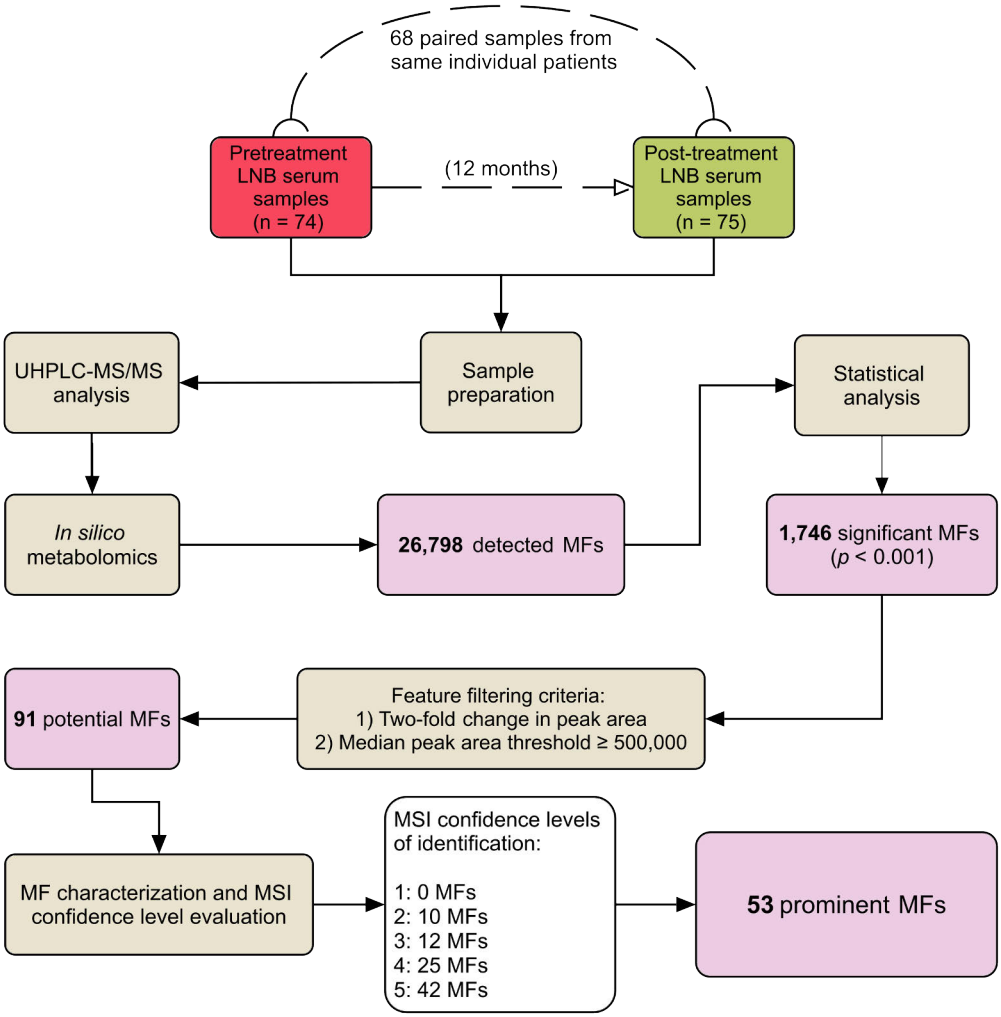

Figure 6. Untargeted metabolomics workflow in **Article I** for serum analysis in Lyme neuroborreliosis (LNB). Molecular features (MFs) were detected and identified using ultrahigh-performance liquid chromatography–tandem mass spectrometry (UHPLC–MS/MS) -based metabolomics, with Metabolomics Standards Initiative[118] (MSI) confidence levels.

3.2.2 Untargeted *in silico* serum metabolomics and prominent molecular features for Lyme neuroborreliosis

In **Article I,** untargeted *in silico* metabolomic analysis of serum samples (n = 149) detected a total of 26,978 MFs from the UHPLC–MS/MS data. Paired, non-parametric comparisons (Wilcoxon signed-rank) between pretreatment and post-treatment sera identified 1,746 MFs that were statistically significant ($p < 0.001$) between pretreatment and post-treatment samples in both raw and IS-standardized datasets. From these, 91 potential MFs were prioritized for detailed statistical analysis and structural identification. Linear mixed modeling was used to evaluate the effects of patient characteristics on MF behavior.

Structural identification uncovered that two of the prioritized MFs were detected in both $[M+H]^+$ and $[M+2H]^{2+}$ charge states. This reduced the number of potential MFs from 91 to 89. Combined with statistical behavior, these findings narrowed the total number of potential MFs to the final 53. For the 89 structurally unique MFs, identification confidence followed the MSI framework[118]: 10 at Level 2 (tentative via MS/MS library/literature), 12 at Level 3 (candidate structures supported by formula and MS/MS), 25 at Level 4 (formula/isotopic/adduct evidence), and 42 at Level 5 (distinct but unclassified spectral features). All reported MFs passed peak quality and alignment criteria and retained consistent RTs within the acquisition window.

In **Article I**, five tentatively identified MFs with the most reliable MSI identification (Figure 7) were acetylcarnitine (Level 2), L-homoarginine (Level 3), leucine-alanine-aspartic acid (Level 3), pipericine (Level 3), and 6-sulfatoxymelatonin (Level 3), when medication-related MFs were excluded.

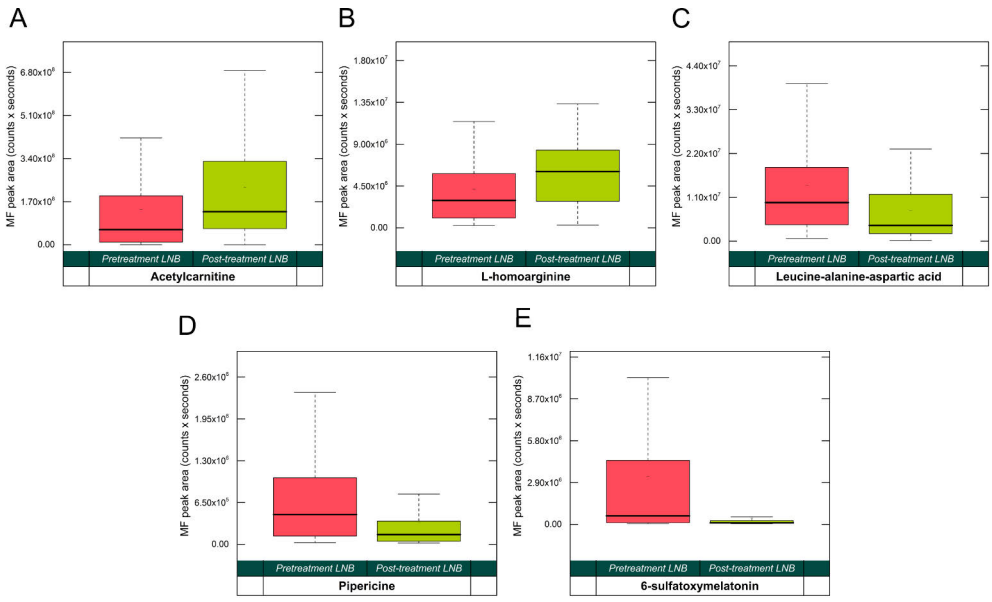

Figure 7. Box-and-whisker plots of standardized serum peak areas for five example molecular features (MFs) showing metabolomic profile changes between acute Lyme neuroborreliosis (LNB; n = 36) and post-treatment LNB (n = 36) states in **Article I**: acetylcarnitine (panel **A**), L-homoarginine (panel **B**), leucine-alanine-aspartic acid tripeptide (panel **C**), pipericine (panel **D**) and 6-sulfatoxymelatonin (panel **E**).

3.3 Machine learning workflow

3.3.1 Machine learning serum sample cohort

The supervised ML classifiers in **Article II** were based on 130 serum samples and their metabolite profiles from three clinically defined cohorts: pretreatment LNB (n = 34), post-treatment LNB (n = 34), and non-LNB controls (n = 62). These samples were organized into 62 analytical data cases for model development. The data cases included 34 fully matched triplets, each comprising a pretreatment LNB sample, a post-treatment LNB sample (12-month follow-up), and an age- and sex-matched non-LNB control. Additionally, 28 unmatched non-LNB control samples were included. The data was split at the case level into a training set (two-thirds of the cases, n = 41) and a test set (one-third of the cases, n = 21) to avoid information leakage and to quantify model performance. The workflow and performance of the supervised ML classifiers are presented in Figure 8.

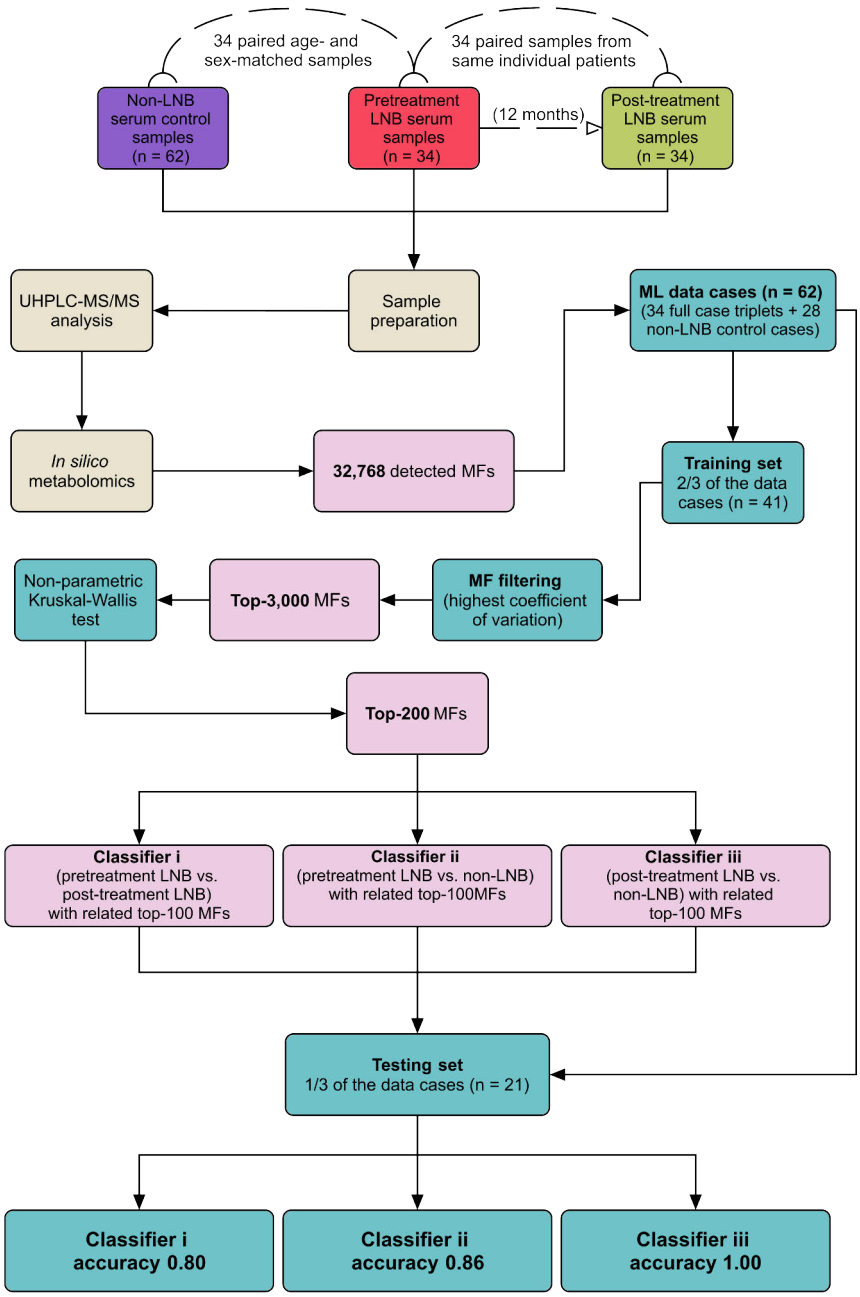

Figure 8. Workflow and performance of supervised machine learning (ML) classifiers in clinically meaningful patient groups in Lyme neuroborreliosis (LNB): (**i**) pretreatment LNB vs. post-treatment LNB (accuracy 0.80), (**ii**) pretreatment LNB vs. *Borrelia* antibody-negative (non-LNB) controls (accuracy 0.86), and (**iii**) post-treatment LNB vs. non-LNB (accuracy 1.00). Classifiers used serum molecular features (MF) from by ultrahigh-performance liquid chromatography–tandem mass spectrometry (UHPLC–MS/MS) -based untargeted metabolomics (**Article II**). Data cases were split into training set and testing set at the case level to prevent information leakage.

3.3.2 Machine learning model-related molecular features and classifier accuracy

In **Article II,** untargeted *in silico* metabolomics of the ML serum cohort detected 32,768 MFs from the UHPLC–MS/MS data. Of these, 27,021 MFs were assigned predicted preliminary molecular formulae, 6,675 MFs received automated preliminary identifications, and 1,606 MFs had pathway associations.

For ML feature selection, the original set of 32,768 MFs was first reduced to the top-3,000 MFs with the highest coefficient of variation and then narrowed to the top-200 features exhibiting the strongest association with the group, determined by a non-parametric Kruskal-Wallis test (training data only). From these, the top-100 discriminatory features were determined for each pairwise classifier with clinical utility: (**i**) pretreatment LNB vs. post-treatment LNB, (**ii**) pretreatment LNB vs. non-LNB, and (**iii**) post-treatment LNB vs. non-LNB. Across the three classifiers, 22 MFs overlapped. Classifier overlaps were as follows: 44 MFs shared between classifiers **i** and **ii**, 50 MFs between **i** and **iii**, and 47 MFs between **ii** and **iii**. Each classifier also retained unique MFs in its top-100 set: 28 unique MFs in classifier **i**, 31 in classifier **ii**, and 25 in classifier **iii**. The shared and unique MF distributions are presented in Figure 9.

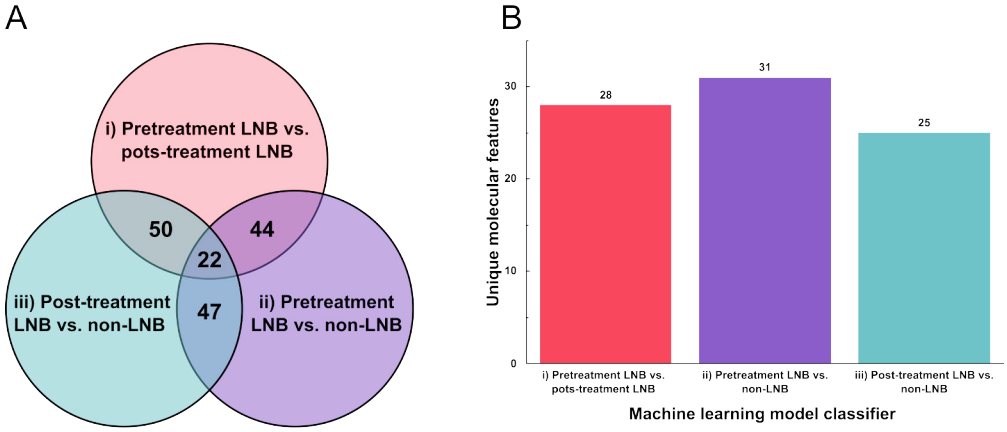

Figure 9. Shared and unique molecular features (MFs) among three machine learning (ML) classifiers **i-iii**. Panel **A** shows the overlap among the top-100 MFs for (**i**) pretreatment LNB vs. post-treatment LNB, (**ii**) pretreatment LNB vs. *Borrelia* antibody-negative (non-LNB) controls, and (**iii**) post-treatment LNB vs. non-LNB in a Venn diagram. Panel **B** depicts ML classifier-specific unique features within the respective top-100 sets in a bar chart.

Random Forest classifiers were trained on two-thirds of the data cases and tested on the one-third validation set. Observed performance (accuracy) was as follows: 0.80 for classifier **i**, 0.86 for classifier **ii**, and 1.00 for classifier **iii**. For reference, the expected (baseline) accuracies (under class prevalence assumptions) were 0.61, 0.58, and 0.63, respectively. In all three tasks, the Random Forest classifier outperformed random classification, demonstrating robust discrimination.

3.4 Cerebrospinal fluid metabolomics workflow

3.4.1 Cerebrospinal fluid sample cohort

The CSF cohort in **Article III** included 181 samples from the following patient groups: acute pretreatment LNB (n = 63), three weeks after antibiotic treatment initiation LNB (n = 36), non-LNB controls (n = 61), and other CNS infections (n = 21). Four different comparisons were investigated: comparison **A**, a paired within-patient analysis between pretreatment LNB and three weeks after treatment initiation (36 matched pairs from same individuals); comparison **B**, a paired case-control analysis between pretreatment LNB (n = 61) and non-LNB controls (n = 61); comparison **C**, an independent group analysis between pretreatment LNB (n = 63) and other CNS infections (n = 21); and comparison **D**, an independent LNB subgroup analysis between pretreatment LNB patients with radiculitis (n = 40) and without radiculitis (n = 23). The CSF metabolomics workflow in **Article III** is presented in Figure 10.

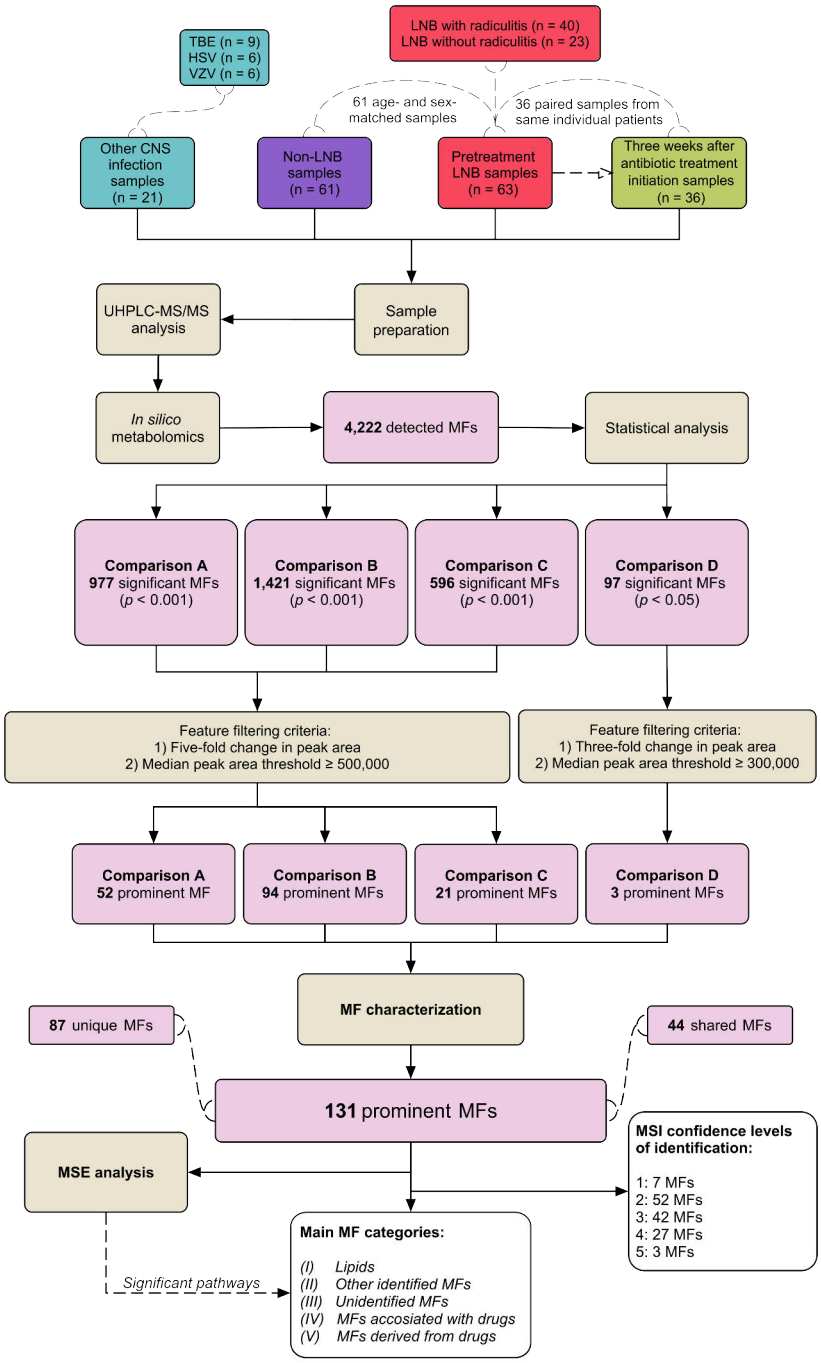

Figure 10. Untargeted metabolomics workflow in **Article III** for cerebrospinal fluid (CSF) analysis in Lyme neuroborreliosis (LNB). Molecular features (MFs) were detected and identified using ultrahigh-performance liquid chromatography–tandem mass spectrometry (UHPLC–MS/MS) -based metabolomics, with assignments supported by Metabolomics Standards Initiative[118] (MSI) confidence levels, MF categories, and Metabolite Set Enrichment (MSE) analysis[149].

3.4.2 Untargeted *in silico* cerebrospinal fluid metabolomics and prominent molecular features for Lyme neuroborreliosis

In **Article III,** the untargeted *in silico* metabolomic analysis detected a total of 4,222 MFs from the CSF samples. In comparison **A**, statistical analysis identified 977 statistically significant ($p < 0.001$) MFs between pretreatment LNB and three weeks after antibiotic treatment initiation LNB. After more detailed statistical evaluation of patient characteristics combined with MF filtering criteria, a total of 60 MFs remained. Closer structural characterization and removal of isotopic replicates narrowed the final number to 52 prominent MFs. The estimated patient group effect (within-factor: time point) was significant in 15 MFs, excluding three doxycycline treatment-associated MFs that were expectedly upregulated at the three-week sampling point. Patient age influenced 40 MFs (notably among lipophilic compounds), sex affected five MFs with lower peak areas in male patients compared to women, CSF CXCL13 was associated with 19 MFs, and the use of APAP impacted six MFs (five identified as APAP metabolites).

In comparison **B**, 1,421 MFs were statistically significant ($p < 0.001$) between pretreatment LNB and non-LNB control groups. After statistical evaluation of patient characteristics and MF filtering criteria, 94 MFs remained. Manual characterization and removal of isotopic replicates yielded 87 prominent MFs. The estimated group effect (within-factor: matched pair) indicated lower MF peak areas in non-LNB samples. The group variable alone explained variation in 55 MFs. Two MFs were notably elevated in non-LNB subjects, identified as DL-glutamine (306.87% increase) and a hypoxanthine-related MF (400.17% increase). Between-factor investigation revealed that age influenced 27 MFs, while sex was associated with four lipid-related MFs. The use of APAP significantly affected seven MFs, but none of them were identified as APAP itself, its known metabolites, or related fragments or adduct ions. Additionally, each of these seven MFs also indicated a statistical association with the patient group and age.

In comparison **C** (an independent comparison), a total of 596 MFs were statistically significant ($p < 0.001$) between pretreatment LNB and other CNS infection groups. Statistical evaluation of patient characteristics and implementation of MF filtering criteria narrowed the selection to 21 prominent MFs prior to closer manual characterization. Group variable differences were detected in four MFs that were exclusively influenced by group. Three of these MFs were structurally related to a purine nucleoside and its two product ions. The fourth MF was identified as acetylcarnitine and confirmed by an authentic reference standard. Age affected two MFs (excluding five MFs directly related to APAP), whereas patient sex showed no statistically significant associations. APAP use influenced 15 MFs, all of which were identified as direct APAP metabolites. Compared with patients taking APAP,

non-users showed a 99.63% lower median effect for these MFs. In comparison **C**, six MFs remained as prominent biomarkers independent of medication-related effects.

In comparison **D** (an independent comparison), 97 MFs were identified as significant ($p < 0.05$) in the LNB radiculitis subgroup analysis. Following statistical evaluation and application of MF filtering criteria, three MFs remained for more detailed investigation. These MFs were associated with the patient group, exhibiting a median estimated group effect of a 117.63% increase in radiculitis. One MF was identified as isopropanolamine myristate, while the two MF remained unknown. All three MFs showed significant association with age and CSF leukocyte count. No significant associations were observed for sex, CSF CXCL13 concentration, or the use of APAP.

None of the final 131 MFs were shared across all four comparisons. Comparison **A** overlapped with comparisons **B** (27 MFs), **C** (one MF), and **D** (one MF). After excluding directly medication-related features (one APAP-related and three doxycycline-related MFs), 45 MFs remained in **A** (16 unique and 29 shared). Comparison **B** shared no MFs with comparisons **C** or **D**, highlighting 60 specific MFs for **B** (eight were influenced by the use of APAP). In comparison **C**, five comparison-specific MFs remained after excluding one MF shared with comparison **A** and 17 MFs related to APAP metabolites. Comparison **D** shared one MF with comparison **A**, leaving two unique comparison-specific MFs.

Manual characterization of prominent MFs was based on exact mass, derived molecular formula, MS/MS patterns, RT, MS databases, statistical behavior, and reference standards. MFs were classified into five categories: lipids/lipid-type features (category **I**: 76 MFs), other identified endogenous/exogenous features (category **II**: 27 MFs), currently unidentified potential LNB features (category **III**: 6 MFs), medication-associated MFs where infection-related processes may also contribute (category **IV**: 8 MFs), and directly medication-related MFs (category **V**: 19 MFs). Categories **II** and **III** shared five MFs. Two MFs in category **IV** and four in category **V** lacked assignable molecular formulae based on exact masses.

MF identification confidence followed the MSI criteria[118]: seven MFs were at Level 1 (confirmed by reference standards), 52 at Level 2 (tentative via MS/MS library/literature), 42 at Level 3 (candidate structures supported by formula and MS/MS), 27 at Level 4 (formula/isotopic/adduct evidence), and 3 at Level 5 (distinct but unclassified spectral features). Pathway analysis identified 25 significant pathways ($p < 0.05$), with nine metabolomic pathways emerging as the most prominent and potentially relevant to LNB.

3.5 Integrative overview and analytical context

The findings of this doctoral dissertation indicate that MS-based metabolomics is capable of detecting metabolic alterations associated with LNB and may serve as a potential complementary tool, alongside more conventional diagnostic methods. Although comprehensive metabolic profiling revealed infection-associated changes, the complexity and heterogeneity of patients' clinical data necessitate careful interpretation of the presented results.

3.5.1 Serum metabolomics and identification of prominent molecular features

In **Article I,** the primary focus was on method development and workflow optimization. During this stage, priority was given to establishing a high-throughput untargeted metabolomics workflow that was capable of robust and reproducible MF coverage, supported by comprehensive statistical evaluation. Within this context, identified Level 2 and Level 3 MFs currently represent the most informative findings between acute pretreatment LNB and post-treatment LNB, supported by either MS library spectra or high-confidence molecular formulae. Definitive metabolite identification (Level 1) requires targeted analyses using authentic reference standards, as later demonstrated in **Article III**.

Acetylcarnitine, identified with an authentic reference standard in **Article III** comparisons **A** and **C** (Level 1: matching *m*/*z*, MS/MS spectra, and RT), is an acetylated carnitine linked to mitochondrial fatty acid transport, neuroprotection, and reduced neuroinflammatory signaling.[153] Acetylcarnitine has also been shown to assist in regulating mitochondrial acetyl-CoA levels and to shuttle two carbon units across mitochondrial membranes.[154] Therefore, changes in its abundance are more likely to reflect alterations in mitochondrial workload rather than being a binary "on/off" disease biomarker.[154]

Serum acetylcarnitine levels (MF peak areas) observed in **Article I** were elevated in LNB post-treatment samples compared to pretreatment LNB samples. However, in **Article III**, CSF samples showed that acetylcarnitine levels were highest in pretreatment LNB and declined three weeks after treatment initiation. Additionally, other known CNS infections (TBE, HSV and VZV) showed higher CSF levels compared to pretreatment LNB. This pattern, shown in Figure 11, fits with the observations of prior CSF metabolomic studies in infectious neuroinflammation, where short-chain acylcarnitines are notably elevated (e.g., in viral and tuberculous meningitides) and then normalized during recovery.[155,156]

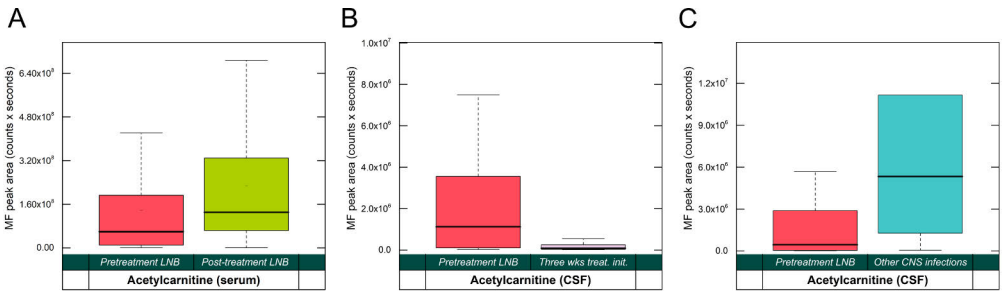

Figure 11. Box-and-whisker plots of standardized peak areas for acetylcarnitine in **Article I** in Lyme neuroborreliosis (LNB) patients' serum [panel **A**; pretreatment LNB (n = 63) vs. post-treatment LNB (n = 63)] and **Article III** cerebrospinal fluid (CSF) comparison A [panel **B**; pretreatment LNB (n = 61) vs. three weeks after treatment initiation (n = 61) and comparison C [panel **C**; pretreatment LNB (n = 63) vs. other known central nervous system (CNS) infections (n = 21)].

Divergences between serum and CSF analyte levels are plausible due to the blood-brain barrier and the blood-CSF barrier, which regulate molecular exchange between the systemic circulation and the CNS.[157,158] Therefore, CSF acetylcarnitine may indicate mitochondrial load during nervous system inflammation, whereas serum acetylcarnitine may reflect systemic recovery and energy repletion.[159,160]

Other identified MFs in **Article I** included L-homoarginine, Leu-Ala-Asp tripeptide, pipericine, and 6-sulfatoxymelatonin (Figure 12). Reduced levels of L-homoarginine in LNB may indicate changes in nitric oxide synthesis and vascular stress.[161,162] During acute LNB, higher levels of Leu-Ala-Asp tripeptide can be consistent with small peptides produced by proteolysis, thus supporting increased protease activity and protein turnover during inflammation.[163–166] The MF annotated as the piperidine alkaloid pipericine from *Piper nigrum* should be interpreted with caution. Although such alkaloids exhibit anti-inflammatory and neuromodulatory effects[167,168], they are also known as dietary xenobiotics and bioenhancers[169,170]. The principal urinary metabolite of melatonin, 6-sulfatoxymelatonin, may indicate circadian-immune coupling, which has been shown to be altered in acute disease states.[171–173]

In accordance with the MSI, untargeted metabolomic findings presented in **Article I** should be regarded as tentative. Definitive identification and better clinical interpretability require confirmation via targeted UHPLC–MS/MS using authentic reference standards to achieve Level 1 confidence with matching RTs and fragmentation patterns.[118,174]

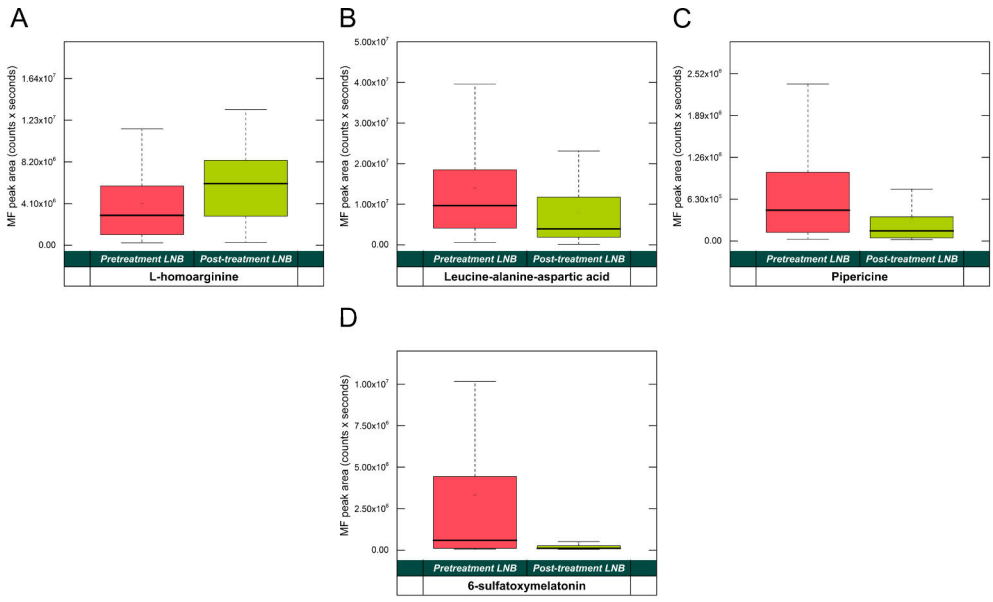

Figure 12. Box-and-whisker plots of standardized peak areas for L-homoarginine (panel **A**), leucine-alanine-aspartic acid (panel **B**), pipericine (panel **C**) and 6-sulfatoxymelatonin (panel **D**) in Lyme neuroborreliosis (LNB) patients' serum [pretreatment LNB (n = 63) vs. post-treatment LNB (n = 63)] in **Article I**.

MFs assigned to MSI confidence levels 4-5 in **Article I** are still considered as prominent biomarkers for LNB. Even though their chemical structures are yet unknown, their statistical discriminative behavior between groups can help the identification of acute LNB from already treated disease. A pragmatic next step is to enhance the MSI identification confidence levels with targeted parallel reaction monitoring (PRM). This would enable selective isolation of known precursor ions and acquisition of their characteristic MS/MS spectra. The resulting fragmentation patterns can then be screened against spectral databases and evaluated through manual identification to generate structural hypotheses, which can subsequently be confirmed using authentic reference standards.

Many of the Level 5 MFs were also detected as $[M+2H]^{2+}$ ions. In (H)ESI, a stable doubly charged ion state ($z = 2$) typically refers to molecules with two or more protonation sites (e.g., peptides, polyamines, or strongly basic, higher-mass metabolites). The characteristic ~0.5 Da isotopic spacing between monoisotopic signals for doubly charged ions enabled calculation of the corresponding neutral masses, even when the molecular formulae and structures remained unknown.[175–177] In addition, (H)ESI behavior also depends on the eluent composition. Small changes in the acidic or basic modifier (e.g., formic acid vs. ammonium acetate) and in the proportion of organic solvent can shift charge states and adduct formation.[178,179] In

practice, acidifying the eluent or switching to ammonium can favor formation of $[M+H]^+$ or $[M+NH_4]^+$, respectively, which may simplify spectral interpretation and compound identification.

3.5.2 Serum metabolomics enhanced with machine learning

In **Article II**, Random Forest-based supervised ML applied to untargeted serum metabolomics was able to distinguish acute pretreatment LNB, post-treatment LNB, and non-LNB controls, indicating that serum metabolic profiles contain biologically relevant information linked both to active disease and to the post-treatment state. Importantly, the study design strengthened this interpretation by combining paired pre- and post-treatment samples from the same individuals, an age- and sex-matched non-LNB comparison group, and an independent training/validation split, thereby increasing sensitivity to individual-level metabolic change while reducing the likelihood that the observed performance reflected only within-dataset fitting.

Before classifier training, the original untargeted data set of 32,768 MFs was reduced to the top-3,000 high-variance features and then to the top-200 most group-associated features, illustrating a deliberate dimensionality-reduction strategy that is appropriate for high-dimensional metabolomics data. The observed classifier performance was clearly above the study-specific naive baselines in all pairwise comparisons: 0.80 versus 0.61 for pretreatment vs. post-treatment LNB, 0.86 versus 0.58 for pretreatment LNB vs. non-LNB controls, and 1.00 versus 0.63 for post-treatment LNB vs. non-LNB controls. Because the comparison groups were not perfectly balanced, these margins above the expected baseline are more informative than the raw accuracy values alone and support the conclusion that the models captured non-random disease-related structure in the serum metabolome. Receiver operating characteristic analyses further supported this interpretation by demonstrating robust discriminatory performance across all three pairwise tasks.

An important methodological observation is that this strong supervised performance was achieved despite only modest global separation in unsupervised ordination, with group differences explaining only a limited proportion of the total variance in the data. This suggests that LNB-related information is not necessarily expressed as a dominant shift visible in exploratory ordination plots, but rather as a distributed multivariate pattern spanning numerous MFs that becomes informative when modeled in a supervised framework. In this respect, the Random Forest approach appears to have captured subtle but systematic serum metabolomic differences that were not fully apparent in unsupervised analysis alone.

A further notable finding was that the discriminatory MFs were not completely classifier-specific, but were partly shared across comparisons. In the model, 22 MFs were present in all three classifiers, and additional overlaps were observed between

the longitudinal and case-control comparisons. This pattern supports the presence of a more persistent infection-related metabolic signature rather than a profile attributable solely to treatment status. At the same time, the clinically most relevant pretreatment LNB vs. non-LNB comparison remained strongly discriminative, indicating that the model did not merely separate recovery status from other clinical backgrounds, but also captured serum features linked to active disease. The especially strong separation between post-treatment LNB and non-LNB controls may suggest that metabolomic alterations persist after clinical recovery and could, in principle, assist in recognizing prior disseminated *Borrelia* exposure in diagnostically uncertain cases. This interpretation is consistent with earlier LB metabolomics studies, in which metabolic biosignatures and ML-based feature selection improved diagnostic discrimination in early disease[68,123], supporting the broader concept that infection-related metabolic changes can be detected even when conventional serological interpretation is limited. However, any "perfect" classification should be interpreted cautiously, as small sample size, biological heterogeneity, MS technical variance, and preprocessing choices may all contribute to optimistic estimates of classifier performance in high-dimensional metabolomics data.

Several factors may contribute to the persistent differences observed after clinical recovery. First, *Borrelia*-specific antibodies can remain elevated for months after successful treatment of disseminated LB.[21–23] Second, host immune signals may also remain altered after treatment in LNB. For example, serum cytokine interferon-α has been shown to persist over a one-year follow-up[180], whereas in early disseminated LB, interferon dominated blood transcriptomes may persist after treatment before normalizing approximately at 6 months.[181] Third, broad spectrum antibiotics (e.g., ceftriaxone) used to treat LNB may disturb the gut microbiome and affect systemic metabolites.[182–184]

In this context, the post-treatment signature identified by the ML model should not be interpreted simply as evidence of ongoing infection, but rather as a composite reflection of convalescence, persistent host-response pathways, and treatment-associated systemic effects. In contrast, the ML models' discriminatory MFs were partially shared across classifiers, including in the pretreatment LNB vs. non-LNB comparison, suggesting that at least part of the signal reflects infection-linked host biology rather than treatment alone. From a translational perspective, this is encouraging because the non-LNB comparison group did not consist only of healthy controls, but of non-LNB individuals evaluated in routine clinical practice, including patients with other suspected infectious, inflammatory, or autoimmune conditions. This makes the classification task clinically more relevant, as future complementary diagnostic tools must distinguish LNB from heterogeneous real-world alternatives rather than from health alone. However, given the limited number of cases, the

current ML model should still be regarded as demonstrating comparative diagnostic potential rather than readiness for clinical use. External validation in larger, temporally separated, and multicenter cohorts will be essential before clinical implementation can be considered. Overall, **Article II** provides proof-of-principle that serum metabolomics enhanced with supervised ML can recover clinically meaningful signatures of acute LNB and post-treatment recovery, thereby offering a rational basis for future targeted biomarker-panel development and external model validation.

3.5.3 Cerebrospinal fluid metabolomics and identification of prominent molecular features

Article III employed UHPLC–MS/MS-based metabolite profiling of CSF to identify LNB-associated metabolic alterations. Four comparisons were investigated: (**A**) a within-patient comparison of acute pretreatment LNB CSF and paired CSF samples collected three weeks after treatment initiation from the same individuals who had ≥ 50 leucocytes/μL in pretreatment CSF; (**B**) a paired comparison between acute LNB CSF and age- and sex-matched non-LNB control CSF samples; (**C**) an independent comparison of acute LNB CSF and other laboratory confirmed CNS infection CSF samples (TBE, HSV and VZV); and (**D**) a comparison among acute LNB cases with and without radiculitis. Of the 4,222 MFs detected, 131 were prioritized based on statistical significance, effect size, and structural characterization, highlighting potential candidate CSF biomarkers.

Several CSF MFs in LNB were linked to tryptophan metabolism and lipid signaling pathways. Multiple MFs are also associated with CSF CXCL13 concentrations, a biomarker used in acute LNB diagnostics.[34,35,40,41] Most elevated MFs in comparison **A** declined at three weeks after treatment initiation (excluding APAP and its related metabolites). Comparison **B** confirmed the specificity of several profile alterations by distinguishing pretreatment LNB and non-LNB controls. Several overlaps between comparisons **A** and **B** suggest the possibility of identifying both disease-specific and general infection biomarkers. Comparison **C** revealed a smaller set of MFs shared with other known CNS infections alongside MFs more specific to LNB. Among the shared endogenous MFs, acetylcarnitine emerged as a general infection biomarker, similarly as in **Article I**. In comparison **D**, fewer significant differences were detected, which may reflect the complex influence of radiculitis on the CSF metabolome and subgroup heterogeneity. Previously, LNB with meningoradiculoneuritis (Garin-Bujadoux-Bannwarth syndrome) has been shown to exhibit a distinct immune profile[185], supporting future targeted metabolomic studies relating to LNB radiculitis.

In **Article III**, a total of 76 MFs were classified in category **I** (lipids and lipid-type compounds). These MFs included lysophospholipids (LysoPLs), sphingolipids, primary fatty acid amides, cyclic phosphatidic acids (cPAs), and other related lipids. The LysoPLs, divided into lysophosphatidylcholine (LysoPC) and lysophosphatidyl-ethanolamine (LysoPE) subclasses, were most abundant in acute LNB (comparisons **A** and **B**) and were reported to be involved in membrane remodeling and intracellular signaling.[186,187] Several LysoPCs were identified, including LysoPC(16:0) and LysoPC(22:6), which have been linked to phospholipase A_2 activity in LNB serum[188]. Additional LysoPCs previously associated with neuroinflammation[189] were also identified, namely LysoPC(P-16:0), LysoPC(P-18:0), and two LysoPC(18:1) isomers. Notably, LysoPC(18:1) elevations have been reported in association with neuropathic pain after peripheral nerve injury[190], and their involvement in LNB remains to be investigated further. Examples of detected LysoPL peak areas for comparisons **A** and **B** are presented in Figure 13.

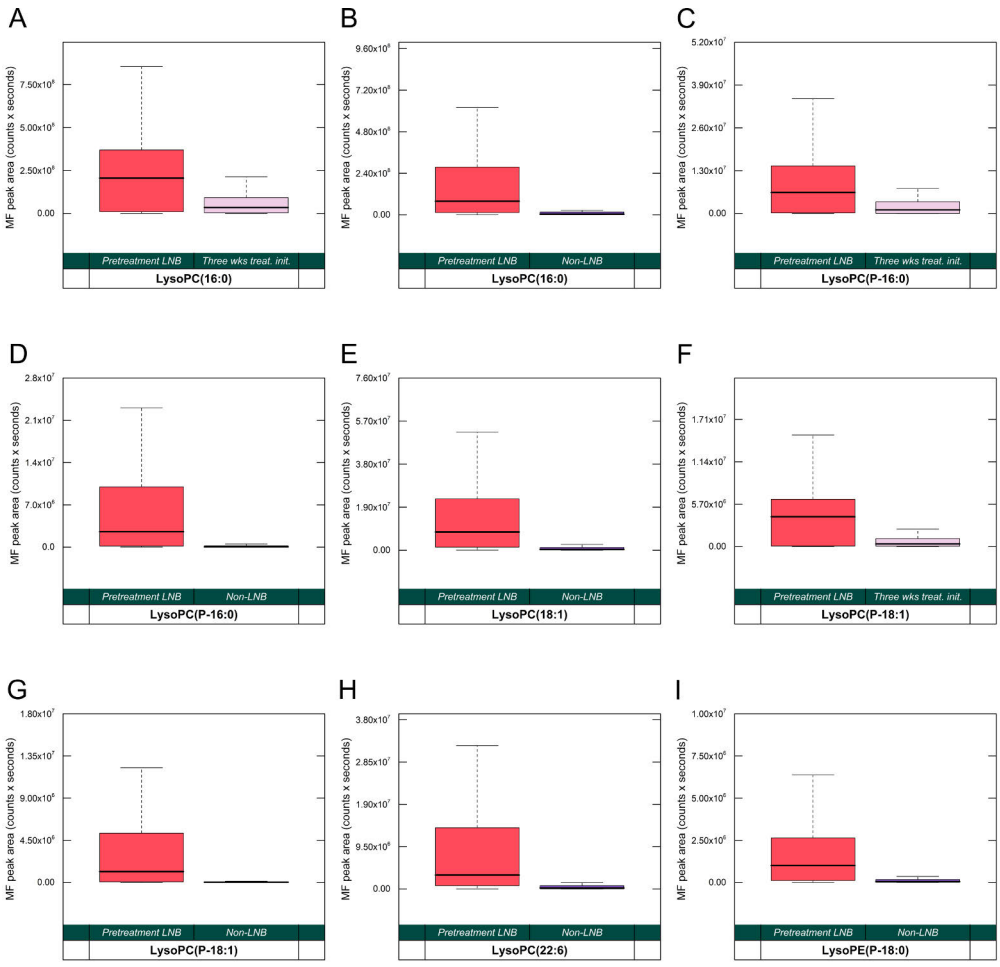

Figure 13. Examples of box-and-whisker plots of standardized CSF molecular feature (MF) peak areas for lysophosphatidylcholines (LysoPCs) and lysophosphatidylethanolamine (LysoPE) detected in **Article III**. Panels depict MFs in comparison A [pretreatment LNB (n = 36) vs. three weeks after treatment initiation from the same individuals (n = 36)] and comparison B [pretreatment LNB (n = 61) vs. *Borrelia* antibody-negative (non-LNB) controls (n = 61)]. Panel assignments are as follows: (**A**) LysoPC(16:0), comparison A; (**B**) LysoPC(16:0), comparison B; (**C**) LysoPC(P-16:0), comparison A; (**D**) LysoPC(P-16:0), comparison B; (**E**) LysoPC(18:1), comparison B; (**F**) LysoPC(P-18:1), comparison A; (**G**) LysoPC(P-18:1), comparison B; (**H**) LysoPC(22:6), comparison B; and (**I**) LysoPE(P-18:0), comparison B.

Sphingolipid-related changes were also detected. Five sphingoid bases were elevated in acute LNB infection in comparisons **A** and **B**: three isomers of C17-sphinganine, d19:0-sphinganine, and 3-ketosphingosine. As precursors of myelin

sphingolipids and bioactive signaling mediators, elevations in d19:0-sphinganine and 3-ketosphingosine have been associated with altered sphingolipid metabolism in multiple sclerosis, neuropathic pain, and neurodegeneration.[191–194] Examples of detected sphingoid base peak areas in comparisons **A** and **B** are presented in Figure 14.

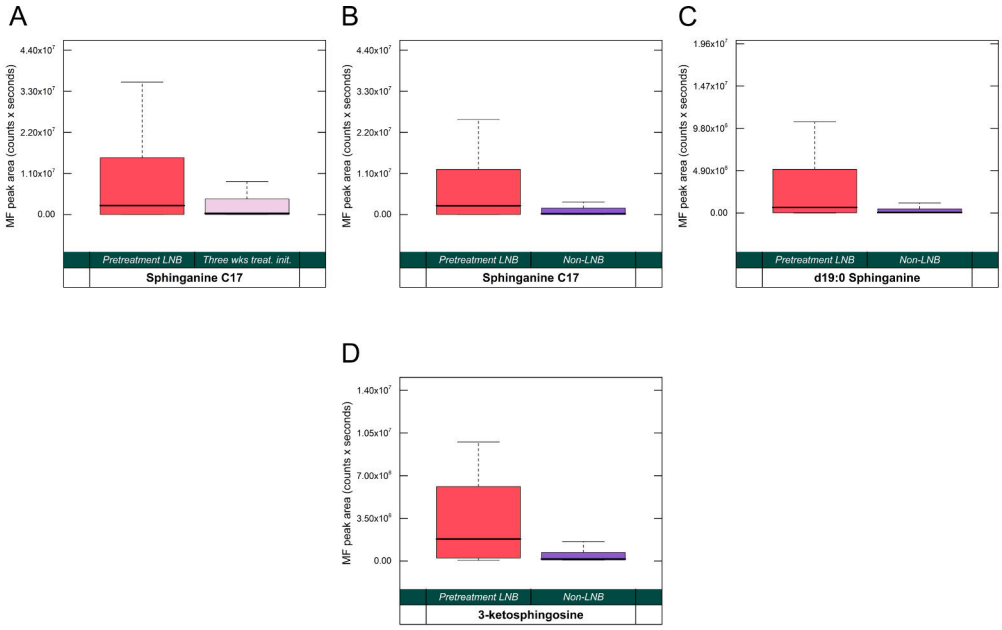

Figure 14. Examples of box-and-whisker plots of standardized CSF molecular feature (MF) peak areas for sphingoid bases detected in **Article III**. Panels depict MFs in comparison A [pretreatment LNB (n = 36) vs. three weeks after treatment initiation from the same individuals (n = 36)] and comparison B [pretreatment LNB (n = 61) vs. *Borrelia* antibody-negative (non-LNB) controls (n = 61)]. Panel assignments are as follows: (**A**) C17-sphinganine, comparison A; (**B**) C17-sphinganine, comparison B; (**C**) d19:0-sphinganine, comparison B; and (**D**) 3-ketosphinganine, comparison B.

A total of four sphingomyelins (SMs) were detected in comparison **A**, SM(d18:1/14:0), SM(d18:1/16:1), SM(d18:1/15:0), and SM(d18:1/16:0), with SM(d18:1/14:0) and SM(d18:1/16:1) also identified in comparison **B**. Elevated CSF sphingomyelins have been reported as biomarkers of active Guillain-Barré syndrome and chronic inflammatory demyelinating polyradiculoneuropathy[195], supporting their potential role also in LNB. Additionally, one phosphoceramide, CerP(d14:0/18:0), was detected in comparison **A**. These features are presented in Figure 15.

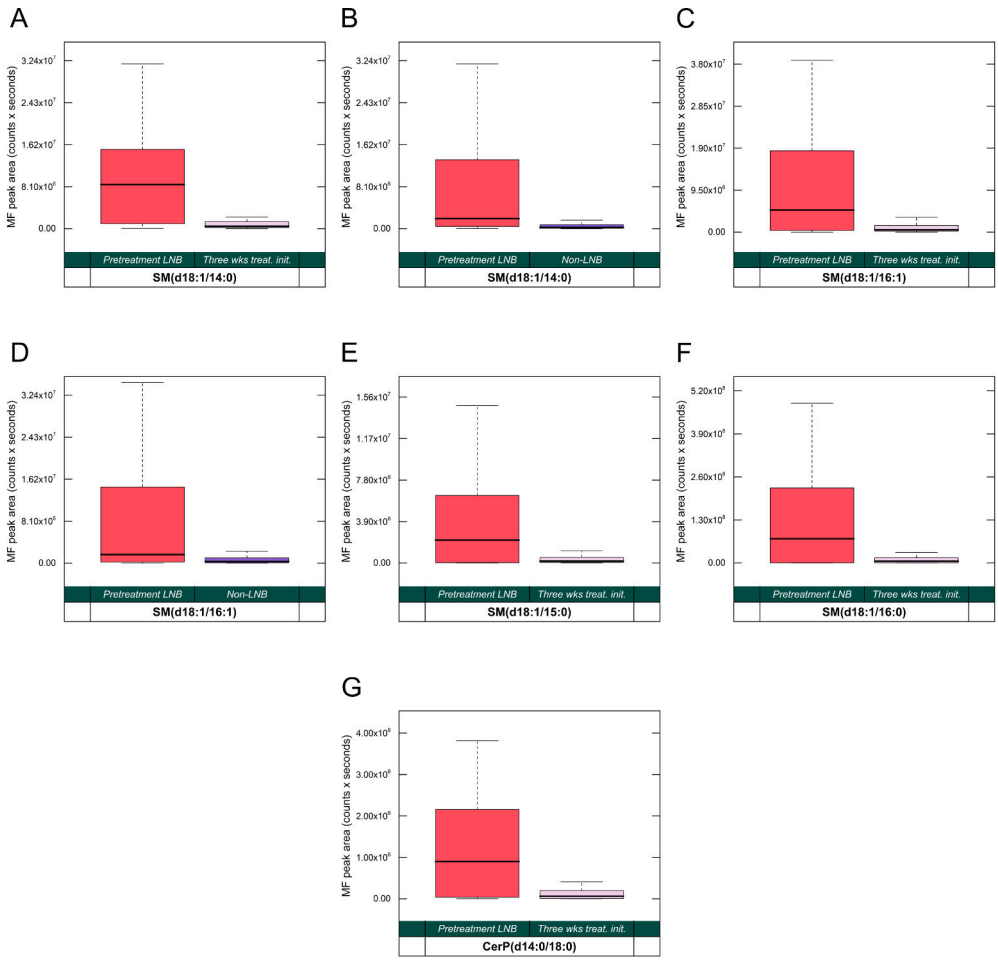

Figure 15. Box-and-whisker plots of standardized CSF molecular feature (MF) peak areas for sphingomyelins (SMs) and a phosphoceramide (CerP) in **Article III**. Panels depict MFs in comparison A [pretreatment LNB (n = 36) vs. three weeks post-treatment from the same individuals (n = 36)] and comparison B [pretreatment LNB (n = 61) vs. *Borrelia* antibody-negative (non-LNB) controls (n = 61)]. Panel assignments are as follows: (**A**) SM(d18:1/14:0), comparison A; (**B**) SM(d18:1/14:0), comparison B; (**C**) SM(d18:1/16:1), comparison A; (**D**) SM(d18:1/16:1), comparison B; (**E**) SM(d18:1/15:0), comparison A; (**F**) SM(d18:1/16:0), comparison A; and (**G**) CerP(d14:0/18:0), comparison A.

Identified CSF primary fatty acid amides (linoleamide, myristamide, palmitoleamide, and oleamide) were found to be statistically significant only in comparison **B**. Primary fatty acid amides are known as neurologically active lipids that have been shown to modulate inflammation, neuronal signaling, and glial function.[196–200] Notably, oleamide has been associated with anti-inflammatory effects in microglia[201], inhibition of glial gap junction communication[202], and multireceptor interactions, with accumulation in CSF during sleep deprivation.[203,204] In addition,

isopropanolamine myristate (a fatty acid derivative) was detected in comparison **D**. Two cPAs, cPA(16:0) and cPA(18:2), were identified in comparison **A**, and cPA(16:0) was also elevated during acute LNB in comparison **B**. Both were statistically associated with CXCL13 concentration in CSF, suggesting a possible link between cPA signaling and chemokine mediated immune activation. Generally, cPAs are known to inhibit cell proliferation, migration, and neuroinflammatory responses.[205,206] Peak areas of the detected primary fatty acids, fatty acid derivative, and cPAs are presented in Figure 16. Additional identified lipid associated MFs were two spirostane-3,6-dione isomers, valenciaxanthin, methyl-12-oxo-octadecanoate, and oxo-octadecanoic acid. However, their biological relevance in LNB remains to be determined.

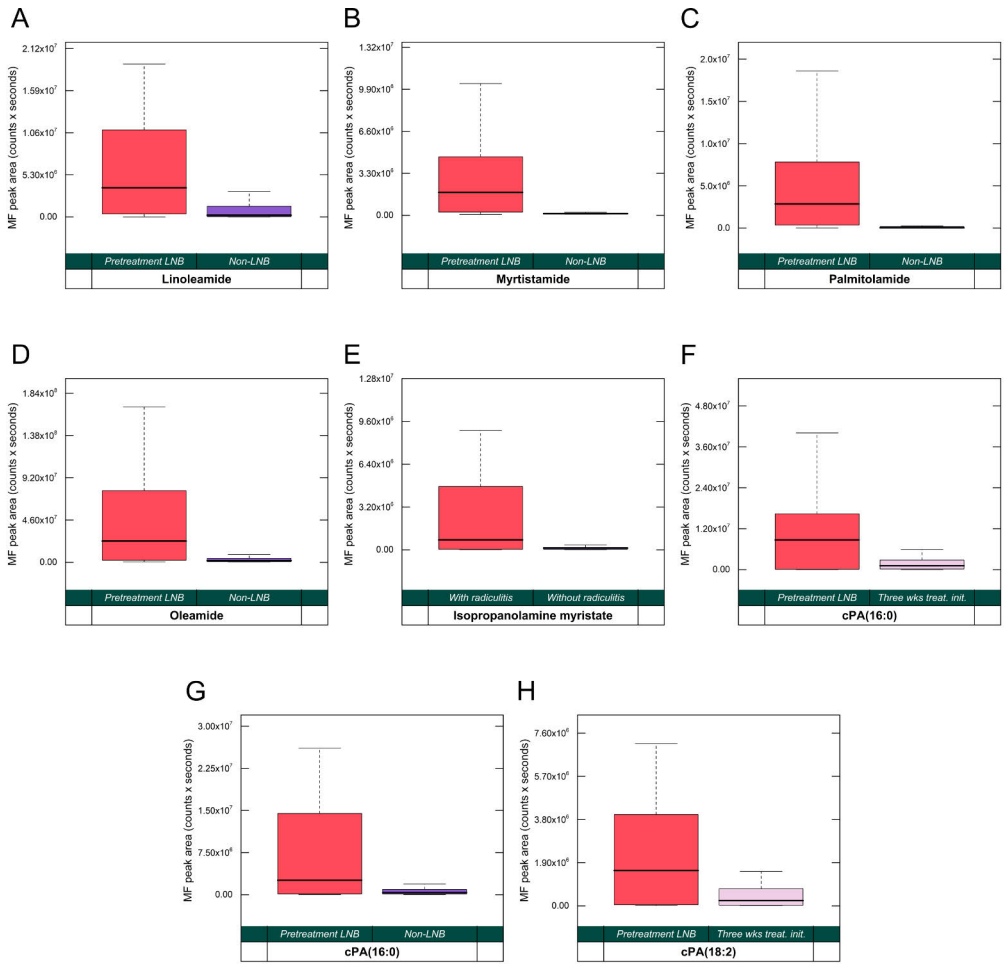

Figure 16. Box-and-whisker plots of standardized CSF molecular feature (MF) peak areas for primary fatty acid amides, fatty acid derivative, and cyclic phosphatidic acids (cPAs) in **Article III**. Panels depict MFs in comparison A [pretreatment LNB (n = 36) vs. three weeks after treatment initiation from the same individuals (n = 36)], comparison B [pretreatment LNB (n = 61) vs. *Borrelia* antibody-negative (non-LNB) controls (n = 61)], and comparison D [LNB with radiculitis (n = 40) vs. LNB without radiculitis (n = 23)]. Panel assignments are as follows: (**A**) linoleamide, comparison B; (**B**) myristamide, comparison B; (**C**) palmitolamide, comparison B; (**D**) oleamide, comparison B; (**E**) isopropanolamine myristate, comparison D; (**F**) cPA(16:0), comparison A; (**G**) cPA(16:0), comparison B; and (**H**) cPA(18:2), comparison A.

The levels of several category **II** endogenous and exogenous MFs were affected, indicating alterations in amino acid metabolism. Endogenous MFs included, for example, DL-kynurenine, quinolinic acid, 5-hydroxytryptophan, acetylcarnitine, glutarylcarnitine, *N*-acetylaspartylglutamate (NAAG), and DL-glutamine. These MFs, except for acetylcarnitine (Figure 11, panels B and C), are presented in Figure 17.

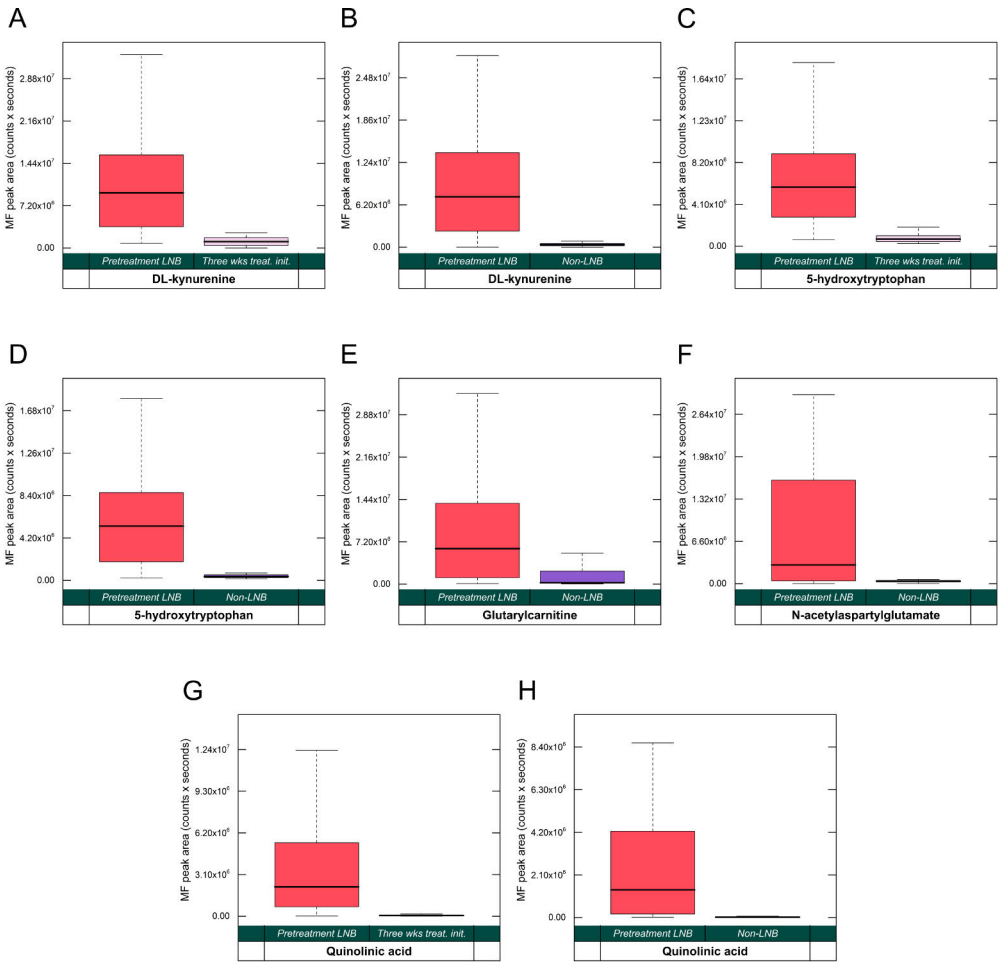

Figure 17. Examples of box-and-whisker plots of standardized CSF molecular feature (MF) peak areas for selected endogenous metabolites in **Article III**. Panels depict MFs in comparison A [pretreatment Lyme neuroborreliosis (LNB; n = 36) vs. three weeks after treatment initiation (n = 36)] and B [pretreatment LNB (n = 61) vs. *Borrelia* antibody-negative (non-LNB) controls (n = 61)]. Panel assignments are as follows: (**A**) DL-kynurenine, comparison A; (**B**) DL-kynurenine, comparison B; (**C**) 5-hydroxytryptophan, comparison A; (**D**) 5-hydroxytryptophan, comparison B; (**E**) glutarylcarnitine, comparison B; (**F**) *N*-acetylaspartylglutamate, comparison B; (**G**) quinolinic acid, comparison A; and (**H**) quinolinic acid, comparison B.

Among the endogenous MFs, NAAG is known as one of the most abundant neuropeptides in the CNS environment that modulates synaptic glutamate release and protects against excitotoxicity.[207] NAAG was statistically associated with the patient groups and with APAP use in comparison **B**. It was therefore classified as a category **II** biomarker, while also showing sensitivity to category **IV**. Both 5-hydroxytryptophan and its MS/MS dehydration fragment were associated with the

use of APAP in comparison **B**. However, the strongest effects were attributed to patient group, followed by age, whereas APAP showed the weakest association.

DL-kynurenine and its kynurenine pathway-related fragmentation products were statistically significant in comparisons **A** and **B** but not in comparison **C**. This finding was consistent with increased tryptophan degradation via the kynurenine pathway in acute LNB and other CNS infections (e.g., TBE).[208–211]

Another kynurenine pathway metabolite, the neuroactive quinolinic acid, which is an *N*-methyl-D-aspartate (NMDA) receptor agonist[212,213], was statistically associated with patient group and CSF CXCL13 concentration in comparison **A**, and with patient group, age, and use of APAP in comparison **B**. Although quinolinic acid is not a product of APAP metabolism, APAP (and acetylsalicylic acid) has shown to inhibit quinolinic acid-induced lipid peroxidation and oxidative damage in animal models.[214] Accordingly, quinolinic acid was statistically significant in both endogenous category **II** and medication associated category **IV** features.

A total of nineteen medication derived MFs in category **V** and eight MFs in category **IV** were detected in the CSF metabolomic data. Sixteen MFs were identified as APAP and its known phase I/II and minor metabolites in **Article III**, supported by characteristic mass shifts, fragments, and adduct ions.[215–219] Three of the APAP-related MFs lacked high-confidence MS/MS data, but the shared molecular formulae and statistical behavior with well-characterized APAP metabolites (e.g., APAP-glucuronide and APAP-cysteine) supported their classification as APAP-derived MFs in category **V**. The three remaining MFs were identified as doxycycline, an in-source MS fragment ion of doxycycline, and a metabolite of doxycycline, all of which were statistically significant in comparison **A**. Their MS signals were observed only during the samples collected three weeks after treatment initiation, consistent with ongoing treatment and supporting the sensitivity of the analytical method.

In contrast, no MFs associated with ceftriaxone or its metabolites reached statistical significance, although ceftriaxone was detected in treated patients (n = 14) in comparison **A**. Its lower peak areas in MS analyses compared with doxycycline (n = 22) likely reflect both pharmacokinetic and analytical differences. Ceftriaxone is highly protein-bound, limiting CNS penetration, while doxycycline is more lipophilic and penetrates CSF more consistently (~10–30% of serum concentrations).[220,221] Moreover, ceftriaxone's polarity and interactions with proteins and Ca^{2+} ions may impair extraction and increase matrix effects, and ionization efficiency may also differ between compounds.[222–225] Ceftriaxone also exhibits delayed and variable CSF penetration, whereas doxycycline shows more stable exposure due to its longer half-life and more predictable CSF penetration.[221,226,227]

MSE pathway analysis identified changes in glycerophospholipid catabolism and phosphatidylinositol metabolism, consistent with prior phospholipidomic

observations of disturbed LysoPC and SM species in LNB plasma.[228] Enrichment of amino acid-related pathways (tryptophan, alanine/aspartate, glutamate/glutamine, and aspartate/asparagine) was consistent with elevated kynurenine pathway activity in acute LNB and in other tick-borne infections, with differential activation reported in pediatric LNB compared to TBE.[208–211,229,230] Signals of branched-chain fatty acid oxidation suggest alterations in mitochondrial energy metabolism and acylcarnitine accumulation[231], with similar changes reported in early LB serum.[69] MSE analysis also highlighted pathways linked to cerebral organic acidurias that may reflect accumulation of metabolic intermediates and overlap with possible neurotoxic mechanisms of inflamed CSF.

3.6 Translational relevance and future perspectives

All samples used in this doctoral dissertation originated from routine diagnostics, which gives the work clear translational relevance. Rather than relying on idealized research-only materials, the studies were based on specimens that reflect everyday clinical laboratory conditions, including routine pre-analytical handling, storage, and patient heterogeneity. This is particularly important in the context of LNB, where current diagnostics rely heavily on CSF analysis and therefore require lumbar puncture. Approaches based on serum or other routinely collected samples could, in the future, complement existing diagnostics by refining diagnostic suspicion, aiding patient stratification, and potentially reducing the need for invasive procedures in selected situations. At present, however, these methods remain preliminary, and their clinical relevance will ultimately depend not only on analytical performance, but also on whether they improve the broader diagnostic pathway, including timeliness, interpretability, and patient management.

From the perspective of practical implementation, the current workflow is better regarded as a development platform than as a ready-to-implement routine assay. Untargeted metabolomics provides broad molecular information, but its routine clinical use would require robust standardization of sample preparation, data acquisition, quality control, and data analysis. Early implementation would therefore most likely be feasible in specialized or university hospital laboratories with existing analytical and computational expertise. Broader clinical use would likely require further refinement of the present workflow into a targeted and standardized biomarker panel with clearly defined thresholds and a fixed analytical pipeline. In this sense, the present work should be viewed as an important step toward clinical translation rather than a fully mature diagnostic solution.

Regulatory applicability is another key consideration. Clinical implementation requires more than promising biomarker discovery: scientific validity, analytical

performance, and clinical performance must all be demonstrated for the intended use of the method. This requirement applies not only to the analytical assay itself, but also to any future computational model used for classification. The use of routine diagnostic samples is advantageous in this regard, as it increases the relevance of the findings to real clinical practice. Nevertheless, external validation, multicenter reproducibility studies, and prospective evaluation in the intended clinical setting will still be necessary before regulatory implementation becomes realistic.

Cost-effectiveness and cost-utility must be assessed at the level of the entire diagnostic pathway rather than the laboratory test alone. Although untargeted metabolomic workflows have traditionally been associated with relatively high instrumentation costs, MS platforms have become more robust, more accessible, and increasingly attractive for clinical use as automation and throughput have improved. It is also important to distinguish between the discovery phase and the eventual clinical assay. High-resolution MS is primarily needed for untargeted biomarker discovery and characterization, whereas a future routine diagnostic application would most likely rely on a targeted method implemented on a triple quadrupole LC–MS/MS platform. Triple quadrupole instruments remain the dominant platform for targeted clinical MS because of their relative affordability, analytical sensitivity, specificity, and suitability for routine quantitative testing. This is also relevant from a practical and economic perspective, as many university hospital laboratories already have triple quadrupole-based LC–MS/MS platforms in routine use. A targeted assay based on the biomarkers identified in this dissertation could therefore, in principle, be implemented without major additional capital investment, meaning that the main additional costs would arise from assay development, validation, and workflow integration rather than from the acquisition of entirely new instrumentation. If such an assay shortens time to diagnosis, reduces unnecessary invasive procedures or additional investigations, and improves diagnostic confidence, it may also provide meaningful clinical and economic value.

At the same time, the present work has limitations that affect its immediate clinical applicability. Because the samples were obtained from routine clinical diagnostics, they were not stored at −80 °C, which may have affected less stable metabolites. This was nevertheless intentional, as the aim was to develop an approach that could ultimately be applied to routine clinical samples without requiring special handling. The storage conditions are therefore justified from a translational perspective, even if they may have influenced metabolite profiles. In addition, detailed clinical metadata was limited for some control samples, which restricted adjustment for potential confounding variables. The complexity of the studied matrices also suggests that late-eluting, hydrophobic lipids may be underrepresented with the current analytical methods. Furthermore, the limited sample size reduces generalizability, and the ML classifiers require external

validation and calibration across clinically relevant subgroups, including different LB manifestations, other tick-borne diseases, and infectious conditions.

Future work should therefore prioritize larger and more diverse patient cohorts, together with matched pairwise serum–CSF sampling, to strengthen both biological interpretation and clinical relevance. Targeted validation of key biomarkers using PRM or multiple reaction monitoring, together with quantitative UHPLC–MS/MS based on authentic reference standards and MS/MS acquired at multiple collision energies, would improve confidence in metabolite identification. Broader lipidomic coverage may require optimization of post-extraction reconstitution conditions, since reconstitution in an aqueous IS solution may have limited the detection of more hydrophobic lipid species. Furthermore, improved annotation of unknown MFs through molecular networking, ion mobility MS, and artificial intelligence-assisted approaches could help clarify serum- and CSF-associated MFs during both active disease and recovery. Overall, the methods presented in this dissertation should currently be regarded as promising translational approaches rather than immediately deployable routine diagnostic tests. If the identified biomarkers and classification strategies can be validated, standardized, and shown to provide clinical and economic benefit, they may in the future become useful complementary tools in specialized clinical laboratories and contribute to less invasive and more efficient diagnostic pathways.

4 Conclusions

This dissertation presents a preliminary investigation of prominent MF panels and associated metabolic alterations, together with ML classifiers for identifying acute LNB, based on integrating untargeted UHPLC–MS/MS metabolomic analysis of clinically relevant serum and CSF samples. **Article I** was primarily methodological, establishing the untargeted UHPLC–MS/MS workflow and analytical foundation for LNB metabolomics of serum samples. **Article II** applied supervised ML to the serum metabolomic dataset generated in **Article I**. **Article III** extended the serum metabolomics workflow to LNB CSF samples.

A central strength of this study was the paired sample research design in which the samples were obtained from the same individuals at different time points. In the serum analyses, pretreatment LNB samples were paired with samples collected 12 months after treatment (**Articles I** and **II**). For CSF analyses, pretreatment LNB samples were paired with a subset of samples collected three weeks after treatment initiation (**Article III**). Most CSF samples originated from the same LNB patients in the serum cohort. The LNB cohorts were compared against matched non-LNB controls in both serum and CSF, and against other laboratory confirmed CNS infections in CSF, allowing the investigation of disease-specific and general infection biomarkers.

The findings of **Article III** revealed metabolic signatures characterized by tryptophan-kynurenine pathway activity, alterations in lipid-signaling, and markers of mitochondrial energy stress (e.g., acetylcarnitine). Several MFs in CSF samples were associated with CXCL13 concentration, supporting a possible link to neuroinflammatory processes. Acetylcarnitine also displayed sample matrix-specific behavior: levels were highest in acute pretreatment LNB CSF samples and declined after treatment, and were also elevated in other CNS infections. In contrast, serum acetylcarnitine increased in the post-treatment state, indicating distinct compartment-specific metabolic responses during the resolution of inflammation.

The supervised serum ML model classifiers in **Article II** performed well above chance across all comparisons, accompanied by strong AUC/ROC performance. These findings indicate that treatment induces a detectable metabolic shift and that treated LNB retains a distinct serum signature compared with non-LNB individuals.

Although such persistent separations may potentially be useful for recognizing prior episodes of disseminated LB or active disease in diagnostically uncertain cases, they should be interpreted cautiously. Notably, overlapping discriminatory features across classifiers suggest an infection-linked signal rather than a purely treatment-driven classification.

In clinical practice, a rapid UHPLC–MS/MS-based metabolomic approach, complemented by supervised ML, may serve as a practical complementary tool to traditional diagnostics. The paired within-patient design demonstrated that longitudinal MF alterations were detectable in each patient and consistently observed across the cohort, suggesting potential to support diagnostic and treatment decisions when interpreted alongside routine laboratory results and clinical data.

In conclusion, this preliminary UHPLC–MS/MS-based metabolomic study outlines a coherent metabolic framework for both serum and CSF matrices. As a complementary approach to clinical evaluation, targeted feature panels derived from the presented results can support both diagnostics and treatment monitoring. With larger and more diverse cohorts, targeted validation of potential biomarkers, expanded MF coverage, improved identification of currently unknown metabolites, and medication-aware analytics, integrated metabolomics workflows have the potential to strengthen clinical decision-making and improve the assessment of nervous system involvement in LB.

Acknowledgements

This multidisciplinary doctoral dissertation was conducted in the Natural Chemistry Research Group (NCRG), Department of Chemistry, University of Turku, during 2022–2026, in close collaboration with the Institute of Biomedicine, University of Turku. I gratefully acknowledge funding from the Research Council of Finland (project NoveLyme, grant 326569 to Jukka Hytönen), the Sakari Alhopuro Foundation (grants 20230181 and 20200177 to Annukka Pietikäinen), and the University of Turku Foundation (grant 081451), as well as travel grants from the University of Turku's Doctoral Programme in Exact Sciences (EXACTUS), the Turku University Foundation, and the Finnish Mass Spectrometry Society (FMSS). This support was pivotal in enabling me to work full-time on my research and to present my results at numerous conferences.

I am deeply grateful to Docent Satu Kurkela and Dr Linda Ahonen for serving as pre-publication examiners and for sharing their professional expertise and constructive comments, which significantly strengthened this work. I also wish to extend my sincere gratitude to Associate Professor Marko Lehtonen for agreeing to act as the opponent for my dissertation.

To Professor Juha-Pekka Salminen, I owe a special debt of gratitude. During my bachelor's and master's studies, he taught by example that precision is a value, curiosity a method, and collaboration a strength. He asked questions that sharpened my thinking, challenged assumptions that needed testing, and insisted on the kind of methodological care that ultimately defines a good analytical chemist. The trust he placed in me, inviting me into projects, letting me learn by doing, and guiding missteps with patience, was invaluable. Many of us who began our careers under his supervision carry these habits forward.

I have been extraordinarily fortunate to have two excellent supervisors. With Docent Maarit Karonen, my first supervisor, our collaboration throughout this doctoral dissertation and beyond has been seamless and encouraging. As I was completing my master's studies, you asked me if I would be interested in *Borrelia*-related metabolomics in the already ongoing NoveLyme project. That invitation quietly opened a new chapter in my life, something I only recognize in hindsight, and I remain profoundly grateful. Like many colleagues before me, I had the

privilege of learning from your immense knowledge of chemistry and of academic life more broadly. You have been a supervisor of rare warmth and care, always approachable, always willing to listen, and your guidance was matched by an equally important gift: the freedom to experiment, make decisions, and learn to stand on my own as a scientist. Because mass spectrometry lies at the heart of my research, your vast expertise proved foundational, from experimental design and instrumental method development to data processing, interpretation, and critical validation. A small ritual I treasure is our shared comfort with quiet at conference breakfasts, watching the sunrise over the sea.

I am equally indebted to Professor Jukka Hytönen, my second supervisor, from the Institute of Biomedicine. Through NoveLyme, you brought the clinical and biomedical dimensions of this work into clear focus and, with thoughtful care, invited me into your research group, where the dialogue between chemistry and biomedicine became part of my daily work. Thanks to your extensive networks and your talent for building partnerships, we have broadened perspectives, strengthened the science, and extended its impact. Like Maarit, you take exceptionally good care of people, colleagues, students, and collaborators alike, and that people-first leadership has been deeply inspiring.

I would especially like to thank Dr Annukka Pietikäinen for all the scientific contributions to my work and all the sample handling through this dissertation. My sincere thanks also go to Doctoral Researcher Varpu Rinne for the collegiality and friendship we have built. Travelling to numerous conferences together, we shared ideas and questions, celebrated results, and, just as importantly, shared everyday conversations beyond science. Your encouragement, sharp feedback, and good humor have made this journey richer, both professionally and personally.

The multidisciplinary nature of this work has brought many new perspectives to my work and thinking. I am particularly grateful to the biostatisticians Saija Hurme and Tiia Rissanen, especially Tiia, for their expert support in designing and conducting the statistical analyses and for helping me interpret the results more broadly. My thanks also go to Professor Leo Lahti and his group for their expertise in designing and developing the machine learning models. From the clinical side, Dr Elisa Kortela has been an especially valuable collaborator, providing essential clinical insight and guidance. I am also grateful to everyone in the Tick-borne Diseases (TBD Turku) consortium for the wonderful collaboration and the many conversations we have shared. A very special thanks goes to the people who quietly keep scientific work running every day: Kirsi Laaksonen, Kari Loikas, and Mauri Nauma. Your help, patience, and practical wisdom have meant more to me than I can easily put into words, and you have been truly invaluable during my time in the Department of Chemistry.

I have been part of the NCRG since my undergraduate years, nearly a decade now, and it has been a privilege to share both the highs and the inevitable lows of research with so many wonderful colleagues. I want to thank the current group members: Jussi Suvanto, Niko Luntamo, Ville Fock, Isabel Möller, Hilla Nieminen, Sofia Rihko, Martta Airola, Alisa Mäntylä, Emmi Tuomi, and Jaakko Huitti. You have made the lab a place of collaboration, curiosity, and good humor. I also want to thank our former group members: Dr Marica Engström, Dr Jorma Kim, Dr Milla Leppä, Dr Marianna Manninen, Dr Iqbal Bin Imran, Dr Valtteri Virtanen, Dr Juuso Laitila, Dr Suvi Vanhakylä, Dr Mimosa Sillanpää, and Anne Koivuniemi. Your support, advice, and camaraderie along the way have meant a great deal to me.

A particularly heartfelt mention to Marianna, Valtteri, Suvi, Niko, Ville, and Mimosa. From you, I have learned the most, and I am very grateful for your friendship. I feel lucky to have shared so many memorable moments with you along the way.

My thanks also go to the friends I made during my years at the university, especially those who became closest and remain part of my life today: Pietari Huuskonen, Aku Kuusisto, Santeri Salminen, and Joona Arvola. Thank you for all the unforgettable moments we've shared: the late-night talks, spontaneous adventures, and the laughter that somehow always finds a way into even the busiest days. You've kept me grounded, reminded me to enjoy life beyond research, and given me memories I know will last a lifetime. Here's to many more!

To my parents, Mom and Dad, thank you for your unwavering guidance, your life lessons, and for believing in me as I found my own path in the world. You have been the steady foundation on which I could build everything else, and your support has shaped not only my career but the person I have become. I am also deeply grateful to my siblings, who have always been there, offering a listening ear and sharing in both the triumphs and the challenges of life.

To my two wonderful children, Aleksanteri and Aleksandra: thank you for filling every single day with joy, laughter, and endless curiosity. Watching you explore the world and wonder at life is a constant inspiration, and you remind me of the beauty and magic in the simplest moments. You mean more to me than words can ever express.

To my wife, Anniina: you have been my anchor and my greatest companion throughout this entire journey. Your patience, understanding, and boundless generosity have carried me through challenges I could never have faced alone. You have celebrated every small victory and offered comfort through every setback, and I cannot imagine having done this without you. From the bottom of my heart, thank you.

April 2026, Turku

Ilari Kuukkanen

"*Impossible only means that you haven't found the solution yet.* "
- Anonymous

"Science and everyday life cannot and should not be separated."
– Rosalind Franklin

List of References

(1) Stanek, G.; Wormser, G. P.; Gray, J.; Strle, F. Lyme Borreliosis. *The Lancet* **2012**, *379* (9814), 461–473. https://doi.org/10.1016/S0140-6736(11)60103-7.

(2) Gern, L.; Estrada-Peña, A.; Frandsen, F.; Gray, J. S.; Jaenson, T. G. T.; Jongejan, F.; Kahl, O.; Korenberg, E.; Mehl, R.; Nuttall, P. A. European Reservoir Hosts of Borrelia Burgdorferi Sensu Lato. *Zentralblatt für Bakteriologie* **1998**, *287* (3), 196–204. https://doi.org/10.1016/S0934-8840(98)80121-7.

(3) Mysterud, A.; Stigum, V. M.; Jaarsma, R. I.; Sprong, H. Genospecies of Borrelia Burgdorferi Sensu Lato Detected in 16 Mammal Species and Questing Ticks from Northern Europe. *Sci. Rep.* **2019**, *9* (1), 5088. https://doi.org/10.1038/s41598-019-41686-0.

(4) Majerová, K.; Hönig, V.; Houda, M.; Papežík, P.; Fonville, M.; Sprong, H.; Rudenko, N.; Golovchenko, M.; Černá Bolfíková, B.; Hulva, P.; Růžek, D.; Hofmannová, L.; Votýpka, J.; Modrý, D. Hedgehogs, Squirrels, and Blackbirds as Sentinel Hosts for Active Surveillance of Borrelia Miyamotoi and Borrelia Burgdorferi Complex in Urban and Rural Environments. *Microorganisms* **2020**, *8* (12), 1908. https://doi.org/10.3390/microorganisms8121908.

(5) Radolf, J. D.; Caimano, M. J.; Stevenson, B.; Hu, L. T. Of Ticks, Mice and Men: Understanding the Dual-Host Lifestyle of Lyme Disease Spirochaetes. *Nat. Rev. Microbiol.* **2012**, *10* (2), 87–99. https://doi.org/10.1038/nrmicro2714.

(6) Steere, A. C.; Strle, F.; Wormser, G. P.; Hu, L. T.; Branda, J. A.; Hovius, J. W. R.; Li, X.; Mead, P. S. Lyme Borreliosis. *Nat. Rev. Dis. Primers* **2016**, *2*, 16090. https://doi.org/10.1038/nrdp.2016.90.

(7) Rollend, L.; Fish, D.; Childs, J. E. Transovarial Transmission of Borrelia Spirochetes by Ixodes Scapularis: A Summary of the Literature and Recent Observations. *Ticks Tick. Borne. Dis.* **2013**, *4* (1–2), 46–51. https://doi.org/10.1016/j.ttbdis.2012.06.008.

(8) van Duijvendijk, G.; Coipan, C.; Wagemakers, A.; Fonville, M.; Ersöz, J.; Oei, A.; Földvári, G.; Hovius, J.; Takken, W.; Sprong, H. Larvae of Ixodes Ricinus Transmit Borrelia Afzelii and B. Miyamotoi to Vertebrate Hosts. *Parasit. Vectors* **2016**, *9* (1), 97. https://doi.org/10.1186/s13071-016-1389-5.

(9) Kurtenbach, K.; Hanincová, K.; Tsao, J. I.; Margos, G.; Fish, D.; Ogden, N. H. Fundamental Processes in the Evolutionary Ecology of Lyme Borreliosis. *Nat. Rev. Microbiol.* **2006**, *4* (9), 660–669. https://doi.org/10.1038/nrmicro1475.

(10) Mannelli, A.; Bertolotti, L.; Gern, L.; Gray, J. Ecology of *Borrelia Burgdorferi Sensu Lato* in Europe: Transmission Dynamics in Multi-Host Systems, Influence of Molecular Processes and Effects of Climate Change. *FEMS Microbiol. Rev.* **2012**, *36* (4), 837–861. https://doi.org/10.1111/j.1574-6976.2011.00312.x.

(11) Martin, A. M.; Buttke, D.; Raphael, J.; Taylor, K.; Maes, S.; Parise, C. M.; Ginsberg, H. S.; Cross, P. C. Deer Management Generally Reduces Densities of Nymphal Ixodes Scapularis, but Not Prevalence of Infection with Borrelia Burgdorferi Sensu Stricto. *Ticks Tick. Borne. Dis.* **2023**, *14* (5), 102202. https://doi.org/10.1016/j.ttbdis.2023.102202.

(12) Cook, M. Lyme Borreliosis: A Review of Data on Transmission Time after Tick Attachment. *Int. J. Gen. Med.* **2014**, 1. https://doi.org/10.2147/IJGM.S73791.

(13) Spielman, A.; Ribeiro, J. M. C.; Mather, T. N.; Piesman, J. Dissemination and Salivary Delivery of Lyme Disease Spirochetes in Vector Ticks (Acari: Ixodidae). *J. Med. Entomol.* **1987**, *24* (2), 201–205. https://doi.org/10.1093/jmedent/24.2.201.

(14) Barthold, S. W.; Persing, D. H.; Armstrong, A. L.; Peeples, R. A. Kinetics of Borrelia Burgdorferi Dissemination and Evolution of Disease after Intradermal Inoculation of Mice. *Am. J. Pathol.* **1991**, *139* (2), 263–273.

(15) Stanek, G.; Fingerle, V.; Hunfeld, K.-P.; Jaulhac, B.; Kaiser, R.; Krause, A.; Kristoferitsch, W.; O'Connell, S.; Ornstein, K.; Strle, F.; Gray, J. Lyme Borreliosis: Clinical Case Definitions for Diagnosis and Management in Europe. *Clin. Microbiol. Infect.* **2011**, *17* (1), 69–79. https://doi.org/10.1111/j.1469-0691.2010.03175.x.

(16) Strle, F.; Stanek, G. Clinical Manifestations and Diagnosis of Lyme Borreliosis. In *Lyme Borreliosis*; Karger: Basel, 2009; pp 51–110. https://doi.org/10.1159/000213070.

(17) Nadelman, R. B.; Nowakowski, J.; Forseter, G.; Goldberg, N. S.; Bittker, S.; Cooper, D.; Aguero-Rosenfeld, M.; Wormser, G. P. The Clinical Spectrum of Early Lyme Borreliosis in Patients with Culture-Confirmed Erythema Migrans. *Am. J. Med.* **1996**, *100* (5), 502–508. https://doi.org/10.1016/S0002-9343(95)99915-9.

(18) Nadelman, R. B.; Wormser, G. P. Erythema Migrans and Early Lyme Disease. *Am. J. Med.* **1995**, *98* (4), 15S-24S. https://doi.org/10.1016/S0002-9343(99)80040-0.

(19) Branda, J. A.; Steere, A. C. Laboratory Diagnosis of Lyme Borreliosis. *Clin. Microbiol. Rev.* **2021**, *34* (2). https://doi.org/10.1128/CMR.00018-19.

(20) Kullberg, B. J.; Vrijmoeth, H. D.; van de Schoor, F.; Hovius, J. W. Lyme Borreliosis: Diagnosis and Management. *BMJ* **2020**, m1041. https://doi.org/10.1136/bmj.m1041.

(21) Feder, H. M.; Gerber, M. A.; Luger, S. W.; Ryan, R. W. Persistence of Serum Antibodies to Borrelia Burgdorferi in Patients Treated for Lyme Disease. *Clinical Infectious Diseases* **1992**, *15* (5), 788–793. https://doi.org/10.1093/clind/15.5.788.

(22) Kalish, R. A.; McHugh, G.; Granquist, J.; Shea, B.; Ruthazer, R.; Steere, A. C. Persistence of Immunoglobulin M or Immunoglobulin G Antibody Responses to Borrelia Burgdorferi 10–20 Years after Active Lyme Disease. *Clinical Infectious Diseases* **2001**, *33* (6), 780–785. https://doi.org/10.1086/322669.

(23) Markowicz, M.; Reiter, M.; Gamper, J.; Stanek, G.; Stockinger, H. Persistent Anti- *Borrelia* IgM Antibodies without Lyme Borreliosis in the Clinical and Immunological Context. *Microbiol. Spectr.* **2021**, *9* (3). https://doi.org/10.1128/Spectrum.01020-21.

(24) Koedel, U.; Fingerle, V.; Pfister, H.-W. Lyme Neuroborreliosis—Epidemiology, Diagnosis and Management. *Nat. Rev. Neurol.* **2015**, *11* (8), 446–456. https://doi.org/10.1038/nrneurol.2015.121.

(25) Halperin, J. J. Diagnosis and Management of Lyme Neuroborreliosis. *Expert Rev. Anti. Infect. Ther.* **2018**, *16* (1), 5–11. https://doi.org/10.1080/14787210.2018.1417836.

(26) Stanek, G.; Strle, F. Lyme Borreliosis–from Tick Bite to Diagnosis and Treatment. *FEMS Microbiol. Rev.* **2018**, *42* (3), 233–258. https://doi.org/10.1093/femsre/fux047.

(27) Berglund, J.; Eitrem, R.; Ornstein, K.; Lindberg, A.; Ringnér, Å.; Elmrud, H.; Carlsson, M.; Runehagen, A.; Svanborg, C.; Norrby, R. An Epidemiologic Study of Lyme Disease in Southern Sweden. *New England Journal of Medicine* **1995**, *333* (20), 1319–1324. https://doi.org/10.1056/NEJM199511163332004.

(28) Henningsson, A. J.; Malmvall, B.-E.; Ernerudh, J.; Matussek, A.; Forsberg, P. Neuroborreliosis—an Epidemiological, Clinical and Healthcare Cost Study from an Endemic Area in the South-East of Sweden. *Clinical Microbiology and Infection* **2010**, *16* (8), 1245–1251. https://doi.org/10.1111/j.1469-0691.2009.03059.x.

(29) Tveitnes, D.; Natås, O. B.; Skadberg, Ø.; Øymar, K. Lyme Meningitis, the Major Cause of Childhood Meningitis in an Endemic Area: A Population Based Study. *Arch. Dis. Child.* **2012**, *97* (3), 215–220. https://doi.org/10.1136/archdischild-2011-300526.

(30) Strle, F.; Ruzic-Sabljic, E.; Cimperman, J.; Lotric-Furlan, S.; Maraspin, V. Comparison of Findings for Patients with Borrelia Garinii and Borrelia Afzelii Isolated from Cerebrospinal Fluid. *Clinical Infectious Diseases* **2006**, *43* (6), 704–710. https://doi.org/10.1086/506936.

(31) van Dam, A. P.; Kuiper, H.; Vos, K.; Widjojokusumo, A.; de Jongh, B. M.; Spanjaard, L.; Ramselaar, A. C. P.; Kramer, M. D.; Dankert, J. Different Genospecies of Borrelia Burgdorferi Are Associated with Distinct Clinical Manifestations of Lyme Borreliosis. *Clinical Infectious Diseases* **1993**, *17* (4), 708–717. https://doi.org/10.1093/clinids/17.4.708.

(32) Balmelli, T.; Piffaretti, J.-C. Association between Different Clinical Manifestations of Lyme Disease and Different Species of Borrelia Burgdorferi Sensu Lato. *Res. Microbiol.* **1995**, *146* (4), 329–340. https://doi.org/10.1016/0923-2508(96)81056-4.

(33) Mygland, Å.; Ljøstad, U.; Fingerle, V.; Rupprecht, T.; Schmutzhard, E.; Steiner, I. EFNS Guidelines on the Diagnosis and Management of European Lyme Neuroborreliosis. *Eur. J. Neurol.* **2010**, *17* (1). https://doi.org/10.1111/j.1468-1331.2009.02862.x.

(34) Hytönen, J.; Kortela, E.; Waris, M.; Puustinen, J.; Salo, J.; Oksi, J. CXCL13 and Neopterin Concentrations in Cerebrospinal Fluid of Patients with Lyme Neuroborreliosis and Other Diseases That Cause Neuroinflammation. *J. Neuroinflammation* **2014**, *11* (1), 103. https://doi.org/10.1186/1742-2094-11-103.

(35) Waiß, C.; Ströbele, B.; Graichen, U.; Klee, S.; Gartlehner, J.; Sonntagbauer, E.; Hirschbichler, S.; Tinchon, A.; Kacar, E.; Wuchty, B.; Novotna, B.; Kühn, Z.; Sellner, J.; Struhal, W.; Bancher, C.; Schnider, P.; Asenbaum-Nan, S.; Oberndorfer, S. CXCL13 as a Biomarker in the Diagnostics of European Lyme Neuroborreliosis - A Prospective Multicentre Study in Austria. *J. Cent. Nerv. Syst. Dis.* **2024**, *16*. https://doi.org/10.1177/11795735241247026.

(36) Pietikäinen, A.; Oksi, J.; Hytönen, J. Point-of-Care Testing for CXCL13 in Lyme Neuroborreliosis. *Diagn. Microbiol. Infect. Dis.* **2018**, *91* (3), 226–228. https://doi.org/10.1016/j.diagmicrobio.2018.02.013.

(37) Cyster, J. G.; Ansel, K. M.; Reif, K.; Ekland, E. H.; Hyman, P. L.; Tang, H. L.; Luther, S. A.; Ngo, V. N. Follicular Stromal Cells and Lymphocyte Homing to Follicles. *Immunol. Rev.* **2000**, *176* (1), 181–193. https://doi.org/10.1034/j.1600-065X.2000.00618.x.

(38) Gunn, M. D.; Ngo, V. N.; Ansel, K. M.; Ekland, E. H.; Cyster, J. G.; Williams, L. T. A B-Cell-Homing Chemokine Made in Lymphoid Follicles Activates Burkitt's Lymphoma Receptor-1. *Nature* **1998**, *391* (6669), 799–803. https://doi.org/10.1038/35876.

(39) Rupprecht, T. A.; Koedel, U.; Fingerle, V.; Pfister, H.-W. The Pathogenesis of Lyme Neuroborreliosis: From Infection to Inflammation. *Molecular Medicine* **2008**, *14* (3–4), 205–212. https://doi.org/10.2119/2007-00091.Rupprecht.

(40) Schmidt, C.; Plate, A.; Angele, B.; Pfister, H.-W.; Wick, M.; Koedel, U.; Rupprecht, T. A. A Prospective Study on the Role of CXCL13 in Lyme Neuroborreliosis. *Neurology* **2011**, *76* (12), 1051–1058. https://doi.org/10.1212/WNL.0b013e318211c39a.

(41) Smíšková, D.; Džupová, O.; Moravcová, L.; Pícha, D. Cerebrospinal Fluid CXCL13 in Non-Borrelial Central Nervous System Infections: Contribution of CXCL13 to the Differential Diagnosis. *Infect. Dis.* **2023**, *55* (8), 551–558. https://doi.org/10.1080/23744235.2023.2222178.

(42) Hartman, T. E.; Lees, H. J. Introduction of Metabolomics: An Overview. In *Metabolomics*; Springer International Publishing: Cham, 2023; pp 1–37. https://doi.org/10.1007/978-3-031-39094-4_1.

(43) Wishart, D. S. Metabolomics for Investigating Physiological and Pathophysiological Processes. *Physiol. Rev.* **2019**, *99* (4), 1819–1875. https://doi.org/10.1152/physrev.00035.2018.

(44) Manzoni, C.; Kia, D. A.; Vandrovcova, J.; Hardy, J.; Wood, N. W.; Lewis, P. A.; Ferrari, R. Genome, Transcriptome and Proteome: The Rise of Omics Data and Their Integration in Biomedical Sciences. *Brief. Bioinform.* **2018**, *19* (2), 286–302. https://doi.org/10.1093/bib/bbw114.

(45) Pinu, F. R.; Beale, D. J.; Paten, A. M.; Kouremenos, K.; Swarup, S.; Schirra, H. J.; Wishart, D. Systems Biology and Multi-Omics Integration: Viewpoints from the Metabolomics Research Community. *Metabolites* **2019**, *9* (4), 76. https://doi.org/10.3390/metabo9040076.

(46) Nalbantoglu, S. Metabolomics: Basic Principles and Strategies. In *Molecular Medicine*; IntechOpen, 2019. https://doi.org/10.5772/intechopen.88563.
(47) Lin, C.; Tian, Q.; Guo, S.; Xie, D.; Cai, Y.; Wang, Z.; Chu, H.; Qiu, S.; Tang, S.; Zhang, A. Metabolomics for Clinical Biomarker Discovery and Therapeutic Target Identification. *Molecules* **2024**, *29* (10), 2198. https://doi.org/10.3390/molecules29102198.
(48) Rinschen, M. M.; Ivanisevic, J.; Giera, M.; Siuzdak, G. Identification of Bioactive Metabolites Using Activity Metabolomics. *Nat. Rev. Mol. Cell Biol.* **2019**, *20* (6), 353–367. https://doi.org/10.1038/s41580-019-0108-4.
(49) Dunn, W. B.; Broadhurst, D.; Begley, P.; Zelena, E.; Francis-McIntyre, S.; Anderson, N.; Brown, M.; Knowles, J. D.; Halsall, A.; Haselden, J. N.; Nicholls, A. W.; Wilson, I. D.; Kell, D. B.; Goodacre, R. Procedures for Large-Scale Metabolic Profiling of Serum and Plasma Using Gas Chromatography and Liquid Chromatography Coupled to Mass Spectrometry. *Nat. Protoc.* **2011**, *6* (7), 1060–1083. https://doi.org/10.1038/nprot.2011.335.
(50) Nagana Gowda, G. A.; Raftery, D. Recent Advances in NMR-Based Metabolomics. *Anal. Chem.* **2017**, *89* (1), 490–510. https://doi.org/10.1021/acs.analchem.6b04420.
(51) Gika, H. G.; Theodoridis, G. A.; Plumb, R. S.; Wilson, I. D. Current Practice of Liquid Chromatography–Mass Spectrometry in Metabolomics and Metabonomics. *J. Pharm. Biomed. Anal.* **2014**, *87*, 12–25. https://doi.org/10.1016/j.jpba.2013.06.032.
(52) Fiehn, O. Metabolomics by Gas Chromatography–Mass Spectrometry: Combined Targeted and Untargeted Profiling. *Curr. Protoc. Mol. Biol.* **2016**, *114* (1), 30.4.1-30.4.32. https://doi.org/10.1002/0471142727.mb3004s114.
(53) Halket, J. M.; Waterman, D.; Przyborowska, A. M.; Patel, R. K. P.; Fraser, P. D.; Bramley, P. M. Chemical Derivatization and Mass Spectral Libraries in Metabolic Profiling by GC/MS and LC/MS/MS. *J. Exp. Bot.* **2005**, *56* (410), 219–243. https://doi.org/10.1093/jxb/eri069.
(54) Hemmer, S.; Manier, S. K.; Wagmann, L.; Meyer, M. R. Comparison of Reversed-Phase, Hydrophilic Interaction, and Porous Graphitic Carbon Chromatography Columns for an Untargeted Toxicometabolomics Study in Pooled Human Liver Microsomes, Rat Urine, and Rat Plasma. *Metabolomics* **2024**, *20* (3), 49. https://doi.org/10.1007/s11306-024-02115-0.
(55) Hosseinkhani, F.; Huang, L.; Dubbelman, A.-C.; Guled, F.; Harms, A. C.; Hankemeier, T. Systematic Evaluation of HILIC Stationary Phases for Global Metabolomics of Human Plasma. *Metabolites* **2022**, *12* (2), 165. https://doi.org/10.3390/metabo12020165.
(56) Naser, F. J.; Mahieu, N. G.; Wang, L.; Spalding, J. L.; Johnson, S. L.; Patti, G. J. Two Complementary Reversed-Phase Separations for Comprehensive Coverage of the Semipolar and Nonpolar Metabolome. *Anal. Bioanal. Chem.* **2018**, *410* (4), 1287–1297. https://doi.org/10.1007/s00216-017-0768-x.
(57) Zhou, B.; Xiao, J. F.; Tuli, L.; Ressom, H. W. LC-MS-Based Metabolomics. *Mol. Biosyst.* **2011**, *8* (2), 470–481. https://doi.org/10.1039/C1MB05350G.
(58) Laaniste, A.; Leito, I.; Kruve, A. ESI Outcompetes Other Ion Sources in LC/MS Trace Analysis. *Anal. Bioanal. Chem.* **2019**, *411* (16), 3533–3542. https://doi.org/10.1007/s00216-019-01832-z.
(59) Kiontke, A.; Billig, S.; Birkemeyer, C. Response in Ambient Low Temperature Plasma Ionization Compared to Electrospray and Atmospheric Pressure Chemical Ionization for Mass Spectrometry. *Int. J. Anal. Chem.* **2018**, *2018*, 1–18. https://doi.org/10.1155/2018/5647536.
(60) Zhang, H.; Lu, K. H.; Ebbini, M.; Huang, P.; Lu, H.; Li, L. Mass Spectrometry Imaging for Spatially Resolved Multi-Omics Molecular Mapping. *npj Imaging* **2024**, *2* (1), 20. https://doi.org/10.1038/s44303-024-00025-3.
(61) Khajavinia, A.; El-Aneed, A. Carbon-Based Nanoparticles and Their Surface-Modified Counterparts as MALDI Matrices. *Anal. Chem.* **2023**, *95* (1), 100–114. https://doi.org/10.1021/acs.analchem.2c04537.
(62) Leeflang, M. M. G.; Ang, C. W.; Berkhout, J.; Bijlmer, H. A.; Van Bortel, W.; Brandenburg, A. H.; Van Burgel, N. D.; Van Dam, A. P.; Dessau, R. B.; Fingerle, V.; Hovius, J. W. R.; Jaulhac, B.; Meijer, B.; Van Pelt, W.; Schellekens, J. F. P.; Spijker, R.; Stelma, F. F.; Stanek, G.; Verduyn-

Lunel, F.; Zeller, H.; Sprong, H. The Diagnostic Accuracy of Serological Tests for Lyme Borreliosis in Europe: A Systematic Review and Meta-Analysis. *BMC Infect. Dis.* **2016**, *16* (1), 140. https://doi.org/10.1186/s12879-016-1468-4.

(63) Roos, K. L.; Berger, J. R. Is the Presence of Antibodies in CSF Sufficient to Make a Definitive Diagnosis of Lyme Disease? *Neurology* **2007**, *69* (10), 949–950. https://doi.org/10.1212/01.wnl.0000271901.94853.24.

(64) Skarpaas, T.; Ljøstad, U.; Søbye, M.; Mygland, Å. Sensitivity and Specificity of a Commercial C6 Peptide Enzyme Immuno Assay in Diagnosis of Acute Lyme Neuroborreliosis. *European Journal of Clinical Microbiology & Infectious Diseases* **2007**, *26* (9), 675–677. https://doi.org/10.1007/s10096-007-0336-y.

(65) Henningsson, A. J.; Christiansson, M.; Tjernberg, I.; Löfgren, S.; Matussek, A. Laboratory Diagnosis of Lyme Neuroborreliosis: A Comparison of Three CSF Anti-Borrelia Antibody Assays. *European Journal of Clinical Microbiology & Infectious Diseases* **2014**, *33* (5), 797–803. https://doi.org/10.1007/s10096-013-2014-6.

(66) Moore, A.; Nelson, C.; Molins, C.; Mead, P.; Schriefer, M. Current Guidelines, Common Clinical Pitfalls, and Future Directions for Laboratory Diagnosis of Lyme Disease, United States. *Emerg. Infect. Dis.* **2016**, *22* (7). https://doi.org/10.3201/eid2207.151694.

(67) Nigrovic, L. E.; Lewander, D. P.; Balamuth, F.; Neville, D. N.; Levas, M. N.; Bennett, J. E.; Garro, A. The Lyme Disease Polymerase Chain Reaction Test Has Low Sensitivity. *Vector-Borne and Zoonotic Diseases* **2020**, *20* (4), 310–313. https://doi.org/10.1089/vbz.2019.2547.

(68) Molins, C. R.; Ashton, L. V.; Wormser, G. P.; Hess, A. M.; Delorey, M. J.; Mahapatra, S.; Schriefer, M. E.; Belisle, J. T. Development of a Metabolic Biosignature for Detection of Early Lyme Disease. *Clinical Infectious Diseases* **2015**, *60* (12), 1767–1775. https://doi.org/10.1093/cid/civ185.

(69) Fitzgerald, B. L.; Molins, C. R.; Islam, M. N.; Graham, B.; Hove, P. R.; Wormser, G. P.; Hu, L.; Ashton, L. V.; Belisle, J. T. Host Metabolic Response in Early Lyme Disease. *J. Proteome Res.* **2020**, *19* (2), 610–623. https://doi.org/10.1021/acs.jproteome.9b00470.

(70) Fitzgerald, B. L.; Graham, B.; Delorey, M. J.; Pegalajar-Jurado, A.; Islam, M. N.; Wormser, G. P.; Aucott, J. N.; Rebman, A. W.; Soloski, M. J.; Belisle, J. T.; Molins, C. R. Metabolic Response in Patients With Post-Treatment Lyme Disease Symptoms/Syndrome. *Clin. Infect. Dis.* **2021**, *73* (7), e2342–e2349. https://doi.org/10.1093/cid/ciaa1455.

(71) Pegalajar-Jurado, A.; Fitzgerald, B. L.; Islam, M. N.; Belisle, J. T.; Wormser, G. P.; Waller, K. S.; Ashton, L. V.; Webb, K. J.; Delorey, M. J.; Clark, R. J.; Molins, C. R. Identification of Urine Metabolites as Biomarkers of Early Lyme Disease. *Sci. Rep.* **2018**, *8* (1), 12204. https://doi.org/10.1038/s41598-018-29713-y.

(72) Kerstholt, M.; Vrijmoeth, H.; Lachmandas, E.; Oosting, M.; Lupse, M.; Flonta, M.; Dinarello, C. A.; Netea, M. G.; Joosten, L. A. B. Role of Glutathione Metabolism in Host Defense against *Borrelia Burgdorferi* Infection. *Proceedings of the National Academy of Sciences* **2018**, *115* (10). https://doi.org/10.1073/pnas.1720833115.

(73) Glader, O.; Puljula, E.; Jokioja, J.; Karonen, M.; Sinkkonen, J.; Hytönen, J. NMR Metabolome of Borrelia Burgdorferi in Vitro and in Vivo in Mice. *Sci. Rep.* **2019**, *9* (1), 8049. https://doi.org/10.1038/s41598-019-44540-5.

(74) Pietikäinen, A.; Glader, O.; Kortela, E.; Kanerva, M.; Oksi, J.; Hytönen, J. Borrelia Burgdorferi Specific Serum and Cerebrospinal Fluid Antibodies in Lyme Neuroborreliosis. *Diagn. Microbiol. Infect. Dis.* **2022**, *104* (3), 115782. https://doi.org/10.1016/j.diagmicrobio.2022.115782.

(75) de Souza, H. M. R.; Pereira, T. T. P.; de Sá, H. C.; Alves, M. A.; Garrett, R.; Canuto, G. A. B. Critical Factors in Sample Collection and Preparation for Clinical Metabolomics of Underexplored Biological Specimens. *Metabolites* **2024**, *14* (1), 36. https://doi.org/10.3390/metabo14010036.

(76) Sitnikov, D. G.; Monnin, C. S.; Vuckovic, D. Systematic Assessment of Seven Solvent and Solid-Phase Extraction Methods for Metabolomics Analysis of Human Plasma by LC-MS. *Sci. Rep.* **2016**, *6* (1), 38885. https://doi.org/10.1038/srep38885.

(77) Tsakelidou, E.; Virgiliou, C.; Valianou, L.; Gika, H.; Raikos, N.; Theodoridis, G. Sample Preparation Strategies for the Effective Quantitation of Hydrophilic Metabolites in Serum by Multi-Targeted HILIC-MS/MS. *Metabolites* **2017**, *7* (2), 13. https://doi.org/10.3390/metabo7020013.

(78) Beale, D. J.; Pinu, F. R.; Kouremenos, K. A.; Poojary, M. M.; Narayana, V. K.; Boughton, B. A.; Kanojia, K.; Dayalan, S.; Jones, O. A. H.; Dias, D. A. Review of Recent Developments in GC–MS Approaches to Metabolomics-Based Research. *Metabolomics* **2018**, *14* (11), 152. https://doi.org/10.1007/s11306-018-1449-2.

(79) Best, C. H.; Taylor, N. B.; West, J. B. *Best and Taylor's Physiological Basis of Medical Practice*, 11th ed.; West, J., Ed.; Waverly Press: Baltimore MD, USA, 1985.

(80) Hagn, G.; Meier-Menches, S. M.; Plessl-Walder, G.; Mitra, G.; Mohr, T.; Preindl, K.; Schlatter, A.; Schmidl, D.; Gerner, C.; Garhöfer, G.; Bileck, A. Plasma Instead of Serum Avoids Critical Confounding of Clinical Metabolomics Studies by Platelets. *J. Proteome Res.* **2024**, *23* (8), 3064–3075. https://doi.org/10.1021/acs.jproteome.3c00761.

(81) Psychogios, N.; Hau, D. D.; Peng, J.; Guo, A. C.; Mandal, R.; Bouatra, S.; Sinelnikov, I.; Krishnamurthy, R.; Eisner, R.; Gautam, B.; Young, N.; Xia, J.; Knox, C.; Dong, E.; Huang, P.; Hollander, Z.; Pedersen, T. L.; Smith, S. R.; Bamforth, F.; Greiner, R.; McManus, B.; Newman, J. W.; Goodfriend, T.; Wishart, D. S. The Human Serum Metabolome. *PLoS One* **2011**, *6* (2), e16957. https://doi.org/10.1371/journal.pone.0016957.

(82) Yu, Z.; Kastenmüller, G.; He, Y.; Belcredi, P.; Möller, G.; Prehn, C.; Mendes, J.; Wahl, S.; Roemisch-Margl, W.; Ceglarek, U.; Polonikov, A.; Dahmen, N.; Prokisch, H.; Xie, L.; Li, Y.; Wichmann, H.-E.; Peters, A.; Kronenberg, F.; Suhre, K.; Adamski, J.; Illig, T.; Wang-Sattler, R. Differences between Human Plasma and Serum Metabolite Profiles. *PLoS One* **2011**, *6* (7), e21230. https://doi.org/10.1371/journal.pone.0021230.

(83) Hooshmand, K.; Xu, J.; Simonsen, A. H.; Wretlind, A.; de Zawadzki, A.; Sulek, K.; Hasselbalch, S. G.; Legido-Quigley, C. Human Cerebrospinal Fluid Sample Preparation and Annotation for Integrated Lipidomics and Metabolomics Profiling Studies. *Mol. Neurobiol.* **2024**, *61* (4), 2021–2032. https://doi.org/10.1007/s12035-023-03666-4.

(84) Mandal, R.; Guo, A. C.; Chaudhary, K. K.; Liu, P.; Yallou, F. S.; Dong, E.; Aziat, F.; Wishart, D. S. Multi-Platform Characterization of the Human Cerebrospinal Fluid Metabolome: A Comprehensive and Quantitative Update. *Genome Med.* **2012**, *4* (4), 38. https://doi.org/10.1186/gm337.

(85) Otto, C.; Kalantzis, R.; Kübler-Weller, D.; Kühn, A. A.; Böld, T.; Regler, A.; Strathmeyer, S.; Wittmann, J.; Ruprecht, K.; Heelemann, S. Comprehensive Analysis of the Cerebrospinal Fluid and Serum Metabolome in Neurological Diseases. *J. Neuroinflammation* **2024**, *21* (1), 234. https://doi.org/10.1186/s12974-024-03218-0.

(86) Židó, M.; Kačer, D.; Valeš, K.; Svobodová, Z.; Zimová, D.; Štětkárová, I. Metabolomics of Cerebrospinal Fluid in Multiple Sclerosis Compared With Healthy Controls: A Pilot Study. *Front. Neurol.* **2022**, *13*. https://doi.org/10.3389/fneur.2022.874121.

(87) Berezhnoy, G.; Laske, C.; Trautwein, C. Metabolomic Profiling of CSF and Blood Serum Elucidates General and Sex-Specific Patterns for Mild Cognitive Impairment and Alzheimer's Disease Patients. *Front. Aging Neurosci.* **2023**, *15*. https://doi.org/10.3389/fnagi.2023.1219718.

(88) Staal, S. L.; Olie, S. E.; van Weeghel, M.; Schomakers, B. V.; Vaz, F. M.; van de Beek, D.; Brouwer, M. C. Cerebrospinal Fluid Metabolome in Central Nervous System Infections: A Study of Diagnostic Accuracy. *Ann. Neurol.* **2025**, *98* (4), 851–863. https://doi.org/10.1002/ana.27291.

(89) Anwardeen, N. R.; Diboun, I.; Mokrab, Y.; Althani, A. A.; Elrayess, M. A. Statistical Methods and Resources for Biomarker Discovery Using Metabolomics. *BMC Bioinformatics* **2023**, *24* (1), 250. https://doi.org/10.1186/s12859-023-05383-0.

(90) Vo, D.-K.; Trinh, K. T. L. Emerging Biomarkers in Metabolomics: Advancements in Precision Health and Disease Diagnosis. *Int. J. Mol. Sci.* **2024**, *25* (23), 13190. https://doi.org/10.3390/ijms252313190.
(91) Beger, R. D.; Goodacre, R.; Jones, C. M.; Lippa, K. A.; Mayboroda, O. A.; O'Neill, D.; Najdekr, L.; Ntai, I.; Wilson, I. D.; Dunn, W. B. Analysis Types and Quantification Methods Applied in UHPLC-MS Metabolomics Research: A Tutorial. *Metabolomics* **2024**, *20* (5), 95. https://doi.org/10.1007/s11306-024-02155-6.
(92) Allwood, J. W.; Williams, A.; Uthe, H.; van Dam, N. M.; Mur, L. A. J.; Grant, M. R.; Pétriacq, P. Unravelling Plant Responses to Stress—The Importance of Targeted and Untargeted Metabolomics. *Metabolites* **2021**, *11* (8), 558. https://doi.org/10.3390/metabo11080558.
(93) Dowling, G. M.; Meyer, M. R. Editorial: Current Trends in Targeted and Non-Targeted Metabolomics in Analytical Toxicology. *Front. Mol. Biosci.* **2025**, *12*. https://doi.org/10.3389/fmolb.2025.1614399.
(94) Almontashiri, N. A. M.; Zha, L.; Young, K.; Law, T.; Kellogg, M. D.; Bodamer, O. A.; Peake, R. W. A. Clinical Validation of Targeted and Untargeted Metabolomics Testing for Genetic Disorders: A 3 Year Comparative Study. *Sci. Rep.* **2020**, *10* (1), 9382. https://doi.org/10.1038/s41598-020-66401-2.
(95) Le Gouellec, A.; Plazy, C.; Toussaint, B. What Clinical Metabolomics Will Bring to the Medicine of Tomorrow. *Frontiers in Analytical Science* **2023**, *3*. https://doi.org/10.3389/frans.2023.1142606.
(96) Xiadong Feng. Improving Quantification and Identification in Metabolomics, University of Groningen, 2023. https://doi.org/10.33612/diss.560940205.
(97) Defossez, E.; Bourquin, J.; von Reuss, S.; Rasmann, S.; Glauser, G. Eight Key Rules for Successful Data-dependent Acquisition in Mass Spectrometry-based Metabolomics. *Mass Spectrom. Rev.* **2023**, *42* (1), 131–143. https://doi.org/10.1002/mas.21715.
(98) Wu, Y.; Wang, Y. A Comparative Study of Data-Independent Acquisition and Data-Dependent Acquisition in Liquid Chromatography-Mass Spectrometry-Based Untargeted Metabolomics Analysis of Panax Genus Sample. *Anal. Bioanal. Chem.* **2025**, *417* (14), 3215–3228. https://doi.org/10.1007/s00216-025-05861-9.
(99) E. Olajide, O.; Y. Kartowikromo, K.; M. Hamid, A. Ion Mobility Mass Spectrometry: Instrumentation and Applications. In *Electron Microscopes, Spectroscopy and Their Applications*; IntechOpen, 2023. https://doi.org/10.5772/intechopen.1002767.
(100) Moses, T.; Burgess, K. Right in Two: Capabilities of Ion Mobility Spectrometry for Untargeted Metabolomics. *Front. Mol. Biosci.* **2023**, *10*. https://doi.org/10.3389/fmolb.2023.1230282.
(101) Naylor, C. N.; Nagy, G. Recent Advances in High-resolution Traveling Wave-based Ion Mobility Separations Coupled to Mass Spectrometry. *Mass Spectrom. Rev.* **2025**, *44* (4), 581–598. https://doi.org/10.1002/mas.21902.
(102) Verenchikov, A. N.; Kirillov, S. N.; Vorobyev, A. V.; Makarov, V. V.; Yavor, M. I.; Tonge, R. P.; Langridge, J. I. Multi Reflecting TOF MS Approaching Resolution of 1,000,000 in a Wide Mass Range. *Int. J. Mass Spectrom.* **2025**, *508*, 117395. https://doi.org/10.1016/j.ijms.2024.117395.
(103) Heil, L. R.; Damoc, E.; Arrey, T. N.; Pashkova, A.; Denisov, E.; Petzoldt, J.; Peterson, A. C.; Hsu, C.; Searle, B. C.; Shulman, N.; Riffle, M.; Connolly, B.; MacLean, B. X.; Remes, P. M.; Senko, M. W.; Stewart, H. I.; Hock, C.; Makarov, A. A.; Hermanson, D.; Zabrouskov, V.; Wu, C. C.; MacCoss, M. J. Evaluating the Performance of the Astral Mass Analyzer for Quantitative Proteomics Using Data-Independent Acquisition. *J. Proteome Res.* **2023**, *22* (10), 3290–3300. https://doi.org/10.1021/acs.jproteome.3c00357.
(104) Alseekh, S.; Aharoni, A.; Brotman, Y.; Contrepois, K.; D'Auria, J.; Ewald, J.; C. Ewald, J.; Fraser, P. D.; Giavalisco, P.; Hall, R. D.; Heinemann, M.; Link, H.; Luo, J.; Neumann, S.; Nielsen, J.; Perez de Souza, L.; Saito, K.; Sauer, U.; Schroeder, F. C.; Schuster, S.; Siuzdak, G.; Skirycz, A.; Sumner, L. W.; Snyder, M. P.; Tang, H.; Tohge, T.; Wang, Y.; Wen, W.; Wu, S.;

Xu, G.; Zamboni, N.; Fernie, A. R. Mass Spectrometry-Based Metabolomics: A Guide for Annotation, Quantification and Best Reporting Practices. *Nat. Methods* **2021**, *18* (7), 747–756. https://doi.org/10.1038/s41592-021-01197-1.

(105) Katajamaa, M.; Orešič, M. Data Processing for Mass Spectrometry-Based Metabolomics. *J. Chromatogr. A* **2007**, *1158* (1–2), 318–328. https://doi.org/10.1016/j.chroma.2007.04.021.

(106) Pluskal, T.; Castillo, S.; Villar-Briones, A.; Orešič, M. MZmine 2: Modular Framework for Processing, Visualizing, and Analyzing Mass Spectrometry-Based Molecular Profile Data. *BMC Bioinformatics* **2010**, *11* (1), 395. https://doi.org/10.1186/1471-2105-11-395.

(107) Antonelli, J.; Claggett, B. L.; Henglin, M.; Kim, A.; Ovsak, G.; Kim, N.; Deng, K.; Rao, K.; Tyagi, O.; Watrous, J. D.; Lagerborg, K. A.; Hushcha, P. V.; Demler, O. V.; Mora, S.; Niiranen, T. J.; Pereira, A. C.; Jain, M.; Cheng, S. Statistical Workflow for Feature Selection in Human Metabolomics Data. *Metabolites* **2019**, *9* (7), 143. https://doi.org/10.3390/metabo9070143.

(108) Westerhuis, J. A.; Hoefsloot, H. C. J.; Smit, S.; Vis, D. J.; Smilde, A. K.; van Velzen, E. J. J.; van Duijnhoven, J. P. M.; van Dorsten, F. A. Assessment of PLSDA Cross Validation. *Metabolomics* **2008**, *4* (1), 81–89. https://doi.org/10.1007/s11306-007-0099-6.

(109) Thévenot, E. A.; Roux, A.; Xu, Y.; Ezan, E.; Junot, C. Analysis of the Human Adult Urinary Metabolome Variations with Age, Body Mass Index, and Gender by Implementing a Comprehensive Workflow for Univariate and OPLS Statistical Analyses. *J. Proteome Res.* **2015**, *14* (8), 3322–3335. https://doi.org/10.1021/acs.jproteome.5b00354.

(110) Xu, R.; Zhang, S.; Li, J.; Zhu, J. Plasma and Serum Metabolic Analysis of Healthy Adults Shows Characteristic Profiles by Subjects' Sex and Age. *Metabolomics* **2024**, *20* (2), 43. https://doi.org/10.1007/s11306-024-02108-z.

(111) Navarro, S. L.; Nagana Gowda, G. A.; Bettcher, L. F.; Pepin, R.; Nguyen, N.; Ellenberger, M.; Zheng, C.; Tinker, L. F.; Prentice, R. L.; Huang, Y.; Yang, T.; Tabung, F. K.; Chan, Q.; Loo, R. L.; Liu, S.; Wactawski-Wende, J.; Lampe, J. W.; Neuhouser, M. L.; Raftery, D. Demographic, Health and Lifestyle Factors Associated with the Metabolome in Older Women. *Metabolites* **2023**, *13* (4), 514. https://doi.org/10.3390/metabo13040514.

(112) Bongaerts, M.; Bonte, R.; Demirdas, S.; Jacobs, E.; Oussoren, E.; van der Ploeg, A.; Wagenmakers, M.; Hofstra, R.; Blom, H.; Reinders, M.; Ruijter, G. Using Out-of-Batch Reference Populations to Improve Untargeted Metabolomics for Screening Inborn Errors of Metabolism. *Metabolites* **2020**, *11* (1), 8. https://doi.org/10.3390/metabo11010008.

(113) Wehrens, R.; Hageman, Jos. A.; van Eeuwijk, F.; Kooke, R.; Flood, P. J.; Wijnker, E.; Keurentjes, J. J. B.; Lommen, A.; van Eekelen, H. D. L. M.; Hall, R. D.; Mumm, R.; de Vos, R. C. H. Improved Batch Correction in Untargeted MS-Based Metabolomics. *Metabolomics* **2016**, *12* (5), 88. https://doi.org/10.1007/s11306-016-1015-8.

(114) Sylvestre, D. A.; Slupsky, C. M.; Aviv, R. I.; Swardfager, W.; Taha, A. Y. Untargeted Metabolomic Analysis of Plasma from Relapsing-Remitting Multiple Sclerosis Patients Reveals Changes in Metabolites Associated with Structural Changes in Brain. *Brain Res.* **2020**, *1732*, 146589. https://doi.org/10.1016/j.brainres.2019.146589.

(115) Rosenbaum, P. R.; Rubin, D. B. The Central Role of the Propensity Score in Observational Studies for Causal Effects. *Biometrika* **1983**, *70* (1), 41–55. https://doi.org/10.1093/biomet/70.1.41.

(116) Laird, N. M.; Ware, J. H. Random-Effects Models for Longitudinal Data. *Biometrics* **1982**, *38* (4), 963. https://doi.org/10.2307/2529876.

(117) Broadhurst, D. I.; Kell, D. B. Statistical Strategies for Avoiding False Discoveries in Metabolomics and Related Experiments. *Metabolomics* **2007**, *2* (4), 171–196. https://doi.org/10.1007/s11306-006-0037-z.

(118) Sumner, L. W.; Amberg, A.; Barrett, D.; Beale, M. H.; Beger, R.; Daykin, C. A.; Fan, T. W.-M.; Fiehn, O.; Goodacre, R.; Griffin, J. L.; Hankemeier, T.; Hardy, N.; Harnly, J.; Higashi, R.; Kopka, J.; Lane, A. N.; Lindon, J. C.; Marriott, P.; Nicholls, A. W.; Reily, M. D.; Thaden, J. J.;

Viant, M. R. Proposed Minimum Reporting Standards for Chemical Analysis. *Metabolomics* **2007**, *3* (3), 211–221. https://doi.org/10.1007/s11306-007-0082-2.

(119) Liebal, U. W.; Phan, A. N. T.; Sudhakar, M.; Raman, K.; Blank, L. M. Machine Learning Applications for Mass Spectrometry-Based Metabolomics. *Metabolites* **2020**, *10* (6). https://doi.org/10.3390/metabo10060243.

(120) Vamathevan, J.; Clark, D.; Czodrowski, P.; Dunham, I.; Ferran, E.; Lee, G.; Li, B.; Madabhushi, A.; Shah, P.; Spitzer, M.; Zhao, S. Applications of Machine Learning in Drug Discovery and Development. *Nat. Rev. Drug Discov.* **2019**, *18* (6), 463–477. https://doi.org/10.1038/s41573-019-0024-5.

(121) Baiges-Gaya, G.; Iftimie, S.; Castañé, H.; Rodríguez-Tomàs, E.; Jiménez-Franco, A.; López-Azcona, A. F.; Castro, A.; Camps, J.; Joven, J. Combining Semi-Targeted Metabolomics and Machine Learning to Identify Metabolic Alterations in the Serum and Urine of Hospitalized Patients with COVID-19. *Biomolecules* **2023**, *13* (1), 163. https://doi.org/10.3390/biom13010163.

(122) Delafiori, J.; Navarro, L. C.; Siciliano, R. F.; de Melo, G. C.; Busanello, E. N. B.; Nicolau, J. C.; Sales, G. M.; de Oliveira, A. N.; Val, F. F. A.; de Oliveira, D. N.; Eguti, A.; dos Santos, L. A.; Dalçóquio, T. F.; Bertolin, A. J.; Abreu-Netto, R. L.; Salsoso, R.; Baía-da-Silva, D.; Marcondes-Braga, F. G.; Sampaio, V. S.; Judice, C. C.; Costa, F. T. M.; Durán, N.; Perroud, M. W.; Sabino, E. C.; Lacerda, M. V. G.; Reis, L. O.; Fávaro, W. J.; Monteiro, W. M.; Rocha, A. R.; Catharino, R. R. Covid-19 Automated Diagnosis and Risk Assessment through Metabolomics and Machine Learning. *Anal. Chem.* **2021**, *93* (4), 2471–2479. https://doi.org/10.1021/acs.analchem.0c04497.

(123) Kehoe, E. R.; Fitzgerald, B. L.; Graham, B.; Islam, M. N.; Sharma, K.; Wormser, G. P.; Belisle, J. T.; Kirby, M. J. Biomarker Selection and a Prospective Metabolite-Based Machine Learning Diagnostic for Lyme Disease. *Sci. Rep.* **2022**, *12* (1), 1478. https://doi.org/10.1038/s41598-022-05451-0.

(124) Zhang, J. D.; Xue, C.; Kolachalama, V. B.; Donald, W. A. Interpretable Machine Learning on Metabolomics Data Reveals Biomarkers for Parkinson's Disease. *ACS Cent. Sci.* **2023**, *9* (5), 1035–1045. https://doi.org/10.1021/acscentsci.2c01468.

(125) Kuang, A.; Kouznetsova, V. L.; Kesari, S.; Tsigelny, I. F. Diagnostics of Thyroid Cancer Using Machine Learning and Metabolomics. *Metabolites* **2023**, *14* (1), 11. https://doi.org/10.3390/metabo14010011.

(126) Radakovich, N.; Nagy, M.; Nazha, A. Machine Learning in Haematological Malignancies. *Lancet Haematol.* **2020**, *7* (7), e541–e550. https://doi.org/10.1016/S2352-3026(20)30121-6.

(127) Mahapatra, D.; Poellinger, A.; Shao, L.; Reyes, M. Interpretability-Driven Sample Selection Using Self Supervised Learning for Disease Classification and Segmentation. *IEEE Trans. Med. Imaging* **2021**, *40* (10), 2548–2562. https://doi.org/10.1109/TMI.2021.3061724.

(128) Topçuoğlu, B.; Lapp, Z.; Sovacool, K.; Snitkin, E.; Wiens, J.; Schloss, P. Mikropml: User-Friendly R Package for Supervised Machine Learning Pipelines. *J. Open Source Softw.* **2021**, *6* (61), 3073. https://doi.org/10.21105/joss.03073.

(129) Johnson, K. W.; Torres Soto, J.; Glicksberg, B. S.; Shameer, K.; Miotto, R.; Ali, M.; Ashley, E.; Dudley, J. T. Artificial Intelligence in Cardiology. *J. Am. Coll. Cardiol.* **2018**, *71* (23), 2668–2679. https://doi.org/10.1016/j.jacc.2018.03.521.

(130) Breiman, L. Random Forests. *Mach. Learn.* **2001**, *45* (1), 5–32. https://doi.org/10.1023/A:1010933404324.

(131) Brereton, R. G.; Lloyd, G. R. Support Vector Machines for Classification and Regression. *Analyst* **2010**, *135* (2), 230–267. https://doi.org/10.1039/B918972F.

(132) Curry, B.; Rumelhart, D. E. MSnet: A Neural Network Which Classifies Mass Spectra. *Tetrahedron Computer Methodology* **1990**, *3* (3–4), 213–237. https://doi.org/10.1016/0898-5529(90)90053-B.

(133) Argelaguet, R.; Velten, B.; Arnol, D.; Dietrich, S.; Zenz, T.; Marioni, J. C.; Buettner, F.; Huber, W.; Stegle, O. Multi-Omics Factor Analysis—a Framework for Unsupervised Integration of Multi-omics Data Sets. *Mol. Syst. Biol.* **2018**, *14* (6). https://doi.org/10.15252/msb.20178124.

(134) Theng, D.; Bhoyar, K. K. Feature Selection Techniques for Machine Learning: A Survey of More than Two Decades of Research. *Knowl. Inf. Syst.* **2024**, *66* (3), 1575–1637. https://doi.org/10.1007/s10115-023-02010-5.
(135) Guo, Y.; Yu, H.; Chen, D.; Zhao, Y.-Y. Machine Learning Distilled Metabolite Biomarkers for Early Stage Renal Injury. *Metabolomics* **2020**, *16* (1), 4. https://doi.org/10.1007/s11306-019-1624-0.
(136) Bersanelli, M.; Mosca, E.; Remondini, D.; Giampieri, E.; Sala, C.; Castellani, G.; Milanesi, L. Methods for the Integration of Multi-Omics Data: Mathematical Aspects. *BMC Bioinformatics* **2016**, *17* (S2), S15. https://doi.org/10.1186/s12859-015-0857-9.
(137) Garali, I.; Adanyeguh, I. M.; Ichou, F.; Perlbarg, V.; Seyer, A.; Colsch, B.; Moszer, I.; Guillemot, V.; Durr, A.; Mochel, F.; Tenenhaus, A. A Strategy for Multimodal Data Integration: Application to Biomarkers Identification in Spinocerebellar Ataxia. *Brief. Bioinform.* **2018**, *19* (6), 1356–1369. https://doi.org/10.1093/bib/bbx060.
(138) Kavakiotis, I.; Tsave, O.; Salifoglou, A.; Maglaveras, N.; Vlahavas, I.; Chouvarda, I. Machine Learning and Data Mining Methods in Diabetes Research. *Comput. Struct. Biotechnol. J.* **2017**, *15*, 104–116. https://doi.org/10.1016/j.csbj.2016.12.005.
(139) Chaudhary, K.; Poirion, O. B.; Lu, L.; Garmire, L. X. Deep Learning–Based Multi-Omics Integration Robustly Predicts Survival in Liver Cancer. *Clinical Cancer Research* **2018**, *24* (6), 1248–1259. https://doi.org/10.1158/1078-0432.CCR-17-0853.
(140) Cao, K.; Bai, X.; Hong, Y.; Wan, L. Unsupervised Topological Alignment for Single-Cell Multi-Omics Integration. *Bioinformatics* **2020**, *36* (Supplement_1), i48–i56. https://doi.org/10.1093/bioinformatics/btaa443.
(141) Kortela, E.; Kanerva, M. J.; Puustinen, J.; Hurme, S.; Airas, L.; Lauhio, A.; Hohenthal, U.; Jalava-Karvinen, P.; Nieminen, T.; Finnilä, T.; Häggblom, T.; Pietikäinen, A.; Koivisto, M.; Vilhonen, J.; Marttila-Vaara, M.; Hytönen, J.; Oksi, J. Oral Doxycycline Compared to Intravenous Ceftriaxone in the Treatment of Lyme Neuroborreliosis: A Multicenter, Equivalence, Randomized, Open-Label Trial. *Clinical Infectious Diseases* **2021**, *72* (8), 1323–1331. https://doi.org/10.1093/cid/ciaa217.
(142) Viljanen, M. K.; Punnonen, J. The Effect of Storage of Antigen-Coated Polystyrene Microwells on the Detection of Antibodies against Borrelia Burgdorferi by Enzyme Immunoassay (EIA). *J. Immunol. Methods* **1989**, *124* (1), 137–141. https://doi.org/10.1016/0022-1759(89)90195-6.
(143) Pence, H. E.; Williams, A. ChemSpider: An Online Chemical Information Resource. *J. Chem. Educ.* **2010**, *87* (11). https://doi.org/10.1021/ed100697w.
(144) Kanehisa, M.; Furumichi, M.; Sato, Y.; Matsuura, Y.; Ishiguro-Watanabe, M. KEGG: Biological Systems Database as a Model of the Real World. *Nucleic Acids Res.* **2025**, *53* (D1), D672–D677. https://doi.org/10.1093/nar/gkae909.
(145) Wishart, D. S.; Guo, A.; Oler, E.; Wang, F.; Anjum, A.; Peters, H.; Dizon, R.; Sayeeda, Z.; Tian, S.; Lee, B. L.; Berjanskii, M.; Mah, R.; Yamamoto, M.; Jovel, J.; Torres-Calzada, C.; Hiebert-Giesbrecht, M.; Lui, V. W.; Varshavi, D.; Varshavi, D.; Allen, D.; Arndt, D.; Khetarpal, N.; Sivakumaran, A.; Harford, K.; Sanford, S.; Yee, K.; Cao, X.; Budinski, Z.; Liigand, J.; Zhang, L.; Zheng, J.; Mandal, R.; Karu, N.; Dambrova, M.; Schiöth, H. B.; Greiner, R.; Gautam, V. HMDB 5.0: The Human Metabolome Database for 2022. *Nucleic Acids Res.* **2022**, *50* (D1), D622–D631. https://doi.org/10.1093/nar/gkab1062.
(146) Schymanski, E. L.; Jeon, J.; Gulde, R.; Fenner, K.; Ruff, M.; Singer, H. P.; Hollender, J. Identifying Small Molecules via High Resolution Mass Spectrometry: Communicating Confidence. *Environ. Sci. Technol.* **2014**, *48* (4), 2097–2098. https://doi.org/10.1021/es5002105.
(147) Huang, R.; Soneson, C.; Ernst, F. G. M.; Rue-Albrecht, K. C.; Yu, G.; Hicks, S. C.; Robinson, M. D. TreeSummarizedExperiment: A S4 Class for Data with Hierarchical Structure. *F1000Res.* **2021**, *9*, 1246. https://doi.org/10.12688/f1000research.26669.2.
(148) Borman, T.; Benedetti, G.; Muluh, G.; Raulo, A.; Valderrama, B.; Sannikov, A.; Peschel, S.; Liu, Y.; Hindström, R.; Pärnänen, K.; Müller, C. L.; Havulinna, A. S.; Shetty, S.; Ramos, M.; Braccia,

D. J.; Bravo, H. C.; Ernst, F. M.; Waldron, L.; Bastiaanssen, T. F. S.; Mallick, H.; Lahti, L. Orchestrating Microbiome Analysis with Bioconductor. October 30, 2025. https://doi.org/10.1101/2025.10.29.685036.

(149) Pang, Z.; Lu, Y.; Zhou, G.; Hui, F.; Xu, L.; Viau, C.; Spigelman, A. F.; MacDonald, P. E.; Wishart, D. S.; Li, S.; Xia, J. MetaboAnalyst 6.0: Towards a Unified Platform for Metabolomics Data Processing, Analysis and Interpretation. *Nucleic Acids Res.* **2024**, *52* (W1), W398–W406. https://doi.org/10.1093/nar/gkae253.

(150) Braisted, J.; Patt, A.; Tindall, C.; Sheils, T.; Neyra, J.; Spencer, K.; Eicher, T.; Mathé, E. A. RaMP-DB 2.0: A Renovated Knowledgebase for Deriving Biological and Chemical Insight from Metabolites, Proteins, and Genes. *Bioinformatics* **2023**, *39* (1). https://doi.org/10.1093/bioinformatics/btac726.

(151) Jassal, B.; Matthews, L.; Viteri, G.; Gong, C.; Lorente, P.; Fabregat, A.; Sidiropoulos, K.; Cook, J.; Gillespie, M.; Haw, R.; Loney, F.; May, B.; Milacic, M.; Rothfels, K.; Sevilla, C.; Shamovsky, V.; Shorser, S.; Varusai, T.; Weiser, J.; Wu, G.; Stein, L.; Hermjakob, H.; D'Eustachio, P. The Reactome Pathway Knowledgebase. *Nucleic Acids Res.* **2019**. https://doi.org/10.1093/nar/gkz1031.

(152) Slenter, D. N.; Kutmon, M.; Hanspers, K.; Riutta, A.; Windsor, J.; Nunes, N.; Mélius, J.; Cirillo, E.; Coort, S. L.; Digles, D.; Ehrhart, F.; Giesbertz, P.; Kalafati, M.; Martens, M.; Miller, R.; Nishida, K.; Rieswijk, L.; Waagmeester, A.; Eijssen, L. M. T.; Evelo, C. T.; Pico, A. R.; Willighagen, E. L. WikiPathways: A Multifaceted Pathway Database Bridging Metabolomics to Other Omics Research. *Nucleic Acids Res.* **2018**, *46* (D1), D661–D667. https://doi.org/10.1093/nar/gkx1064.

(153) Ferreira, G. C.; McKenna, M. C. L-Carnitine and Acetyl-l-Carnitine Roles and Neuroprotection in Developing Brain. *Neurochem. Res.* **2017**, *42* (6), 1661–1675. https://doi.org/10.1007/s11064-017-2288-7.

(154) Izzo, L. T.; Trefely, S.; Demetriadou, C.; Drummond, J. M.; Mizukami, T.; Kuprasertkul, N.; Farria, A. T.; Nguyen, P. T. T.; Murali, N.; Reich, L.; Kantner, D. S.; Shaffer, J.; Affronti, H.; Carrer, A.; Andrews, A.; Capell, B. C.; Snyder, N. W.; Wellen, K. E. Acetylcarnitine Shuttling Links Mitochondrial Metabolism to Histone Acetylation and Lipogenesis. *Sci. Adv.* **2023**, *9* (18). https://doi.org/10.1126/sciadv.adf0115.

(155) Al-Mekhlafi, A.; Waqas, F. H.; Krueger, M.; Klawonn, F.; Akmatov, M. K.; Müller-Vahl, K.; Trebst, C.; Skripuletz, T.; Stangel, M.; Sühs, K.-W.; Pessler, F. Elevated Phospholipids and Acylcarnitines C4 and C5 in Cerebrospinal Fluid Distinguish Viral CNS Infections from Autoimmune Neuroinflammation. *J. Transl. Med.* **2023**, *21* (1), 776. https://doi.org/10.1186/s12967-023-04637-y.

(156) Plaatjie, O. N.; van Furth, A. M. T.; Solomons, R.; van der Kuip, M.; Mason, S. CSF Carnitine Is a Potential Biomarker in Paediatric Tuberculous Meningitis. *Sci. Rep.* **2025**, *15* (1), 29366. https://doi.org/10.1038/s41598-025-15000-0.

(157) Carstens, G.; Verbeek, M. M.; Rohlwink, U. K.; Figaji, A. A.; te Brake, L.; van Laarhoven, A. Metabolite Transport across Central Nervous System Barriers. *Journal of Cerebral Blood Flow & Metabolism* **2024**, *44* (7), 1063–1077. https://doi.org/10.1177/0271678X241241908.

(158) Okura, T.; Kato, S.; Deguchi, Y. Functional Expression of Organic Cation/Carnitine Transporter 2 (OCTN2/SLC22A5) in Human Brain Capillary Endothelial Cell Line HCMEC/D3, a Human Blood-Brain Barrier Model. *Drug Metab. Pharmacokinet.* **2014**, *29* (1), 69–74. https://doi.org/10.2133/dmpk.DMPK-13-RG-058.

(159) Plaatjie, O. N.; van Furth, A. M. T.; van der Kuip, M.; Mason, S. LC–MS Metabolomics and Lipidomics in Cerebrospinal Fluid from Viral and Bacterial CNS Infections: A Review. *Front. Neurol.* **2024**, *15*. https://doi.org/10.3389/fneur.2024.1403312.

(160) McCann, M. R.; George De la Rosa, M. V.; Rosania, G. R.; Stringer, K. A. L-Carnitine and Acylcarnitines: Mitochondrial Biomarkers for Precision Medicine. *Metabolites* **2021**, *11* (1), 51. https://doi.org/10.3390/metabo11010051.

(161) Vallance, P.; Chan, N. Endothelial Function and Nitric Oxide: Clinical Relevance. *Heart* **2001**, *85* (3), 342–350. https://doi.org/10.1136/heart.85.3.342.
(162) Karetnikova, E. S.; Jarzebska, N.; Markov, A. G.; Weiss, N.; Lentz, S. R.; Rodionov, R. N. Is Homoarginine a Protective Cardiovascular Risk Factor? *Arterioscler. Thromb. Vasc. Biol.* **2019**, *39* (5), 869–875. https://doi.org/10.1161/ATVBAHA.118.312218.
(163) Pasini, E.; Corsetti, G.; Aquilani, R.; Romano, C.; Picca, A.; Calvani, R.; Dioguardi, F. Protein-Amino Acid Metabolism Disarrangements: The Hidden Enemy of Chronic Age-Related Conditions. *Nutrients* **2018**, *10* (4), 391. https://doi.org/10.3390/nu10040391.
(164) Ling, Z.-N.; Jiang, Y.-F.; Ru, J.-N.; Lu, J.-H.; Ding, B.; Wu, J. Amino Acid Metabolism in Health and Disease. *Signal Transduct. Target. Ther.* **2023**, *8* (1), 345. https://doi.org/10.1038/s41392-023-01569-3.
(165) Bakochi, A.; Mohanty, T.; Pyl, P. T.; Gueto-Tettay, C. A.; Malmström, L.; Linder, A.; Malmström, J. Cerebrospinal Fluid Proteome Maps Detect Pathogen-Specific Host Response Patterns in Meningitis. *Elife* **2021**, *10*. https://doi.org/10.7554/eLife.64159.
(166) Bharucha, T.; Gangadharan, B.; Kumar, A.; Myall, A. C.; Ayhan, N.; Pastorino, B.; Chanthongthip, A.; Vongsouvath, M.; Mayxay, M.; Sengvilaipaseuth, O.; Phonemixay, O.; Rattanavong, S.; O'Brien, D. P.; Vendrell, I.; Fischer, R.; Kessler, B.; Turtle, L.; de Lamballerie, X.; Dubot-Pérès, A.; Newton, P. N.; Zitzmann, N.; SEAe Consortium. Deep Proteomics Network and Machine Learning Analysis of Human Cerebrospinal Fluid in Japanese Encephalitis Virus Infection. *J. Proteome Res.* **2023**, *22* (6), 1614–1629. https://doi.org/10.1021/acs.jproteome.2c00563.
(167) Pei, H.; Xue, L.; Tang, M.; Tang, H.; Kuang, S.; Wang, L.; Ma, X.; Cai, X.; Li, Y.; Zhao, M.; Peng, A.; Ye, H.; Chen, L. Alkaloids from Black Pepper (*Piper Nigrum* L.) Exhibit Anti-Inflammatory Activity in Murine Macrophages by Inhibiting Activation of NF-KB Pathway. *J. Agric. Food Chem.* **2020**, *68* (8), 2406–2417. https://doi.org/10.1021/acs.jafc.9b07754.
(168) Azam, S.; Park, J.-Y.; Kim, I.-S.; Choi, D.-K. Piperine and Its Metabolite's Pharmacology in Neurodegenerative and Neurological Diseases. *Biomedicines* **2022**, *10* (1), 154. https://doi.org/10.3390/biomedicines10010154.
(169) Han, H.-K. The Effects of Black Pepper on the Intestinal Absorption and Hepatic Metabolism of Drugs. *Expert Opin. Drug Metab. Toxicol.* **2011**, *7* (6), 721–729. https://doi.org/10.1517/17425255.2011.570332.
(170) Guo, R.; Fang, Y.; Li, J.; Gao, H.; Niu, Z.; Lv, Y.; You, L.; Zhang, J.; Wang, X.; Wu, G.; Wang, T.; Hu, W.; Gu, F. A Comprehensive Review on the Main Alkamides in Piper Nigrum and Anti-Inflammatory Properties of Piperine. *Phytochemistry Reviews* **2025**. https://doi.org/10.1007/s11101-025-10127-4.
(171) Bojkowski, C. J.; Arendt, J.; Shih, M. C.; Markey, S. P. Melatonin Secretion in Humans Assessed by Measuring Its Metabolite, 6-Sulfatoxymelatonin. *Clin. Chem.* **1987**, *33* (8), 1343–1348. https://doi.org/10.1093/clinchem/33.8.1343.
(172) Abeysuriya, R. G.; Lockley, S. W.; Robinson, P. A.; Postnova, S. A Unified Model of Melatonin, 6-sulfatoxymelatonin, and Sleep Dynamics. *J. Pineal Res.* **2018**, *64* (4). https://doi.org/10.1111/jpi.12474.
(173) Carrillo-Vico, A.; Lardone, P.; Álvarez-Sánchez, N.; Rodríguez-Rodríguez, A.; Guerrero, J. Melatonin: Buffering the Immune System. *Int. J. Mol. Sci.* **2013**, *14* (4), 8638–8683. https://doi.org/10.3390/ijms14048638.
(174) Metz, T. O.; Chang, C. H.; Gautam, V.; Anjum, A.; Tian, S.; Wang, F.; Colby, S. M.; Nunez, J. R.; Blumer, M. R.; Edison, A. S.; Fiehn, O.; Jones, D. P.; Li, S.; Morgan, E. T.; Patti, G. J.; Ross, D. H.; Shapiro, M. R.; Williams, A. J.; Wishart, D. S. Introducing "Identification Probability" for Automated and Transferable Assessment of Metabolite Identification Confidence in Metabolomics and Related Studies. *Anal. Chem.* **2025**, *97* (1), 1–11. https://doi.org/10.1021/acs.analchem.4c04060.
(175) Pizzala, N. J.; Chao, H.; Faye, B. K. S.; McLuckey, S. A. Precursor Resolution via Ion Z-State Manipulation: A Tandem Mass Spectrometry Approach for the Analysis of Mixtures of

Multiply-Charged Ions. *Journal of Mass Spectrometry* **2025**, *60* (4). https://doi.org/10.1002/jms.5124.

(176) Babele, P.; Yadav, A. K. Back2Basics: Mass-to-Charge Ratio (m/z) in Proteomics. *J. Proteins Proteom.* **2023**, *14* (4), 223–226. https://doi.org/10.1007/s42485-023-00115-7.

(177) Nagornov, K. O.; Kozhinov, A. N.; Gasilova, N.; Menin, L.; Tsybin, Y. O. Transient-Mediated Simulations of FTMS Isotopic Distributions and Mass Spectra to Guide Experiment Design and Data Analysis. *J. Am. Soc. Mass Spectrom.* **2020**, *31* (9), 1927–1942. https://doi.org/10.1021/jasms.0c00190.

(178) Kruve, A.; Kaupmees, K. Adduct Formation in ESI/MS by Mobile Phase Additives. *J. Am. Soc. Mass Spectrom.* **2017**, *28* (5), 887–894. https://doi.org/10.1007/s13361-017-1626-y.

(179) Liigand, J.; Laaniste, A.; Kruve, A. PH Effects on Electrospray Ionization Efficiency. *J. Am. Soc. Mass Spectrom.* **2017**, *28* (3), 461–469. https://doi.org/10.1007/s13361-016-1563-1.

(180) Hernández, S. A.; Ogrinc, K.; Korva, M.; Kastrin, A.; Bogovič, P.; Rojko, T.; Kelley, K. W.; Weis, J. J.; Strle, F.; Strle, K. Association of Persistent Symptoms after Lyme Neuroborreliosis and Increased Levels of Interferon-α in Blood. *Emerg. Infect. Dis.* **2023**, *29* (6). https://doi.org/10.3201/eid2906.221685.

(181) Petzke, M. M.; Volyanskyy, K.; Mao, Y.; Arevalo, B.; Zohn, R.; Quituisaca, J.; Wormser, G. P.; Dimitrova, N.; Schwartz, I. Global Transcriptome Analysis Identifies a Diagnostic Signature for Early Disseminated Lyme Disease and Its Resolution. *mBio* **2020**, *11* (2). https://doi.org/10.1128/mBio.00047-20.

(182) Fishbein, S. R. S.; Mahmud, B.; Dantas, G. Antibiotic Perturbations to the Gut Microbiome. *Nat. Rev. Microbiol.* **2023**, *21* (12), 772–788. https://doi.org/10.1038/s41579-023-00933-y.

(183) He, M.; Shi, J.; Liu, A.; Xu, Y.-J.; Liu, Y. Antibiotic-Induced Gut Microbiota Dysbiosis Altered Host Metabolism. *Mol. Omics* **2023**, *19* (4), 330–339. https://doi.org/10.1039/D2MO00284A.

(184) Fujisaka, S.; Ussar, S.; Clish, C.; Devkota, S.; Dreyfuss, J. M.; Sakaguchi, M.; Soto, M.; Konishi, M.; Softic, S.; Altindis, E.; Li, N.; Gerber, G.; Bry, L.; Kahn, C. R. Antibiotic Effects on Gut Microbiota and Metabolism Are Host Dependent. *Journal of Clinical Investigation* **2016**, *126* (12), 4430–4443. https://doi.org/10.1172/JCI86674.

(185) Ogrinc, K.; Hernández, S. A.; Korva, M.; Bogovič, P.; Rojko, T.; Lusa, L.; Chiumento, G.; Strle, F.; Strle, K. Unique Clinical, Immune, and Genetic Signature in Patients with Borrelial Meningoradiculoneuritis1. *Emerg. Infect. Dis.* **2022**, *28* (4). https://doi.org/10.3201/eid2804.211831.

(186) Wepy, J. A.; Galligan, J. J.; Kingsley, P. J.; Xu, S.; Goodman, M. C.; Tallman, K. A.; Rouzer, C. A.; Marnett, L. J. Lysophospholipases Cooperate to Mediate Lipid Homeostasis and Lysophospholipid Signaling. *J. Lipid Res.* **2019**, *60* (2), 360–374. https://doi.org/10.1194/jlr.M087890.

(187) Choi, J. W.; Chun, J. Lysophospholipids and Their Receptors in the Central Nervous System. *Biochimica et Biophysica Acta (BBA) - Molecular and Cell Biology of Lipids* **2013**, *1831* (1), 20–32. https://doi.org/10.1016/j.bbalip.2012.07.015.

(188) Łuczaj, W.; Moniuszko-Malinowska, A.; Groth, M.; Skrzydlewska, E. Changes in the Serum Phospholipid Profile of Neuroborreliosis Patients, Foresters, and Patients Subjected to Long-Term Therapy According to ILADS Methods. *Prostaglandins Other Lipid Mediat.* **2025**, *177*, 106966. https://doi.org/10.1016/j.prostaglandins.2025.106966.

(189) Stoessel, D.; Stellmann, J.-P.; Willing, A.; Behrens, B.; Rosenkranz, S. C.; Hodecker, S. C.; Stürner, K. H.; Reinhardt, S.; Fleischer, S.; Deuschle, C.; Maetzler, W.; Berg, D.; Heesen, C.; Walther, D.; Schauer, N.; Friese, M. A.; Pless, O. Metabolomic Profiles for Primary Progressive Multiple Sclerosis Stratification and Disease Course Monitoring. *Front. Hum. Neurosci.* **2018**, *12*. https://doi.org/10.3389/fnhum.2018.00226.

(190) Ren, J.; Yu, L.; Lin, J.; Liu, Y.; Ma, L.; huang, Y.; Sun, N.; Deng, Y.; Zhong, D.; Zhou, B.; Jiang, B.; Yan, M. Elevated 18:1 Lysophosphatidylcholine Contributes to Neuropathic Pain in Peripheral Nerve Injury. *Reg. Anesth. Pain Med.* **2025**, rapm-2024-106195. https://doi.org/10.1136/rapm-2024-106195.

(191) Podbielska, M.; Ariga, T.; Pokryszko-Dragan, A. Sphingolipid Players in Multiple Sclerosis: Their Influence on the Initiation and Course of the Disease. *Int. J. Mol. Sci.* **2022**, *23* (10), 5330. https://doi.org/10.3390/ijms23105330.
(192) Wang, J.; Zheng, G.; Wang, L.; Meng, L.; Ren, J.; Shang, L.; Li, D.; Bao, Y. Dysregulation of Sphingolipid Metabolism in Pain. *Front. Pharmacol.* **2024**, *15*. https://doi.org/10.3389/fphar.2024.1337150.
(193) Alaamery, M.; Albesher, N.; Aljawini, N.; Alsuwailm, M.; Massadeh, S.; Wheeler, M. A.; Chao, C.; Quintana, F. J. Role of Sphingolipid Metabolism in Neurodegeneration. *J. Neurochem.* **2021**, *158* (1), 25–35. https://doi.org/10.1111/jnc.15044.
(194) Shi, L.; Ghezzi, L.; Fenoglio, C.; Pietroboni, A. M.; Galimberti, D.; Pace, F.; Hardy, T. A.; Piccio, L.; Don, A. S. CSF Sphingolipids Are Correlated with Neuroinflammatory Cytokines and Differentiate Neuromyelitis Optica Spectrum Disorder from Multiple Sclerosis. *J. Neurol. Neurosurg. Psychiatry* **2025**, *96* (1), 54–67. https://doi.org/10.1136/jnnp-2024-333774.
(195) Capodivento, G.; De Michelis, C.; Carpo, M.; Fancellu, R.; Schirinzi, E.; Severi, D.; Visigalli, D.; Franciotta, D.; Manganelli, F.; Siciliano, G.; Beronio, A.; Capello, E.; Lanteri, P.; Nobile-Orazio, E.; Schenone, A.; Benedetti, L.; Nobbio, L. CSF Sphingomyelin: A New Biomarker of Demyelination in the Diagnosis and Management of CIDP and GBS. *J. Neurol. Neurosurg. Psychiatry* **2021**, *92* (3), 303–310. https://doi.org/10.1136/jnnp-2020-324445.
(196) Castillo-Peinado, L. S.; López-Bascón, M. A.; Mena-Bravo, A.; Luque de Castro, M. D.; Priego-Capote, F. Determination of Primary Fatty Acid Amides in Different Biological Fluids by LC–MS/MS in MRM Mode with Synthetic Deuterated Standards: Influence of Biofluid Matrix on Sample Preparation. *Talanta* **2019**, *193*, 29–36. https://doi.org/10.1016/j.talanta.2018.09.088.
(197) Groth, M.; Skrzydlewska, E.; Czupryna, P.; Biernacki, M.; Moniuszko-Malinowska, A. Lipid Mediators of Cerebrospinal Fluid in Response to TBE and Bacterial Co-Infections. *Free Radic. Biol. Med.* **2023**, *207*, 272–278. https://doi.org/10.1016/j.freeradbiomed.2023.07.027.
(198) Kim, M.; Snowden, S.; Suvitaival, T.; Ali, A.; Merkler, D. J.; Ahmad, T.; Westwood, S.; Baird, A.; Proitsi, P.; Nevado-Holgado, A.; Hye, A.; Bos, I.; Vos, S.; Vandenberghe, R.; Teunissen, C.; ten Kate, M.; Scheltens, P.; Gabel, S.; Meersmans, K.; Blin, O.; Richardson, J.; De Roeck, E.; Sleegers, K.; Bordet, R.; Rami, L.; Kettunen, P.; Tsolaki, M.; Verhey, F.; Sala, I.; Lléo, A.; Peyratout, G.; Tainta, M.; Johannsen, P.; Freund-Levi, Y.; Frölich, L.; Dobricic, V.; Engelborghs, S.; Frisoni, G. B.; Molinuevo, J. L.; Wallin, A.; Popp, J.; Martinez-Lage, P.; Bertram, L.; Barkhof, F.; Ashton, N.; Blennow, K.; Zetterberg, H.; Streffer, J.; Visser, P. J.; Lovestone, S.; Legido-Quigley, C. Primary Fatty Amides in Plasma Associated with Brain Amyloid Burden, Hippocampal Volume, and Memory in the European Medical Information Framework for Alzheimer's Disease Biomarker Discovery Cohort. *Alzheimer's & Dementia* **2019**, *15* (6), 817–827. https://doi.org/10.1016/j.jalz.2019.03.004.
(199) Ezzili, C.; Otrubova, K.; Boger, D. L. Fatty Acid Amide Signaling Molecules. *Bioorg. Med. Chem. Lett.* **2010**, *20* (20), 5959–5968. https://doi.org/10.1016/j.bmcl.2010.08.048.
(200) Divito, E. B.; Cascio, M. Metabolism, Physiology, and Analyses of Primary Fatty Acid Amides. *Chem. Rev.* **2013**, *113* (10), 7343–7353. https://doi.org/10.1021/cr300363b.
(201) Kita, M.; Ano, Y.; Inoue, A.; Aoki, J. Identification of P2Y Receptors Involved in Oleamide-Suppressing Inflammatory Responses in Murine Microglia and Human Dendritic Cells. *Sci. Rep.* **2019**, *9* (1), 3135. https://doi.org/10.1038/s41598-019-40008-8.
(202) Guan, X.; Cravatt, B. F.; Ehring, G. R.; Hall, J. E.; Boger, D. L.; Lerner, R. A.; Gilula, N. B. The Sleep-Inducing Lipid Oleamide Deconvolutes Gap Junction Communication and Calcium Wave Transmission in Glial Cells. *J. Cell Biol.* **1997**, *139* (7), 1785–1792. https://doi.org/10.1083/jcb.139.7.1785.
(203) Fedorova, I.; Hashimoto, A.; Fecik, R. A.; Hedrick, M. P.; Hanuš, L. O.; Boger, D. L.; Rice, K. C.; Basile, A. S. Behavioral Evidence for the Interaction of Oleamide with Multiple Neurotransmitter Systems. *J. Pharmacol. Exp. Ther.* **2001**, *299* (1), 332–342. https://doi.org/10.1016/S0022-3565(24)29334-4.

(204) Akanmu, M.; Adeosun, S.; Ilesanmi, O. Neuropharmacological Effects of Oleamide in Male and Female Mice. *Behavioural Brain Research* **2007**, *182* (1), 88–94. https://doi.org/10.1016/j.bbr.2007.05.006.

(205) Uchiyama, A.; Mukai, M.; Fujiwara, Y.; Kobayashi, S.; Kawai, N.; Murofushi, H.; Inoue, M.; Enoki, S.; Tanaka, Y.; Niki, T.; Kobayashi, T.; Tigyi, G.; Murakami-Murofushi, K. Inhibition of Transcellular Tumor Cell Migration and Metastasis by Novel Carba-Derivatives of Cyclic Phosphatidic Acid. *Biochimica et Biophysica Acta (BBA) - Molecular and Cell Biology of Lipids* **2007**, *1771* (1), 103–112. https://doi.org/10.1016/j.bbalip.2006.10.001.

(206) Gotoh, M.; Sano-Maeda, K.; Murofushi, H.; Murakami-Murofushi, K. Protection of Neuroblastoma Neuro2A Cells from Hypoxia-Induced Apoptosis by Cyclic Phosphatidic Acid (CPA). *PLoS One* **2012**, *7* (12), e51093. https://doi.org/10.1371/journal.pone.0051093.

(207) Neale, J. H.; Yamamoto, T. N-Acetylaspartylglutamate (NAAG) and Glutamate Carboxypeptidase II: An Abundant Peptide Neurotransmitter-Enzyme System with Multiple Clinical Applications. *Prog. Neurobiol.* **2020**, *184*, 101722. https://doi.org/10.1016/j.pneurobio.2019.101722.

(208) Sühs, K.-W.; Novoselova, N.; Kuhn, M.; Seegers, L.; Kaever, V.; Müller-Vahl, K.; Trebst, C.; Skripuletz, T.; Stangel, M.; Pessler, F. Kynurenine Is a Cerebrospinal Fluid Biomarker for Bacterial and Viral Central Nervous System Infections. *J. Infect. Dis.* **2019**, *220* (1), 127–138. https://doi.org/10.1093/infdis/jiz048.

(209) Ahlberg Weidenfors, J.; Griška, V.; Li, X.; Pranckevičienė, A.; Pakalnienė, J.; Atlas, A.; Franzén-Röhl, E.; Piehl, F.; Lindquist, L.; Mickienė, A.; Engberg, G.; Schwieler, L.; Erhardt, S. Dysregulation of the Kynurenine Pathway Is Related to Persistent Cognitive Impairment in Tick-Borne Encephalitis. *Brain Behav. Immun.* **2025**, *125*, 452–465. https://doi.org/10.1016/j.bbi.2025.02.005.

(210) Wickström, R.; Fowler, Å.; Goiny, M.; Millischer, V.; Ygberg, S.; Schwieler, L. The Kynurenine Pathway Is Differentially Activated in Children with Lyme Disease and Tick-Borne Encephalitis. *Microorganisms* **2021**, *9* (2), 322. https://doi.org/10.3390/microorganisms9020322.

(211) Coutinho, L. G.; Christen, S.; Bellac, C. L.; Fontes, F. L.; de Souza, F. R. S.; Grandgirard, D.; Leib, S. L.; Agnez-Lima, L. F. The Kynurenine Pathway Is Involved in Bacterial Meningitis. *J. Neuroinflammation* **2014**, *11* (1), 169. https://doi.org/10.1186/s12974-014-0169-4.

(212) Zhao, H.; Zhang, Y.; Liu, B.; Zhang, L.; Bao, M.; Li, L.; Zhao, N.; Hussain, M.; Wang, Y.; Yi, J.; Chen, P.; Lu, C. A Pilot Study to Identify the Longitudinal Serum Metabolite Profiles to Predict the Development of Hyperuricemia in Essential Hypertension. *Clinica Chimica Acta* **2020**, *510*, 466–474. https://doi.org/10.1016/j.cca.2020.08.002.

(213) Guillemin, G. J. Quinolinic Acid, the Inescapable Neurotoxin. *FEBS J.* **2012**, *279* (8), 1356–1365. https://doi.org/10.1111/j.1742-4658.2012.08485.x.

(214) Maharaj, H.; Maharaj, D. S.; Daya, S. Acetylsalicylic Acid and Acetaminophen Protect against Oxidative Neurotoxicity. *Metab. Brain Dis.* **2006**, *21* (2–3), 180–190. https://doi.org/10.1007/s11011-006-9012-7.

(215) Dargue, R.; Grant, I.; Nye, L. C.; Nicholls, A.; Dare, T.; Stahl, S. H.; Plumb, R. S.; Lee, K.; Jalan, R.; Coen, M.; Wilson, I. D. The Analysis of Acetaminophen (Paracetamol) and Seven Metabolites in Rat, Pig and Human Plasma by U(H)PLC–MS. *Bioanalysis* **2020**, *12* (7), 485–500. https://doi.org/10.4155/bio-2020-0015.

(216) David, A.; Chaker, J.; Léger, T.; Al-Salhi, R.; Dalgaard, M. D.; Styrishave, B.; Bury, D.; Koch, H. M.; Jégou, B.; Kristensen, D. M. Acetaminophen Metabolism Revisited Using Non-Targeted Analyses: Implications for Human Biomonitoring. *Environ. Int.* **2021**, *149*, 106388. https://doi.org/10.1016/j.envint.2021.106388.

(217) Zhang, X.; Li, R.; Hu, W.; Zeng, J.; Jiang, X.; Wang, L. A Reliable LC-MS/MS Method for the Quantification of *N* -acetyl- *p* -benzoquinoneimine, Acetaminophen Glutathione and Acetaminophen Glucuronide in Mouse Plasma, Liver and Kidney: Method Validation and Application to a Pharmacokinetic Study. *Biomedical Chromatography* **2018**, *32* (11). https://doi.org/10.1002/bmc.4331.

(218) Rousar, T.; Handl, J.; Capek, J.; Nyvltova, P.; Rousarova, E.; Kubat, M.; Smid, L.; Vanova, J.; Malinak, D.; Musilek, K.; Cesla, P. Cysteine Conjugates of Acetaminophen and P-Aminophenol Are Potent Inducers of Cellular Impairment in Human Proximal Tubular Kidney HK-2 Cells. *Arch. Toxicol.* **2023**, *97* (11), 2943–2954. https://doi.org/10.1007/s00204-023-03569-2.

(219) Hairin, T.; Marzilawati, A. R.; Didi, E. M. H.; Mahadeva, S.; Lee, Y. K.; Abd. Rahman, N.; Mustafa, A. M.; Chik, Z. Quantitative LC/MS/MS Analysis of Acetaminophen–Cysteine Adducts (APAP–CYS) and Its Application in Acetaminophen Overdose Patients. *Analytical Methods* **2013**, *5* (8), 1955. https://doi.org/10.1039/c3ay26614a.

(220) Nau, R.; Sörgel, F.; Eiffert, H. Penetration of Drugs through the Blood-Cerebrospinal Fluid/Blood-Brain Barrier for Treatment of Central Nervous System Infections. *Clin. Microbiol. Rev.* **2010**, *23* (4), 858–883. https://doi.org/10.1128/CMR.00007-10.

(221) Haddad, N.; Carr, M.; Balian, S.; Lannin, J.; Kim, Y.; Toth, C.; Jarvis, J. The Blood–Brain Barrier and Pharmacokinetic/Pharmacodynamic Optimization of Antibiotics for the Treatment of Central Nervous System Infections in Adults. *Antibiotics* **2022**, *11* (12), 1843. https://doi.org/10.3390/antibiotics11121843.

(222) Kamel, A. M.; Brown, P. R.; Munson, B. Electrospray Ionization Mass Spectrometry of Tetracycline, Oxytetracycline, Chlorotetracycline, Minocycline, and Methacycline. *Anal. Chem.* **1999**, *71* (5), 968–977. https://doi.org/10.1021/ac9807114.

(223) Krishna, Ac.; Sathiyaraj, M.; Saravanan, R.; Chelladurai, R.; Vignesh, R. A Novel and Rapid Method to Determine Doxycycline in Human Plasma by Liquid Chromatography Tandem Mass Spectrometry. *Indian J. Pharm. Sci.* **2012**, *74* (6), 541. https://doi.org/10.4103/0250-474X.110599.

(224) Sun, H.; Xing, H.; Tian, X.; Zhang, X.; Yang, J.; Wang, P. UPLC-MS/MS Method for Simultaneous Determination of 14 Antimicrobials in Human Plasma and Cerebrospinal Fluid: Application to Therapeutic Drug Monitoring. *J. Anal. Methods Chem.* **2022**, *2022* (1). https://doi.org/10.1155/2022/7048605.

(225) Wongchang, T.; Winterberg, M.; Tarning, J.; Sriboonvorakul, N.; Muangnoicharoen, S.; Blessborn, D. Determination of Ceftriaxone in Human Plasma Using Liquid Chromatography–Tandem Mass Spectrometry. *Wellcome Open Res.* **2022**, *4*, 47. https://doi.org/10.12688/wellcomeopenres.15141.3.

(226) Buke, A. Does Dexamethasone Affect Ceftriazone Penetration into Cerebrospinal Fluid in Adult Bacterial Meningitis. *Int. J. Antimicrob. Agents* **2003**, *21* (5), 452–456. https://doi.org/10.1016/S0924-8579(03)00041-4.

(227) Kumta, N.; Heffernan, A. J.; Liu, X.; Parker, S. L.; Cotta, M. O.; Wallis, S. C.; Livermore, A.; Starr, T.; Wai, W. T.; Joynt, G. M.; Lipman, J.; Roberts, J. A. Ceftriaxone Population Pharmacokinetics in Plasma and Cerebrospinal Fluid of Neurocritical Care Patients. *Int. J. Antimicrob. Agents* **2025**, *65* (5), 107461. https://doi.org/10.1016/j.ijantimicag.2025.107461.

(228) Łuczaj, W.; Domingues, P.; Domingues, M. R.; Pancewicz, S.; Skrzydlewska, E. Phospholipidomic Analysis Reveals Changes in Sphingomyelin and Lysophosphatidylcholine Profiles in Plasma from Patients with Neuroborreliosis. *Lipids* **2017**, *52* (1), 93–98. https://doi.org/10.1007/s11745-016-4212-3.

(229) Halperin, J. J.; Heyes, M. P. Neuroactive Kynurenines in Lyme Borreliasis. *Neurology* **1992**, *42* (1), 43–43. https://doi.org/10.1212/WNL.42.1.43.

(230) Gasse, T.; Murr, C.; Meyersbach, P.; Schmutzhard, E.; Wachter, H.; Fuchs, D. Neopterin Production and Tryptophan Degradation in Acute Lyme Neuroborreliosis Versus Late Lyme Encephalopathy. *cclm* **1994**, *32* (9), 685–690. https://doi.org/10.1515/cclm.1994.32.9.685.

(231) Guerra, I. M. S.; Ferreira, H. B.; Melo, T.; Rocha, H.; Moreira, S.; Diogo, L.; Domingues, M. R.; Moreira, A. S. P. Mitochondrial Fatty Acid β-Oxidation Disorders: From Disease to Lipidomic Studies—A Critical Review. *Int. J. Mol. Sci.* **2022**, *23* (22), 13933. https://doi.org/10.3390/ijms232213933.

TURUN
YLIOPISTO
UNIVERSITY
OF TURKU

Painosalama, Turku, Finland 2026

ISBN 978-952-02-0686-4 (PRINT)
ISBN 978-952-02-0687-1 (PDF)
ISSN 0082-7002 (Print)
ISSN 2343-3175 (Online)